

**Unraveling the molecular mechanisms underlying the  
cell death pathway induced by *Vibrio parahaemolyticus*  
Thermostable Direct Hemolysin, an atypical  
pore-forming toxin**

**Pratima Verma**

*A thesis submitted for the partial fulfillment of  
the degree of Doctor of Philosophy*



Department of Biological Sciences  
Indian Institute of Science Education and Research Mohali  
Knowledge city, Sector 81, SAS Nagar, Manauli PO, Mohali 140306, Punjab, India.

February 2024



*Dedicated to  
my beloved parents...*



## **Declaration**

The work presented in this thesis has been carried out by me under the guidance of **Prof. Kausik Chattopadhyay** at the Indian Institute of Science Education and Research Mohali. This work has not been submitted in part or in full for a degree, a diploma, or a fellowship to any other university or institute. Whenever contributions of others are involved, every effort is made to indicate this clearly, with due acknowledgement of collaborative research and discussions. This thesis is a bonafide record of original work done by me and all sources listed within have been detailed in the bibliography.

**Pratima Verma**

In my capacity as the supervisor of the candidate's thesis work, I certify that the above statements by the candidate are true to the best of my knowledge.

**Prof. Kausik Chattopadhyay**

Department of Biological Sciences

Indian Institute of Science Education and Research Mohali



## Acknowledgments

The completion of this thesis would not have been possible without the unwavering support and guidance of numerous individuals. I am deeply grateful to each and every one of them for their invaluable contributions.

With due respect, I would like to express my sincere gratitude to my Ph.D. supervisor, Prof. Kausik Chattopadhyay, whose constant guidance, patience, and encouragement have been instrumental throughout my research journey. His exceptional vision, dedication, and profound knowledge have been a constant source of inspiration for me. I am truly grateful for his continuous support and mentorship.

I would like to extend my deep gratitude toward the immense contribution of Prof. Arunika Mukhopadhaya, for her pivotal role in shaping up my thesis work. Her profound expertise and valuable insights have significantly enriched the quality of my research work. I am deeply grateful to her for granting me unrestricted access to all the resources in her laboratory.

I am thankful to my doctoral committee members, Prof. Arunika Mukhopadhaya and Dr. Indranil Banerjee, for their timely evaluation of my work. Their valuable feedback and scientific criticism have definitely refined the quality of this work.

A note of thanks to Dr. Reena Thakur for her critical review and insightful comments on my manuscript drafts.

I would like to express my gratitude to all the past AM-KC lab members; Dr. G.V.R. Krishna Prasad, Dr. Nidhi Kundu, Dr. Aakanksha Gulati, Dr. Deepinder Kaur, Dr. Reema Kathuria, Dr. Vinica Dhar, Dr. Anish Kumar Mondal, for being the generous seniors. A special thanks to Dr. G.V.R. Krishna Prasad Dr. Nidhi Kundu for their patience and guidance throughout various experiments and lab techniques. My deepest thanks to the present AM-KC lab members; Dr. Reena, Dr. Vidushi, Shraddha, Arpita, Yogesh, Kusum, Mahendra, Shashi, Shamaita, Sanjeev, Dwipjyoti, Sindhoora, Aakanksha, Sougata, Koyel, Riya and Tanya, for fostering a supportive and collaborative environment in the lab. A special mention to Aakanksha Chauhan, Dr. Reena Thakur, Kusum Lata and Arpita Sharma, for generously extending their assistance and support during the revision work.

My heartfelt thanks to my dear batchmates and friends around the campus, Shraddha, Arpita Sharma, Arpita Mrigwani, Neeladrita, Babita, Roman, Tejal, Kusum, Garima, Sai, Nisha for their constant encouragement, love and friendship during these years.

I am extremely grateful to my off campus support systems, Piyush (Ishaan), Dipti Di and Salwa, for holding my back in every good and bad and for being warm and considerate during challenging times.

Words cannot express my gratitude to my parents for everything that they have done for me. Thank you Mumma and Papa, for your unconditional love, constant support and motivation during all the ups and downs of this journey. I thank my siblings, Anchal and Gaurav for being my best buddies, cheering me up and supporting me with all their love and care.

Lastly, I am humbly grateful to the Almighty for His blessings throughout this journey.

**Pratima Verma**

## List of publications

1. **Verma, P.\***, Chauhan, A.\*, Thakur, R., Lata, K., Sharma, A., Chattopadhyay, K., & Mukhopadhyaya, A. (2023). *Vibrio parahaemolyticus* thermostable direct haemolysin induces non-classical programmed cell death despite caspase activation. *Molecular microbiology*, 10.1111/mmi.15180. (\*equal contribution)
2. Bhutani, G., **Verma, P.**, Jayachandran, A., Paul, S., Chattopadhyay, K., & De, A. K. (2023). Unveiling the Role of Hidden Isomers in Large Stokes Shift in mKeima: Harnessing pH-Sensitive Dual-Emission in Bioimaging. *The journal of physical chemistry. B*, 127(14), 3197–3207.
3. Kaur, D.\*, **Verma, P.\***, Singh, M., Sharma, A., Lata, K., Mukhopadhyaya, A., & Chattopadhyay, K. (2022). Pore formation-independent cell death induced by a  $\beta$ -barrel pore-forming toxin. *FASEB journal : official publication of the Federation of American Societies for Experimental Biology*, 36(10), e22557. (\*equal contribution)
4. **Verma, P.**, & Chattopadhyay, K. (2021). Current Perspective on the Membrane-Damaging Action of Thermostable Direct Hemolysin, an Atypical Bacterial Pore-forming Toxin. *Frontiers in molecular biosciences*, 8, 717147.
5. **Verma, P.**, Gandhi, S., Lata, K., & Chattopadhyay, K. (2021). Pore-forming toxins in infection and immunity. *Biochemical Society transactions*, 49(1), 455–465.
6. Mondal, A. K., **Verma, P.**, Lata, K., Singh, M., Chatterjee, S., & Chattopadhyay, K. (2020). Sequence Diversity in the Pore-Forming Motifs of the Membrane-Damaging Protein Toxins. *The Journal of membrane biology*, 253(5), 469–478.
7. Kundu, N., **Verma, P.**, Kumar, A., Dhar, V., Dutta, S., & Chattopadhyay, K. (2020). N-Terminal Region of *Vibrio parahemolyticus* Thermostable Direct Hemolysin Regulates the Membrane-Damaging Action of the Toxin. *Biochemistry*, 59(4), 605–614.
8. Mondal, A. K., Sreekumar, A., Kundu, N., Kathuria, R., **Verma, P.**, Gandhi, S., & Chattopadhyay, K. (2018). Structural Basis and Functional Implications of the Membrane Pore-Formation Mechanisms of Bacterial Pore-Forming Toxins. *Advances in experimental medicine and biology*, 1112, 281–291.



## List of illustrations

<b>Illustration 1. General mechanism of pore-formation at the membrane surface by pore-forming toxins (PFTs). .....</b>	<b>6</b>
<b>Illustration 2. Damage and repair responses triggered by the PFTs.....</b>	<b>12</b>
<b>Illustration 3. Distinct immunological and cell death responses triggered by pore-forming toxins. ....</b>	<b>14</b>
<b>Illustration 4. Schematic representation of extrinsic and intrinsic pathways of apoptosis. ....</b>	<b>21</b>
<b>Illustration 5. Simplified representation of MPT-driven necrosis.....</b>	<b>23</b>
<b>Illustration 6. Schematic representation of necroptosis pathway.....</b>	<b>25</b>
<b>Illustration 7. Schematic representation of canonical and non-canonical pyroptosis pathways.....</b>	<b>26</b>
<b>Illustration 8. Diagrammatic representation of molecular mechanism of ferroptosis . .....</b>	<b>27</b>
<b>Illustration 9. Schematic representation of parthanatos cell death pathway. ....</b>	<b>29</b>
<b>Illustration 10. Schematic representing autophagy pathway. ....</b>	<b>30</b>
<b>Illustration 11. Structural features of TDH. ....</b>	<b>37</b>
<b>Illustration 12. TDH-mediated pathophysiological responses.....</b>	<b>39</b>
<b>Illustration 13. Diagrammatic representation of TDH-mediated caspase-independent cell death in target cells.....</b>	<b>115</b>



## List of figures

Figure 1. SDS-PAGE/Coomassie staining profile and hemolytic activity of purified TDH. ....	67
Figure 2. TDH exhibits potent cytotoxicity in Caco-2 and THP-1 cells. ....	69
Figure 3. TDH induces morphological changes in the target nucleated mammalian cells.....	71
Figure 4. TDH induces phosphatidylserine flipping and nuclear disintegration in target cells.....	73
Figure 5. TDH induces DNA fragmentation in Caco-2 cells, similar to that observed during apoptosis.....	74
Figure 6TDH-mediated cell death is independent of caspase-activation. ....	77
Figure 7. TDH triggers mitochondrial membrane permeability transition (MMPT) in target cells. ....	79
Figure 8. TDH-mediated ATP depletion in Caco-2 cells.....	80
Figure 9. TDH induces loss of cytochrome c in the target cells.....	82
Figure 10. TDH-induced MMPT causes the release of apoptosis inducing factor (AIF) from the mitochondria, which further translocates to the nucleus . ....	83
Figure 11. TDH-induced MMPT leads to the nuclear translocation of endonuclease G (Endo G) in target cells. ....	85
Figure 12. TDH induces ROS production in Caco-2 cells. ....	86
Figure 13. ROS production does not appear to be the sole player of TDH-mediated cell death pathway. ....	87
Figure 14. TDH induces ROS-mediated calcium influx, while calcium chelation does not affect TDH-mediated cytotoxicity in the target cells. ....	89
Figure 15. TDH exhibits significant propensity to translocate to the mitochondria of target cells. ....	92

**Figure 16. TDH exhibits association with isolated mitochondria of Caco-2 cells without inducing AIF release from them. .... 95**

**Figure 17. TDH induces elevated bax/bcl-2 ratio and increased mitochondrial translocation of Bax in target cells. .... 97**

**Figure 18. TDH induces lysosomal membrane permeabilization in Caco-2 cells.. 98**

**Figure 19. TDH treatment augments PARP-1 cleavage in the target cells..... 99**

## **List of tables**

**Table 1. Cellular responses-mediated by PFTs in their target hosts .....9**

**Table 2. Cell death responses by PFTs .....15**



## Abbreviations

AIF	Apoptosis Inducing factor
ANT	Adenine Nucleotide Translocator
BID	BH3 interacting-domain death agonist
BIR	Baculovirus IAP repeats
BSA	Bovine serum albumin
CADs	Caspase-activated DNases
CARD	Caspase recruitment domain
CTR	C-terminal region
DAMPs	Damage-associated molecular patterns
DCFDA	2', 7'-dichlorofluorescein diacetate
DISC	Death-inducing signaling complex
DNA	Deoxyribonucleic acid
DTT	Dithiothreitol
EDTA	Ethylenediaminetetraacetic acid
ER	Endoplasmic reticulum
ERK	Extracellular signal-regulated kinase
FADD	Fas-associated death domain
FBS	Fetal bovine serum
FITC	Fluorescein Isothiocyanate
FSC	Forward scatter
GAPDH	Glyceraldehyde-3-phosphate dehydrogenase
GSDMD	Gasdermin D
HBSS	Hanks' balanced salt solution
HEPES	4-(2-Hydroxyethyl)-1-piperazine ethanesulfonic acid
HRP	Horseradish peroxidase
IAP	Inhibitor of apoptosis
IPTG	Isopropyl $\beta$ -D-1-thiogalactopyranoside
JNK	Jun N-terminal kinase
LB	Luria broth
LDH	Lactate dehydrogenase
LMP	Lysosomal membrane permeabilization

LPS	Lipopolysaccharide
MAC	Membrane attack complex
MAPK	Mitogen-activated protein kinases
MIF	Macrophage migration inhibitory factor
MLKL	Mixed-lineage kinase domain-like pseudokinase
MMPT	Mitochondrial membrane permeability transition
MOMP	Mitochondrial outer membrane permeabilization
MPTP	Mitochondrial permeability transition pore
MSHA	Mannose-sensitive hemagglutinin
NAC	N-acetyl cysteine
NOD	Nucleotide oligomerization domain
OD	Optical density
PAAN	Parthanatos-associated AIF nuclease
PAGE	Polyacrylamide gel electrophoresis
PAI	Pathogenicity island
PAMPs	Pathogen-associated molecular patterns
PAR	Poly-(ADP-ribose)
PARP	Poly-(ADP-ribose) polymerase-1
PBS	Phosphate buffer saline
PCD	Programmed cell death
PCNA	Proliferating cell nuclear antigen
PDB	Protein data bank
PFP	Pore-forming proteins
PFT	Pore-forming toxins
PI	Propidium iodide
PMA	Phorbol 12-myristate 13-acetate
PS	Phosphatidylserine
PVDF	Polyvinylidene difluoride
RHIM	RIP homotypic interaction motif
RIPK1/3	Receptor-interacting protein kinase 1/3
RNA	Ribonucleic acid
ROS	Reactive oxygen species
RT-PCR	Real time - polymerase chain reaction
SDS	Sodium dodecyl sulfate

SSC	Side scatter
TAE	Tris acetate EDTA
TBST	Tris buffer saline- Tween20
TDH	Thermostable Direct Hemolysin
TLH	Thermolabile Hemolysin
TLR	Toll-like Receptor
TNF- $\alpha$	Tumor Necrosis Factor- $\alpha$
TNFR	Tumor Necrosis Factor Receptor
TRADD	TNF receptor-associated death domain
TRAIL	TNF-related apoptosis-inducing ligand
TRH	TDH-Related Hemolysin
UPR	Unfolded protein response
VCC	Vibrio cholerae Cytolysin
VDAC	Voltage-gated anion channel
XIAP	X-linked inhibitor of apoptosis
ZVAD-fmk	N-Benzylloxycarbonyl-Val-Ala-Asp(O-Me) fluoromethyl

ketone



# Contents

Declaration .....	i
Acknowledgments .....	iii
List of publications .....	v
List of illustrations.....	vii
List of figures .....	ix
List of tables .....	xi
Abbreviations .....	xiii
Abstract.....	1
<b>Section-1 Introduction and literature review.....</b>	<b>3</b>
1.0. Introduction .....	5
1.1. Pore-forming (proteins) toxins .....	6
1.2. Role of PFTs in membrane damage and beyond: PFT-mediated cellular responses	8
a. Membrane-repair responses .....	11
b. Activation of stress response pathways.....	11
c. Unfolded Protein Response (UPR) .....	12
d. Modulation of host immune responses.....	13
e. PFT-induced death signaling in the host cells.....	15
1.3. Cell death.....	18
1.3.1. Apoptosis .....	18
1.3.2. MPT-driven necrosis .....	22
1.3.3. Necroptosis .....	24
1.3.4. Pyroptosis .....	25
1.3.5. Ferroptosis .....	27
1.3.6. Parthanatos .....	28
1.3.7. Autophagy .....	29
1.4. <i>Vibrio parahaemolyticus</i> .....	31

1.4.1. Pathophysiology.....	31
1.4.2. Pathogenicity.....	31
a. Adhesins .....	32
b. Toxins.....	32
c. Type III secretion systems (T3SS).....	33
d. Type VI secretion system (T6SS) .....	34
e. Iron acquisition system .....	34
1.5. Thermostable Direct Hemolysin .....	35
1.5.1. Regulation and secretion of TDH by <i>V. parahaemolyticus</i> .....	35
1.5.2. Structural and physicochemical properties of TDH.....	36
1.5.4. Pathophysiological functions of TDH .....	38
1.6. Aim of the study: .....	41
<b>Section-2 Materials and methods .....</b>	<b>43</b>
2.1. Ethics statement .....	45
2.2. Expression and purification of TDH.....	45
2.3. Hemolytic activity assay .....	46
2.4. Cell culture conditions .....	46
2.5. Lactate dehydrogenase release assay of cytotoxicity.....	47
2.6. Analysis of morphological changes by flow cytometry .....	47
2.7. Analysis of morphological changes by phase contrast microscopy.....	48
2.8. Annexin V-FITC and propidium iodide staining .....	48
2.9. DNA fragmentation analysis by agarose gel electrophoresis .....	49
2.10. Whole cell lysate preparation for cleaved caspase-3 detection.....	50
2.11. Active caspase-3 detection by flow cytometry .....	51
2.12. JC-1 dye assay for Mitochondrial Membrane Permeability Transition.....	51
2.13. ATP determination assay .....	52
2.14. Assay for the detection of loss of cytochrome c from mitochondria .....	52

2.15. Mitochondrial fraction preparation for AIF, TDH and Bax translocation .....	53
2.16. Nuclear fraction preparation for AIF and Endo G translocation .....	54
2.17. DCFDA fluorescence assay for the detection of intracellular ROS production....	55
2.18. NAC-mediated inhibition studies .....	56
2.19. Mitochondrial ROS detection .....	56
2.20. Calcium measurement assay.....	57
2.21. Co-localization study using confocal microscopy.....	58
2.22. Effect of TDH on isolated mitochondria .....	59
2.23. Semi-quantitative RT-PCR analysis for <i>bax</i> and <i>bcl-2</i> .....	61
2.24. Detection of lysosomal membrane permeabilization .....	62
2.25. Detection of cleaved PARP-1 in whole cell lysates .....	62
2.26. Statistical analyses .....	63
<b>Section-3 Results .....</b>	<b>65</b>
3.1. Purification and hemolytic activity of TDH .....	67
3.2. TDH displays potent cytotoxicity in the nucleated mammalian cells .....	68
3.3. TDH induces morphological alterations in target cells .....	70
3.4. TDH induces membrane phosphatidylserine flipping and DNA fragmentation resembling the features of apoptosis-like programmed cell death .....	72
3.5. TDH-mediated cell death does not involve caspases as the key executioners .....	75
3.6. TDH induces mitochondrial membrane permeability transition (MMPT) in the target cells	78
3.7. TDH causes depletion of ATP pools in the target cells.....	80
3.8. TDH triggers the release of cytochrome c from the mitochondria due to mitochondrial damage .....	81
3.9. TDH induces the translocation of apoptosis-inducing factor (AIF) from the mitochondria to the nucleus of target cells .....	82
3.10. TDH causes the translocation of endonuclease G to the nucleus of target cells, justifying the DNA-laddering pattern in caspase-independent cell death.....	84

3.11. TDH induces ROS production in the target cells.....	85
3.12. TDH induces ROS-mediated calcium influx in target cells.....	88
3.13. TDH translocates to the mitochondria of the target cells .....	90
3.14. TDH association with the isolated mitochondria does not induce mitochondrial damage .....	93
3.15. TDH causes increased <i>bax/bcl-2</i> ratio along with mitochondrial recruitment of active bax molecules in the target cells.....	95
3.16. TDH induces permeabilization of lysosomal membrane .....	97
3.17. TDH induces PARP-1 cleavage in target cells .....	98
<b>Section-4 Discussion &amp; conclusion .....</b>	<b>101</b>
References .....	117
Synopsis .....	141

## Abstract

Thermostable Direct Hemolysin (TDH) is an atypical pore-forming toxin and a key virulence factor secreted by *Vibrio parahaemolyticus*, a human gastrointestinal pathogen. Owing to its membrane-damaging pore-forming activity, TDH exerts several pathophysiological effects in the target cells. The manifestation of bloody mucous diarrhea during *V. parahaemolyticus* infections is attributed to the potent cytotoxicity of TDH, also reported against various nucleated mammalian cells. Nevertheless, the precise mechanism of TDH-induced cell death remains largely unexplored. The present work elucidates the mechanistic insights into the cytotoxic cell death responses elicited by TDH in the nucleated mammalian cells. The study reveals that TDH triggers features of apoptosis-like programmed cell death in the target cells. However, the involvement of caspases is not observed in TDH-mediated cell death. Therefore, TDH evokes a caspase-independent programmed cell death pathway, predominantly marked by mitochondrial damage. TDH prompts mitochondrial membrane permeability transition (MMPT), resulting in the release of mitochondrial factors like AIF and Endo G, responsible for the execution of caspase-independent cell death. Furthermore, this work documents ROS production, calcium influx, lysosomal membrane permeabilization and PARP-1 cleavage in response to TDH. Interestingly, a fraction of TDH and active Bax are found to translocate to the target cell mitochondria. TDH itself remains insufficient to induce mitochondrial damage, implying towards the Bax-mediated mitochondrial damage. Altogether, this study unravels significant executioners of the TDH-mediated caspase-independent programmed cell death. Furthermore, it provides critical new insights into the role of TDH in the context of host-pathogen interaction processes.



## **Section-1**

### **Introduction and literature review**



# 1. Introduction and literature review

## 1.0. Introduction

The plasma membrane of all living cells is an extremely crucial component that supports and maintains cellular integrity and facilitates various biological processes required for the proper functioning and survival of the cell [1]. In order to get past this barrier and modulate the normal physiology of the target cells, living organisms employ a specialized class of proteins called the 'pore-forming proteins' or PFPs. These proteins have the ability to destroy the plasma membrane by punching holes on them and, in turn, disrupt the physiological balance of the cell [2]. The PFPs are conserved across all the domains of life such as bacteria, fungi, plants and higher vertebrates like humans [3]. Therefore, these proteins are considered Nature's ancient and favourite cell-killing machinery.

Bacteria secrete pore-forming proteins, generally termed as the bacterial pore-forming toxins (PFTs). These are the most well-studied protein toxins and constitute the largest class of known bacterial toxins [3]. Bacteria utilize PFTs for various benefits, such as nutrient retrieval from their host, killing other bacterial cells competing for the same resources, and facilitating the entry of other bacterial effectors [4-6]. During bacterial infections, PFTs help in breaching the epithelial and endothelial barriers, aiding the pathogen's entry and dissemination into host cells [7]. Moreover, bacterial pathogens replicating inside host cells secrete PFTs to assist their spread by rupturing intracellular vesicles [8]. Interaction of bacterial PFTs with target host cells may trigger diverse cellular responses, including repair, survival, immunological and cell death responses that can modulate the course of infection [4]. Altogether, these functionalities make the PFTs an extremely critical member of a bacterium's virulence arsenals.

In this direction, the current thesis work aims to understand and elucidate the cell death responses generated by a major PFT of *Vibrio parahaemolyticus*, Thermostable Direct Hemolysin.

## 1.1. Pore-forming (proteins) toxins

Pore-forming (proteins) toxins (PFTs) are a distinct class of membrane-attacking proteins that form pores on the target cell membrane, thereby destroying the permeability barrier function of the plasma membrane [3, 9]. This is accompanied by the unregulated exchange of ions, water and other molecules between the cell and the extracellular milieu, leading to perturbed cellular homeostasis and subsequent cell death [3, 4, 10]. PFTs are amphipathic molecules undergoing substantial structural rearrangements from water-soluble monomeric to transmembrane-oligomeric conformations [11]. The general scheme of the pore-formation mechanism adopted by PFTs involves: (i) adsorption of water-soluble PFT monomers to the membrane and their specific interaction with the membrane surface receptors, (ii) oligomerization of PFT monomers on the membrane surface resulting in an oligomeric pre-pore intermediate, and (iii) subsequent insertion of the pore-forming motifs into the lipid bilayer to form an active transmembrane pore (Illustration 1) [12, 13].

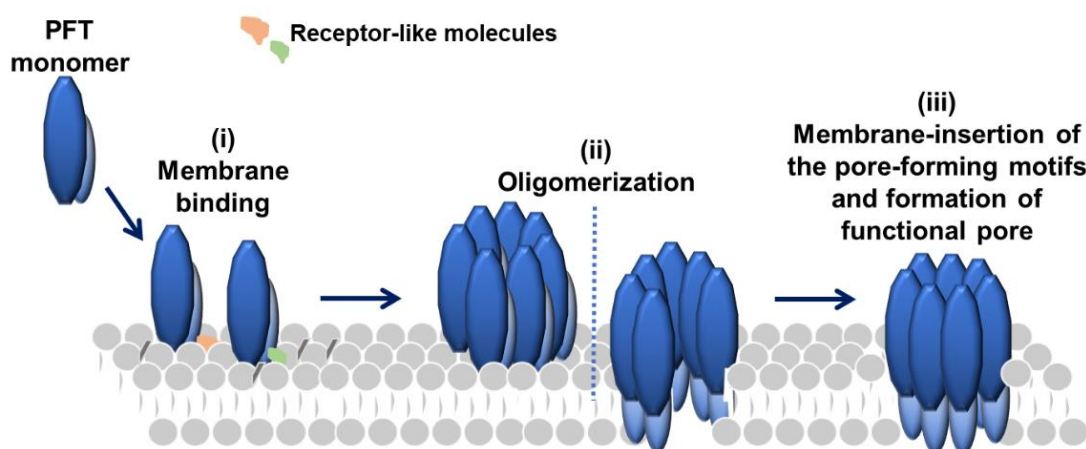


**Illustration 1. General mechanism of pore-formation at the membrane surface by pore-forming toxins (PFTs).** PFTs are secreted as water-soluble monomers interacting with specific receptors on the membrane surface. Subsequently, the membrane-bound monomers oligomerize on the membrane surface and undergo structural reorganizations resulting in the insertion and formation of a functional transmembrane pore. For some PFTs, the insertion of the pore-forming motif can be concurrent with the oligomerization step leading to the formation of arcs that eventually grow to form complete pores.

Interestingly, different PFTs may have unique physicochemical properties such as their secretion through the bacterium, their in-solution state, oligomeric stoichiometry, pre-pore intermediates, distinct pore-forming motifs, pore-size etc. For instance, *Vibrio cholerae* cytolysin is released in association with the outer membrane vesicles secreted by the bacterium, while Pneumolysin, a PFT from *Streptococcus pneumoniae*, is secreted upon autolysis of the bacterial cell [14, 15]. Unlike most of the PFTs that remain as monomers in solution, Thermostable Direct Hemolysin (TDH) exhibits a water-soluble tetrameric assembly that binds to the target membrane [16, 17]. Most  $\beta$ -PFTs shows an oligomeric pre-pore intermediate before insertion, while  $\alpha$ -PFTs follow sequential insertion of pore-forming motifs along with concomitant oligomerization forming arc-like structures that eventually grow from partial to complete pores [3]. These unique characteristics of PFTs may reflect upon their unique and distinct steps of pore-formation mechanisms.

Based on the membrane-traversing motifs secondary structure ( $\alpha$ -helices or  $\beta$ -sheets), the PFTs are categorized as  $\alpha$ - and  $\beta$ -PFTs [18]. Actinoporins secreted by sea anemones, cytolysin A and colicins from *Escherichia coli* are the typical examples of  $\alpha$ -PFTs [10, 18]. Cholesterol-dependent cytolysins (CDCs), Aerolysin and *Vibrio cholerae* cytolysin are some of the prominent examples of  $\beta$ -PFTs [10].

Depending on PFT's pore-architecture, two pore models have been proposed. Archetypical PFTs form a transmembrane scaffold comprising the insertion motifs to generate a water-filled lumen lined mainly by the hydrophilic side chains. In contrast, the lipid bilayer side is marked mostly by the hydrophobic residues of the protein toxin. Pores with such a structural disposition are called 'protein-only pores'. For example, members of gasdermin family form protein-only pores on target membranes [19]. Another type of transmembrane-pore scaffold is the 'toroidal pore model', where the pore-lining is constituted by the contribution of protein motifs from the PFT and the membrane phospholipid head groups. For example, Bax and Bak are mammalian pore-forming proteins that are proposed to form toroidal pores on mitochondrial membranes during apoptotic cell death induction [19, 20].

## **1.2. Role of PFTs in membrane damage and beyond: PFT-mediated cellular responses**

PFTs are found associated with diverse biological processes ranging from the pathogenesis of the bacteria to the effectors responsible for the execution of immunological or cell death responses in humans. Various studies exploring the role of PFTs beyond membrane damage have surfaced over the decade and challenged the classical notion about PFTs that their attack and effects are limited to the membrane [21-24]. In fact, diverse cellular responses have been reported in response to PFTs' assaults (Table 1). The primary consequences of compromised plasma-membrane integrity, like the dysregulation of ionic flow (calcium influx and potassium efflux), ATP depletion and disturbed cellular homeostasis, may act as the mechanical cues triggering various damage and repair response signaling in the host cells. Elevated calcium levels in the cytosol are sensed and reciprocated with membrane-repair response, activation of survival and defence mechanisms in the host. However, if high concentration of cytosolic calcium persists for long, it may cause organelle dysfunction and trigger regulated cell death [23, 25]. The efflux of potassium by PFTs has been observed to induce cellular responses like autophagy and NLRP3 inflammasome activation [26, 27]. ATP-depletion by the PFTs has also been associated with mitochondrial dysfunction and cell death [28]. The physico-chemical properties of a PFT and the associated target site contribute significantly in deciding whether a distinct pathway or overlapping cellular processes or responses will be activated in the target cell. Different PFTs vary from each other in terms of size, structure, stoichiometry, architecture, stability, specificity and conductance of the pore for different ions. Individual PFTs may have various membrane-bound conformational states and intermediates during the pore-formation process. In addition, the concentration of a PFT at the target site and the extent of ion flux may vary. Considering these factors, it would be appropriate to say that the exact nature and extent of the host cellular responses is specific to the nature and the degree of assault by the PFT in question. Therefore, it is important to focus upon the mechanism of action of PFTs and their effects on the target cells.

The mammalian hosts also employ various PFPs in diverse responses to tackle the assaults of different PFTs and play roles in the execution of various effector functions like immunological responses and cell death to combat disease and infections. For instance, perforins are the PFPs secreted by the cytotoxic T-cells and natural killer cells.

They form large pores on infected cells and aid the entry of granzymes into the target cells that kill them by inducing apoptosis [29]. The complement system serves as an essential tool employed by the host defense system for the clearance of bacteria and parasites. Activation of the complement pathway comprises of a pore-forming protein complex i.e. membrane-attack complex (MAC). The MAC forms pore on the target pathogen's membrane causing its lysis. Moreover, MAC activation may accompany apoptosis of the infected cells [30]. Mixed-lineage kinase domain-like pseudokinase (MLKL) is another critical PFP that forms pores on the plasma membrane during necroptosis, a form of inflammatory cell death [31]. Gasdermins are a distinct family of pore-forming proteins, out of which Gasdermin D is an essential player in another inflammatory cell death called pyroptosis [32]. Members of the bcl-2 family, Bax and Bak are pro-apoptotic molecules that primarily form pores in the outer mitochondrial membrane. The permeabilization of outer mitochondrial membrane by Bax and Bak may lead to disrupted mitochondrial membrane potential, and also facilitates the release of mitochondrial factors essential for the programmed cell death [33].

**Table 1. Cellular responses-mediated by PFTs in their target hosts**

<i>PFT</i>	<i>Pathogen</i>	<i>Cellular responses</i>	<i>Ref.</i>
Pneumolysin (PLY)	<i>Streptococcus pneumoniae</i>	Inflammation, complement activation, NLRP3 inflammasome activation, barrier dysfunction, hijacking of host factors, cell death of non-immune cells	[34-38]
Panton-Valentine Leukocidin (PVL)	<i>Staphylococcus aureus</i>	Pro-inflammatory responses and lysis of Polymorphonuclear Leukocytes, soft tissue necrosis	[39-41]
$\alpha$ -hemolysin or $\alpha$ -toxin (Hla)	<i>Staphylococcus aureus</i>	Disruption of epithelial and endothelial barriers, cell death by different pathways, triggers p38 MAPK and endocytosis-mediated cell survival responses	[42]

Perfringolysin (PFO)	<i>Clostridium perfringens</i>	TLR-4 mediated inflammatory responses, vasoconstriction, cytotoxicity toward macrophages, actomyosin reorganizations and ER vacuolation	[43-45]
Listeriolysin O (LLO)	<i>Listeria monocytogenes</i>	Intracellular survival of pathogen and hijacks host factors, induces UPR pathway upon ER stress, pro-inflammatory responses, triggers cell death responses in both immune and non-immune cell types	[46]
Hemolysin A (HlyA)	<i>Escherichia coli</i>	Cytotoxic to various cell types, disrupts cell adhesion, induces cytokines production from epithelial cells and monocytes by activating NLRP3 inflammasome	[47, 48]
<i>Vibrio cholerae</i> Cytolysin (VCC)	<i>Vibrio cholerae</i>	Induces apoptosis in immune and non-immune cells in a caspase-dependent manner, damages epithelial cells by vacuolation, pro-inflammatory responses in macrophages, monocytes, intestinal epithelial cells, autophagic cell survival responses	[49]
Motility associated killing factor A (MakA)	<i>Vibrio cholerae</i>	Suppresses tumor cell proliferation by blocking PIP5 $\alpha$ /Akt lipid-signaling pathway, activates non-canonical autophagy in target cells	[50, 51]
ESAT-6	<i>Mycobacterium tuberculosis</i>	Phagosome lysis for bacterial dissemination, ROS-mediated ER stress and apoptosis in macrophages, interferes with macrophage	[52-54]

		differentiation and polarization, blocks fusion of autophagosome and lysosome	
Vacuolating toxin A (VacA)	<i>Helicobacter pylori</i>	Immunosuppression of myeloid and T-cells, inhibition of antigen presentation and T-cell proliferation, induction of apoptosis, mTORC1 inhibition-dependent autophagy induction, cytoskeletal rearrangements	[55-57]

Following are the extensively studied damage, repair and defense responses triggered in mammalian hosts upon encountering PFTs:

**a. Membrane-repair responses:** Upon encountering a PFT at the membrane surface, the cell's first obvious response is to remove it from the membrane itself to limit further damage. The plasma membrane undergoes dramatic reorganizations to counter PFT's membrane-damaging effects [58]. Membrane-repair strategies initiated by the target host cells involve *shedding* the toxin lesions from the membrane in small vesicles in the extracellular milieu or *endocytosis* of the transmembrane-complexes of PFTs to destroy them intracellularly [27, 59, 60] (Illustration 2). *Clogging* of the pore, membrane *patching* and *blebbing* are the other strategies of membrane-repair adopted by the cells to clear off the PFT lesions [59]. Studies emphasize on the occurrence of different membrane-repair mechanisms simultaneously in response to a single PFT. For example, alpha-hemolysin from *Staphylococcus aureus* undergoes shedding after being endocytosed and failed lysosomal degradation [61].

**b. Activation of stress response pathways:** The membrane-damaging activity of PFTs invokes stress conditions in the target cells that, in turn, can trigger the stress-response signaling pathway(s). MAPKs (mitogen-activated protein kinases) such as p38, JNK and ERK are the critical mediators of the stress-response signaling cascade(s) (Illustration 2). p38 and/or JNK MAPK-mediated pathways have been observed in response to the PFTs' attack [62]. The PFT-mediated osmotic stress, ionic imbalance (calcium influx and potassium efflux) and ATP depletion within the cells are recognized as the primary

triggers for the MAPK activation. Interaction of PFTs with specific cell surface receptors may also trigger the downstream pathways, ultimately leading to different MAPKs' activation [49]. Upon activation, MAPK signaling may overlap and contribute to multiple other cell signaling responses involving inflammatory responses, repair mechanisms, cell survival strategies or the programmed cell death pathways [63].

**c. Unfolded Protein Response (UPR):** PFT-mediated assaults result in the modulation of intracellular calcium and its stores, imposing a stressful condition over the endoplasmic reticulum (ER). The ER stress in the cells triggers an adaptive cellular response that monitors ER protein homeostasis called the unfolded protein response (UPR) [64] (Illustration 2). Generally, the UPR pathway tackles the protein-folding stress to relieve the ER stress by inhibiting protein synthesis while enhancing protein folding and degradation. It has been documented that UPR activation in response to PFTs provides defensive roles to the target cells [65]. However, it is necessary to consider here that excessive and prolonged ER stress may end up in inducing cell death [66].

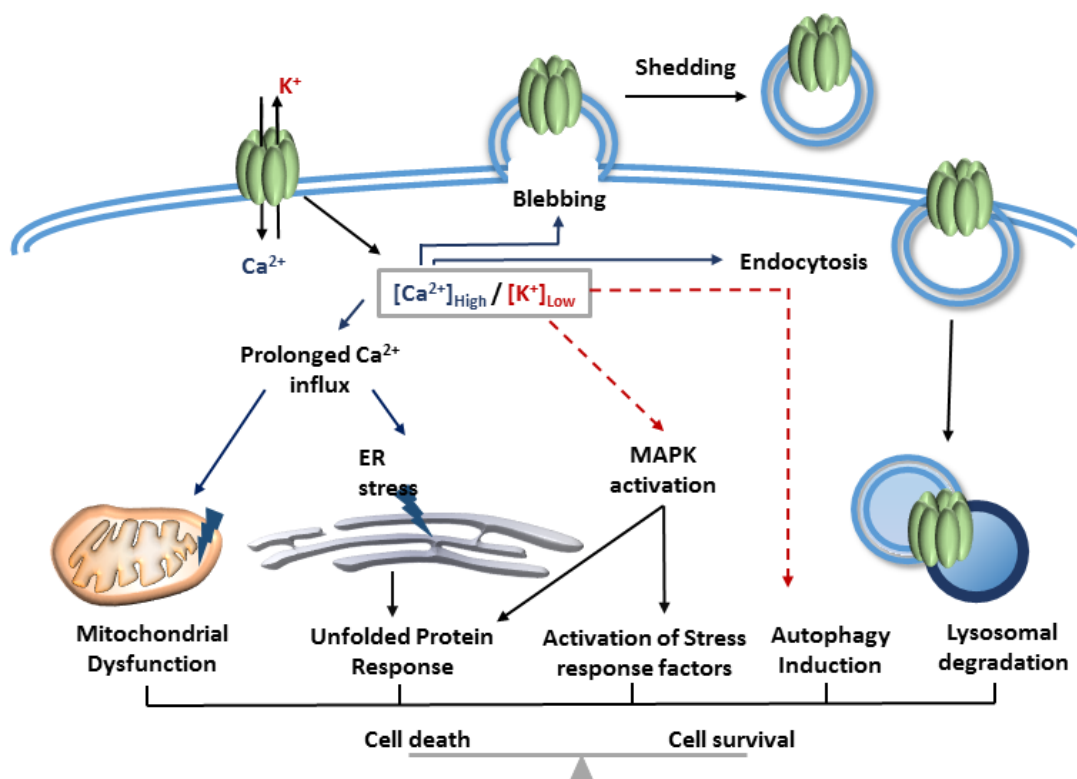


**Illustration 2. Damage and repair responses triggered by the PFTs.** Diagrammatic representation of induction of cellular defense and repair processes triggered in response

to assaults by PFTs. Pore-formation activity of PFTs leads to calcium influx and potassium efflux, which are instantly sensed by the cell and evoke various responses to repair the membrane damage and restore cell homeostasis. Blebbing and shedding the damaged membrane fractions in the form of vesicles containing the PFT is one of the repair mechanisms adopted by the cell. Endocytosis of PFTs for lysosomal degradation serves as another cell repair/survival response. Autophagy induction is another cell survival response triggered in affected cells. The persistent imbalance of ions induces organelle stress, such as calcium-mediated ER and mitochondrial stress resulting in UPR and mitochondrial dysfunction. Low potassium levels lead to the activation of stress response factors. Overwhelming damage with no scope of repair eventually ends up in cell death.

**d. Modulation of host immune responses:** The mammalian defense system nurtures various immune cells like monocytes, macrophages, and neutrophils that try to combat the pathogenic infection as first responders. The potent cell-killing activity of PFTs has been documented against all these cell types [67-70]. Essentially, PFTs have various immunomodulatory effects, aiding the pathogen in evading the immune surveillance system of the mammalian host. PFTs are recognized as PAMPs (pattern-associated molecular patterns) by the immune cells' surface receptors called PRRs or the pattern recognition receptors [24, 71]. TLRs or Toll-like receptors are the most common PRRs associated with PFT recognition by the immune cells. A signaling cascade is activated downstream to the TLR activation, leading to the pro-inflammatory responses that result into the release of pro-inflammatory cytokines such as TNF- $\alpha$ , IL-6 and nitric oxide [24, 72]. The production of these cytokines is mediated either through a canonical NF- $\kappa$ B pathway or a non-canonical MAPKs (p38 and JNK)-dependent manner (Illustration 3).

As mentioned earlier, the PFTs disintegrate from the membrane-surface during the host's cell membrane-repair process. In the extracellular milieu, these proteoliposomes containing lipid membrane and the PFTs may behave as DAMPs (damage-associated molecular patterns) and activate the immune cells [73]. Other inflammatory responses observed against PFT attacks include inflammasome activation in immune cells [36, 74]. Inflammasomes are multimeric complexes that sense and assemble in response to infections. Their activation is linked with the efflux of potassium

due to PFTs' assaults. Activation of NLRP3 inflammasome, in turn, activates Gasdermin D, a key executioner of inflammatory cell death called pyroptosis. The active form of Gasdermin D assists the secretion of inflammatory cytokine, IL-1 $\beta$ , by forming pores on the cell membrane, causing pyroptosis [32, 70] (Illustration 3).

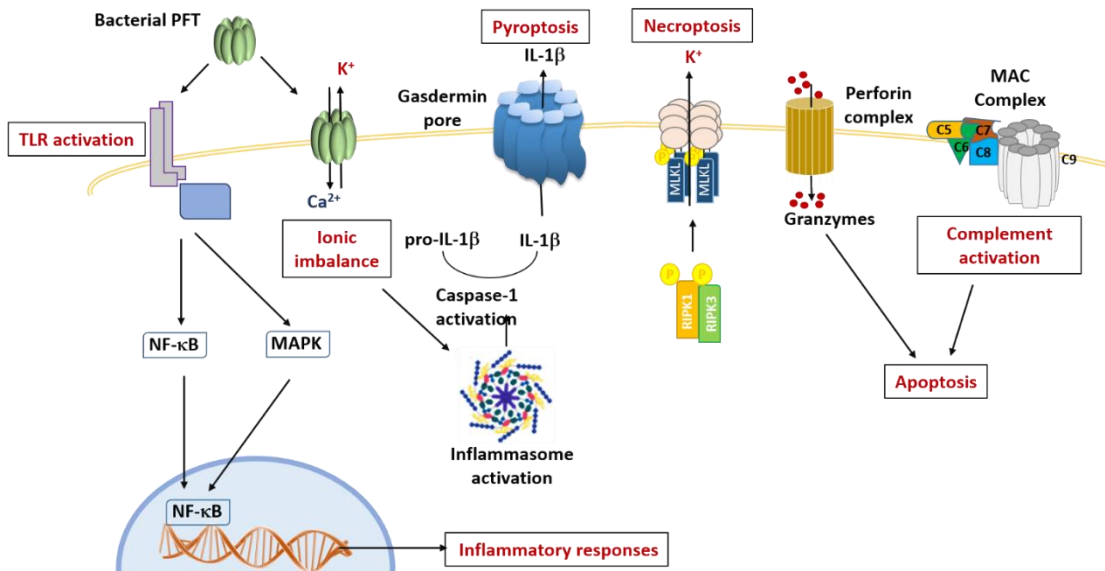


**Illustration 3. Distinct immunological and cell death responses triggered by pore-forming toxins.** PFTs upon recognition as PAMPs by the PRRs (TLRs) of immune cells, which leads to their activation and triggers downstream signaling which may lead to inflammatory responses in the form of cytokines production. Pore-forming activity of PFTs accompany ionic imbalance which triggers inflammasome activation which leads to the inflammatory cell death, pyroptosis. Certain PFTs may trigger MLKL-mediated plasma membrane permeabilization, causing necroptosis. Some immune cells secrete perforins that form large pores on infected cells and facilitate the entry of granzymes and killing such cells by triggering apoptosis. PFTs can also activate the complement system in the host cells. The MAC complex of the activated complement system can kill the bacterial cells by forming pores on their membranes and may trigger apoptosis in the host cells.

PFTs are also perceived to modulate the adaptive immune responses in the target host. Upon immunization with purified PFTs, antigen-specific B-lymphocytes activation

and antibody generation have been observed, suggesting their impact on the adaptive immune system. Dendritic cells are considered as the link between the innate and adaptive arms of the immune system. Therefore, the activation of dendritic cells by the PFTs could potentially modulate the T-cells responses [75]. Besides, PFTs can efficiently suppress the host's adaptive immune system, aiding pathogen evasion from the host defense mechanisms. For instance, listeriolysin O inhibits antigen presentation, leaving the T-cells unresponsive [76]. Also, downregulation of the inflammatory responses by pneumolysin upon recognition by mannose receptor C type 1 on macrophages or dendritic cells suppresses the T-cell activation [77].

**e. PFT-induced death signaling in the host cells:** When the PFT assaults become overwhelming for the host cell, and the damage crosses the threshold leaving no scope for repair, the cell death becomes inevitable (Illustration 2). The cross-talk between different damage, repair, survival and defense pathways with the signaling of cell death pathways eventually decides the fate of the cell in terms of survival or death (Illustration 2 and 3). Various reports suggest different cell death mechanisms in response to different PFTs (Table 2).

**Table 2. Cell death responses by PFTs**

<i>PFT</i>	<i>Cell death pathway(s)</i>	<i>Target cells</i>	<i>Characteristics</i>	<i>Ref.</i>
Pneumolysin (PLY)	Apoptosis	Microglial cells, rat cochlear cells, dendritic cells, neuronal cells	Induces high calcium influx , mitochondrial damage and release of AIF in microglial cells, lysosomal permeabilization associated apoptosis in macrophages, Mitochondrial translocation of toxin inducing its dysfunctioning and release of AIF in neuronal cells	[72, 78]
	Necroptosis	Respiratory epithelium and alveolar macrophages	Calcium and potassium imbalance-mediated necroptosis	

	Pyroptosis	Microglial cells	Activation of caspase-1, production of IL-1 $\alpha$ , IL-1 $\beta$ , IL-18	
$\alpha$ -hemolysin or $\alpha$ -toxin (Hla)	Apoptosis	Jurkat T cells, B cells, mononuclear cells, endothelial cells, Bladder epithelial cells	Mitochondrial pathway in T-cells, death receptor and ligands - mediated in mononuclear cells	[79-82]
	Necroptosis	T-cells and macrophages	MLKL pore-formation IL-	
	Pyroptosis	Monocytes, macrophages, microglial cells, keratinocytes	1 $\beta$ secretion, inflammasome activation	
	Autophagy	Epithelial and endothelial cells	Autophagy induction imparts tolerance against infection	
Listeriolysin O (LLO)	Apoptosis	Primary immune cells such as BMDCs, BMMs, primary T- cells and cell lines CB1 murine dendritic cell line and A5, T- cell hybridoma	Granzymes-mediated rapid T-cell apoptosis	[83, 84]
	Pyroptosis	Peripheral blood mononuclear cells (PBMCs)	NLRP3 inflammasome activation and IL-1 $\beta$ secretion	
Hemolysin A (HlyA)	Apoptosis	Epithelial and endothelial cells, Neutrophils	Outer-membrane vesicles- mediated translocation to mitochondria, caspase-3,-9 and PARP-mediated apoptosis	[74, 85]
	Pyroptosis	Macrophages, Bladder epithelial cells	NLRP3 inflammasome activation, IL-1 $\beta$ secretion and Caspase-1/-4-	

			dependent inflammatory cell death	
Panton-Valentine Leukocidin (PVL)	Apoptosis Necrosis	Neutrophils, monocytes, macrophages, keratinocytes	Activation of caspase-9, -3, chromatin condensation, DNA fragmentation, mitochondrial localization of the toxin	[40, 67, 86]
<i>Vibrio cholerae</i> Cytolysin (VCC)	Apoptosis Autophagy	Intestinal epithelial cells Intestinal epithelial cells	Caspase-dependent, DNA fragmentation, mitochondrial translocation of the toxin, mitochondrial damage, pore-formation independent cell death Protective role of autophagy against infection	[22, 87]
Vacuolating toxin A (VacA)	Apoptosis Autophagy	Epithelial cells Gastric epithelial cells	Mitochondrial translocation of toxin, MOMP results in apoptosis ER stress-mediated autophagic cell death	[56, 88]

The form of cell death triggered by a PFT may depend on the target cell type and also the toxin's dose and incubation time. Certain PFTs have been observed to induce apoptosis at sub-lytic concentrations, while higher doses resulted in the necrotic alterations [45, 81]. Extensive pore-formation at high concentrations of PFT leads to rapid damage and rupture of plasma membrane resulting into oncosis or necrosis [89]. Apparently, the participation of pore-forming activity of a PFT has been rendered essential to trigger cell death responses. In contrast, apoptotic cell death independent of the pore-formation activity has been documented recently for *Vibrio cholerae* cytolysin in human intestinal epithelial cells [22]. For certain instances, the mechanistic cues like calcium influx and activation of stress kinases may also contribute as the deciding factors for the type of cell death [25, 63]. As the central theme of the study, various types of general cell death processes have been discussed further in detail.

### **1.3. Cell death**

Cell death is a process of irreversible loss of vital functions and integrity of a cell. It is an inevitable process that is crucial for homeostasis of the organisms under both physiological (organismal development or tissue turnover) and pathological scenarios (defense mechanisms) [90]. The dysregulation of this process results in several pathologies. Earlier, cell death was considered a phenomenon that either have specific sets of cellular effectors or is executed in a regulated and programmed manner or the unregulated swelling and rupturing of the cell following a severe insult. The former type of cell death was termed 'apoptosis,' and the latter was termed 'necrosis' [91]. Apoptosis and programmed cell death (PCD) were used interchangeably. Later, PCD was recognised as a much broader term inclusive of various forms of cell death executed in a programmed manner. Interestingly, different PCD pathways can operate in a cell at the same time. Multiple forms of cell death are largely interpreted and defined by the morphological, biological and functional perspectives like the display of distinct morphological features, involvement of specific organelle functions and specific executioners (proteins and enzymes) and the underlying molecular mechanism [90, 92]. Based on the molecular mechanisms of the cell death pathways, the Nomenclature Committee on Cell Death (2018) proposed the universal classification of different forms of cell death [90]. Following are the distinct and established forms of cell death:

#### **1.3.1. Apoptosis**

The term 'Apoptosis' was first introduced and described in a report published in 1972 by Kerr, Wyllie and Currie, as a morphologically distinct form of cell death [93]. It is defined as the physiologically controlled suicide of a cell in response to numerous perturbations involving embryonic development, immunological regulations, or purging diseased or infected cells. External perturbations like irradiation, heat, chemicals, etc., can also trigger apoptosis [91]. Cells undergoing apoptosis display morphological alterations like shrinkage of cytoplasm, pyknosis (chromatin condensation), karyorrhexis (nuclear fragmentation), plasma membrane blebbing and budding of apoptotic bodies [94]. These apoptotic bodies are engulfed and disposed of by the phagocytic cells, a process technically termed as efferocytosis [95].

The critical players of the apoptotic mode of cell death are deemed to be the cytosolic proteases called 'caspases', conserved across all metazoans, including *Caenorhabditis elegans*, *Drosophila*, mouse and humans [96, 97]. Caspases are cysteine-dependent proteases that catalytically act upon the aspartate residues in their specific substrates. These proteases are observed in both immune and non-immune cells. Caspases are constitutively expressed in the cells' cytoplasm as zymogens (enzymatically inactive) called procaspases. Activation of single chain zymogens involves the processing of the pro-domain part, followed by an autoproteolytic cleavage to remove the inter-linker between the large and small subunit of the caspases. The activation of caspases is followed by their dimerization or cleavage required for their catalytic activity. Based on their involvement in the type of cell death, caspases have been categorized as either apoptotic caspases or inflammatory caspases [96].

**Apoptotic caspases:** These caspases are involved in the initiation and execution of both the intrinsic and extrinsic arms of apoptosis and based on their order of involvement, caspases are sub-categorized as initiator and effector/ executioner caspases. Caspase-2, -8, -9 and -10 are the initiator caspases which are activated by the apoptotic stimuli and, in turn, activate effector caspases [98]. Caspase-3, -6 and -7 are the effector caspases which upon their activation by the initiator caspases, cleaves and activate multiple other cellular proteins involved in apoptosis [98]. The key substrates of caspases in apoptotic pathway are the caspase-activated DNases (CADs) [99]. Executioner caspases degrades the inhibitory domain of CADs (iCAD) rendering them free to dimerize and translocate to the nucleus where these proteases cleave the DNA into small oligonucleosomal units. Poly(ADP-ribose) Polymerase (PARP) is another substrate cleaved by the executioner caspases [99].

**Inflammatory caspases:** Caspase-1, -4, -5, -11 and -12 are enlisted as the inflammatory caspases [96]. These caspases are activated by the multimeric protein assembly called inflammasomes. Activation of inflammatory caspases triggers a lytic and inflammatory form of cell death termed as pyroptosis [96].

**Mechanism of Apoptosis:** Depending on the mode of initiation, specific adaptor molecules and the initiator caspases involved, apoptosis is classified into two pathways: the intrinsic and the extrinsic pathway.

**Intrinsic pathway:** This pathway is mainly executed in the cells with compromised mitochondrial integrity in response to apoptotic stimuli like DNA damage, Reactive Oxygen Species (ROS) overload, ER stress, mitotic defects, etc. Such stress stimuli signal the pro-apoptotic molecules like Bax (Bcl-2 associated X) or Bak (Bcl-2 antagonist/killer), which translocate to the mitochondria and subsequently results in mitochondrial outer membrane permeabilization (MOMP) [90]. The mitochondrial disintegrity, accompanied by loss of mitochondrial membrane potential, plays a central role in different forms of cell death, including intrinsic apoptosis [100]. The loss of mitochondrial integrity leads to the release of multiple mitochondrial factors responsible for the regulation and execution of different types of cell death. During intrinsic apoptosis, MOMP causes the cytosolic release of apoptogenic factors normally present in the mitochondrial inter-membrane space like cytochrome c, Smac/Diablo, Omi/ Htra2 [101-103].

Upon its release in the cytoplasm, cytochrome c serves as a cofactor that interacts with Apaf-1 (apoptosis protease activating factor-1) and exposes its nucleotide-binding site. The ATP-bound heptameric assembly of Apaf-1 undergoes further conformational changes leading to the exposure of its CARD domain that interacts with the pro-domain (or the CARD domain) of procaspase-9 [101]. This heptameric adaptor protein complex constituted of cytochrome c, Apaf-1, dATP and procaspase-9 is termed as apoptosome [104]. The activation of initiator caspase-9 by the apoptosome in turn leads to the activation of downstream effector caspases (caspase-3, -7 and -6).

Other mitochondrial factors like Smac/Diablo or Omi/Htra2 promote the apoptotic pathway by impeding the inhibitors of apoptosis proteins (IAPs) through their proteasomal degradation, that otherwise hamper the activity of caspases [102, 103].

**Extrinsic pathway:** This arm of apoptosis is triggered mainly by the interaction of a specific extracellular ligand activating its specific death receptors [90]. The well-established members of the death receptor family and their ligands involve Tumor necrosis factor receptor-1 (TNFR-1)-TNF- $\alpha$ , Fas (CD95/APO-1)- Fas L (CD95 L), TNF-related apoptosis-inducing ligand receptor-1 (TRAIL-1)- TRAIL [105]. Activation of death receptors by cognate death ligands results in receptor homo-trimerization, followed by the recruitment of adaptor molecules like FADD (Fas-associated death domain) or TRADD (TNF receptor-associated death domain) at the cytoplasmic death domain of the

death receptors. Adaptor molecules, in turn, associate with procaspase-8 forming a multimeric platform termed DISC or death-inducing signaling complex. This complex promotes proximity-mediated autoproteolytic activation of caspase-8, in turn activating effector caspases -3, -7 and -6 [92].

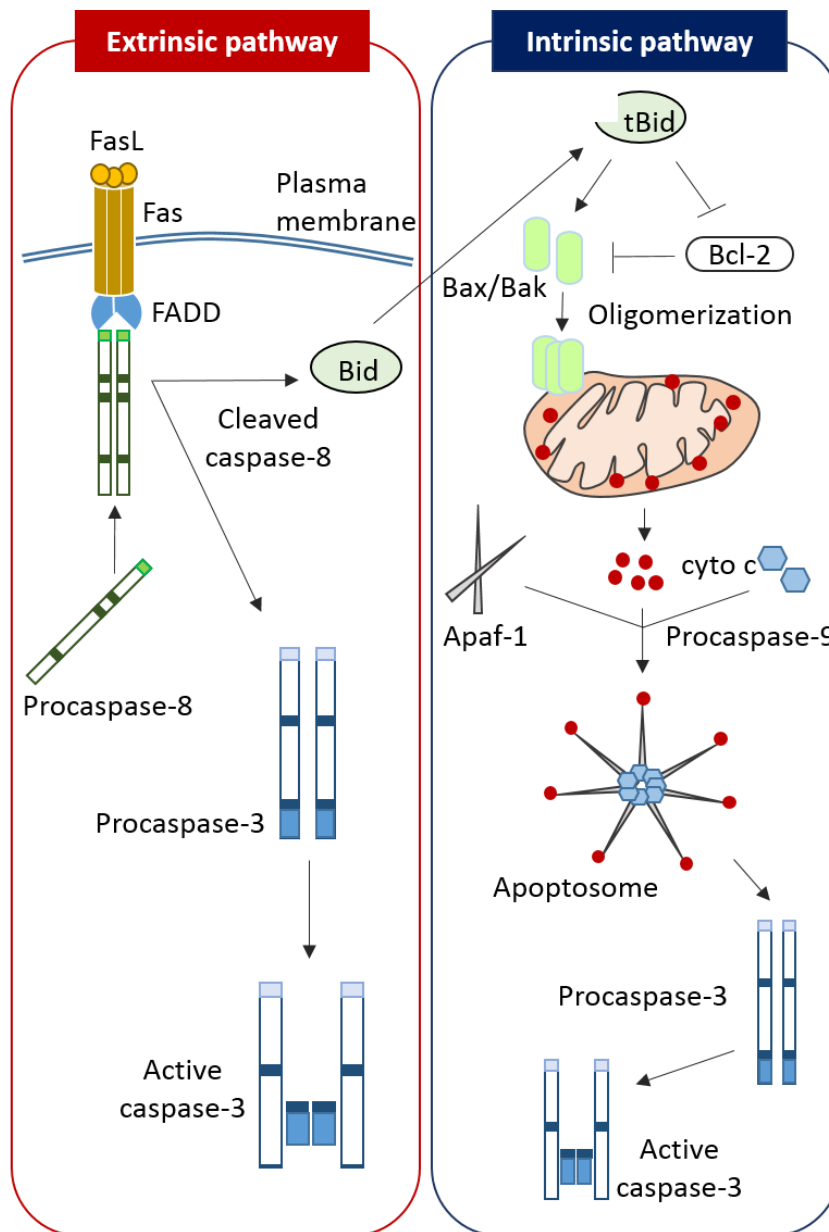


**Illustration 4. Schematic representation of extrinsic and intrinsic pathways of apoptosis.** During extrinsic pathway (left panel), the death receptors (Fas) at the plasma membrane interacts with a death ligand (FasL), inducing the receptor trimerization. The adaptor molecules (FADD) are recruited at the cytoplasmic death domain of the death

receptor which further recruits and activates procaspase-8. The active caspase-8 causes the activation of downstream effector caspase-3 or it can cause Bid cleavage, which may account for MOMP. The intrinsic arm of apoptosis (right panel) involves MOMP induction by pro-apoptotic molecules Bax/Bak resulting in cytochrome c release through the mitochondria. Cytochrome c interacts with Apaf-1 in the cytosol which leads to the formation of apoptosome that recruits procaspase-9 for its activation. The active caspase-9 downstream to it, mediates caspase-3 activation.

**Bridging the gap between extrinsic and intrinsic pathway:** Studies highlight an intricate connection between both the apoptotic pathways. Active caspase-8 from the extrinsic pathway cleaves Bcl-2 homology 3 (BH3)-interacting domain (Bid), a death agonist converting it into its truncated form (tBid). tBid may activate the pro-apoptotic molecules, Bak and Bax, causing MOMP and eventually leading to the intrinsic apoptosis pathway [90, 106].

**1.3.2. MPT-driven necrosis:** MPT refers to Mitochondrial (membrane) permeability transition that is triggered in response to perturbations like oxidative stress or cytosolic calcium overload. Such stimuli cause the abrupt increase in the permeability of the inner mitochondrial membrane to small solute molecules, resulting in subsequent dissipation of mitochondrial membrane potential and complete breakdown of the mitochondria, eventually leading to cell death [107, 108]. This form of cell death generally exhibits morphological features of necrosis. The molecular model proposed for MPT-driven necrosis suggests that the prolonged and irreversible opening of a multiprotein complex that forms a pore, MPTP (mitochondrial permeability transition pore), at the juxtaposition of outer and inner mitochondrial membrane triggers the implications mentioned above [108]. However, under certain conditions where mitochondrial membrane permeability transition (MMPT) is transient and not so prolonged, apoptosis or parthanatos like cell death can also operate [108]. The exact composition, mechanism and regulation of MPTP are still debatable. Reports have validated the *in vivo* requirement of only cyclophilin D (CypD) as an essential component for MPT induction [109]. Apart from cypD, other putative components of MPTP are adenine-nucleotide

translocator (ANT) and voltage-dependent anion channel (VDAC), F<sub>1</sub>F<sub>0</sub>-ATPase-c subunit, inorganic phosphate carrier (PHC) and paraplegin matrix AAA peptidase subunit (SPG7). However, the role of these components is reported to be dispensable for MPTP. Additionally, multiple physical and functional activators of MPTP have been identified such as MOMP regulators of apoptosis (Bax, Bak, Bid, Bcl-2, and Bcl-xl), Drp1 and p53 [90].

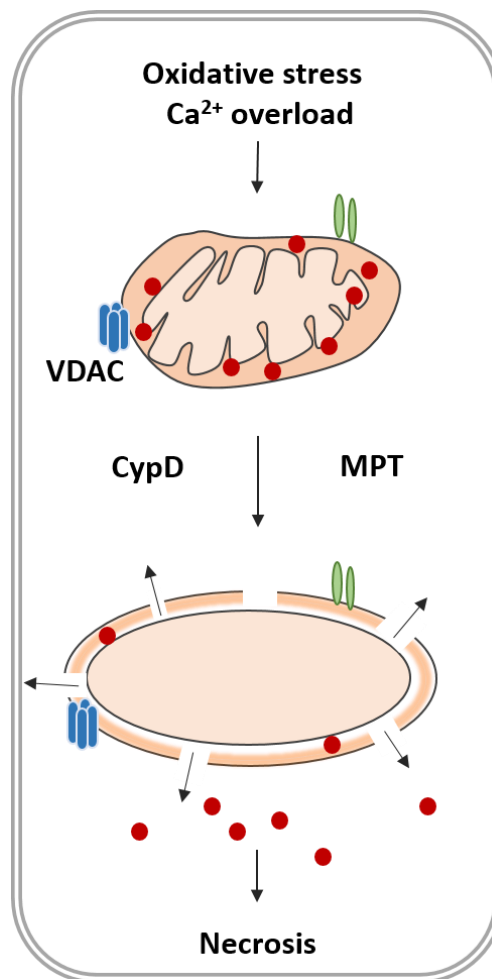


**Illustration 5. Simplified representation of MPT-driven necrosis.** Prolonged oxidative stress and calcium overload conditions results into Cyp D-mediated sensitization of MPTP. This tends to continuous opening of MPTP and increased permeability of both outer and inner mitochondrial membranes, resulting into necrosis.

**1.3.3. Necroptosis:** Necroptosis is a type of cell death that manifests necrotic morphological features mediated by either ligation of death receptors involved in apoptosis or endogenous cues such as viral nucleic acids. Various studies have now established that necroptosis is a basic form of cell death that takes part in adaptive cellular functions, development, and maintenance of homeostasis. Necroptosis is an inflammatory mode of cell death culminating into plasma membrane permeabilization [110]. At the molecular level, necroptosis is triggered by the activation of cellular receptors like death receptors (TNF or Fas) or other pattern recognition receptors (PRRs) like Toll-like receptors (TLR4 or TLR3). In the absence of caspase-8 activation, downstream to death receptors RIPK1 (receptor-interacting protein kinase 1) is activated, which further recruits and phosphorylates RIPK3 in a complex named, ripoptosome. The RIPK1 and RIPK3 interact through a common motif RIP homotypic interaction motif (RHIM). The RIPK1/RIPK3 complex, in turn, recruits and phosphorylates MLKL (mixed-lineage kinase domain-like) protein, thus, forming the complex called necrosome. The formation of necrosome is considered critical for the execution of necroptosis, followed by plasma membrane permeabilization by phosphorylated MLKL. In certain instances, RIPK1 is found dispensable and could be inhibitory for the activation of necroptosis [110, 111].

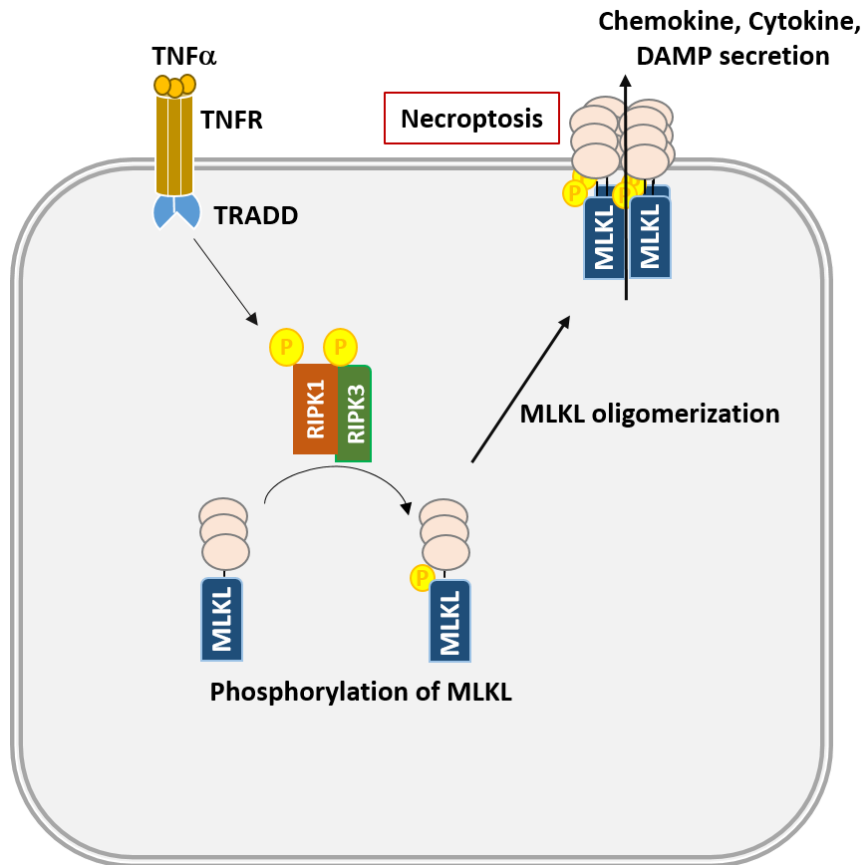


**Illustration 6. Schematic representation of necroptosis pathway.** The molecular mechanisms underlying necroptosis can be triggered upon the ligation of death receptors in response to the extracellular signals or due to some endogenous cues. RIPK1 activation leads to its interaction with RIPK3 and its phosphorylation that further recruits MLKL in a complex called necrosome. MLKL phosphorylation results into its oligomerization at the plasma membrane surface leading to its permeabilization and release of inflammatory factors.

**1.3.4. Pyroptosis:** Pyroptosis is a highly inflammatory mode of cell death triggered in response to the PAMPs and DAMPs by the innate immune system. The pyroptotic stimuli sensitize and activate the inflammasome sensors to form a multimeric protein complex called inflammasomes that prevent pathogen spread by activating molecules resulting in cell lysis [112]. The inflammasome complex is primarily constituted of three components: (i) NLRs or the nucleotide oligomerization domain (NOD)-like receptors, (ii) the adapter apoptosis-associated speck-like protein with a CARD domain (ASC), (iii) pro-caspase-1 [36, 96]. In the canonical pathway of pyroptosis, the formation of this

assembly releases the active form of caspase-1, which processes the pyroptotic executioner Gasdermin D into N-terminal and C-terminal fragments. The N-terminal component of Gasdermin D perforates the plasma membrane by forming oligomeric pores, leading to cell swelling and subsequent cell lysis [32]. Moreover, caspase-1 cleaves the zymogens of IL-1 $\beta$  and IL-18, facilitating their release through Gasdermin D pores. The non-canonical pyroptosis pathway is induced by the direct interaction of LPS with CARD domain of caspase-4, -5 (or caspase-11, mouse orthologue) triggering the non-canonical activation of inflammasome [113].

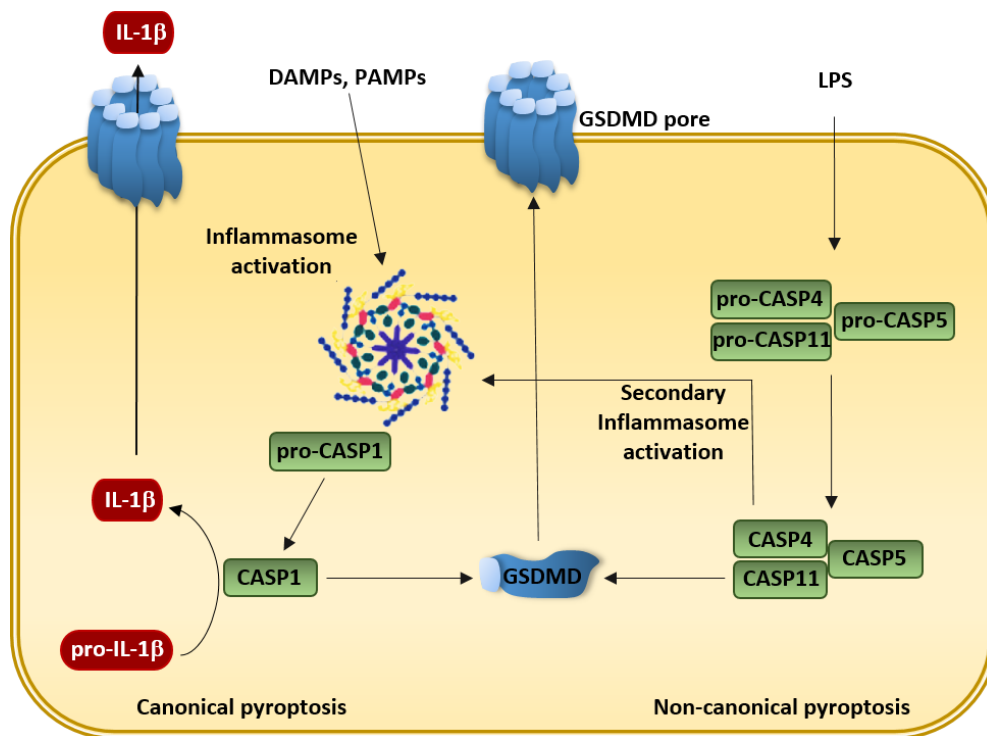


**Illustration 7. Schematic representation of canonical and non-canonical pyroptosis pathways.** In canonical pyroptosis (right), DAMPs or PAMPs mediate the recruitment of a multimeric assembly, NLRP3 inflammasome that activates caspase-1. In the non-canonical pyroptosis (left), caspase-4, -5, -11 are activated by LPS which in turn activates the inflammasome. Both these pathways lead to the cleavage and activation of a common executioner protein, Gasdermin D (GSDMD). The cleaved N-terminal domain of GSDMD forms pore on the plasma membrane and facilitates the release of mature IL-1 $\beta$  and IL-18.

**1.3.5. Ferroptosis:** Ferroptosis is an iron-dependent form of regulated cell death, transpired by severe lipid peroxides accumulation due to oxidative stress and iron availability [90]. Ferroptosis serves essential regulatory roles during the occurrence and development of multiple diseases. Ferroptosis manifests morphological features distinct from typical apoptosis or necrosis, like mitochondrial shrinkage with a reduction in cristae and increased membrane density [114]. At the molecular level, a glutathione-dependent antioxidant enzyme, glutathione peroxidase (GPX4), is crucial for the regulation of ferroptosis. Under physiological conditions, GPX4 catalyses the lipid hydroperoxides to lipid alcohols, therefore, limiting the production of lipid peroxides. However, during stress-induced perturbations, inhibition of GPX4 results in increased lipid peroxidation by utilizing the hydroxyl radicals and accumulated intracellular labile iron [115]. Various reports have probed multiple factors and pathways directly or indirectly associated with GPX4 that may ultimately trigger ferroptosis and that iron chelators and lipophilic antioxidants can inhibit it [108, 114].

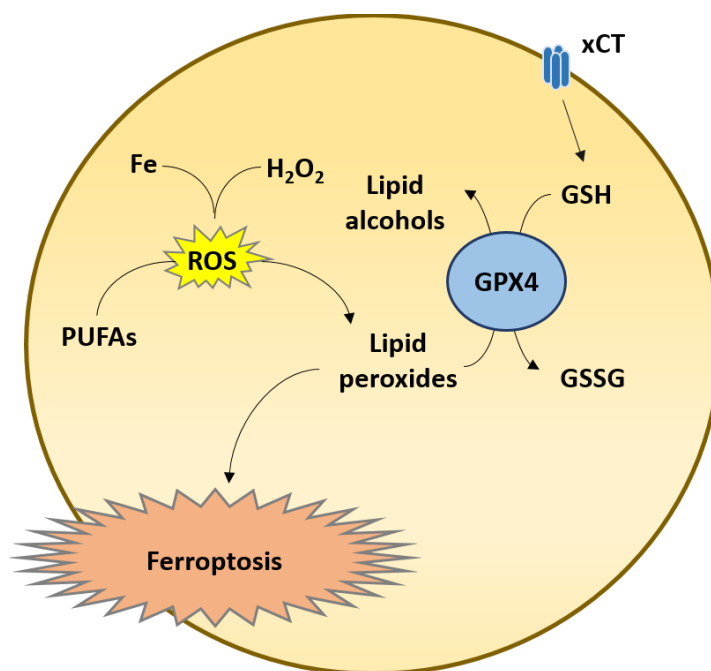


**Illustration 8. Diagrammatic representation of molecular mechanism of ferroptosis .**

Under physiological conditions, ferroptosis remains inhibited by GPX4 by reducing lipid peroxides and ROS by utilising glutathione (GSH). Stress-stimulated inhibition of GPX4

activity and iron and ROS accumulation results into increased lipid peroxidation leading to ferroptosis.

**1.3.6. Parthanatos:** Parthanatos is a form of cell death exhibited due to hyperactivation of a DNA repair enzyme Poly-(ADP-ribose) Polymerase 1 or PARP1 in response to excessive DNA damage by prolonged exposure to alkylating agents, hypoxia, oxidative stress etc. [90, 116]. Morphological changes observed during parthanatos are similar to that in necrosis or apoptosis such as loss of membrane integrity, loss of mitochondrial potential, nuclear shrinkage and chromatin condensation DNA fragmentation (15-50 kb). The hyperactivation of PARP1 utilises  $\text{NAD}^+$  and ATP pools of the cells to form poly-(ADP-ribose) or PAR polymers. Consequently, the over-accumulation of PAR polymers and their translocation from the nucleus to mitochondria serves as a death signal to induce mitochondrial outer membrane permeabilization (MOMP), disruption of mitochondrial membrane potential, and the translocation of a mitochondrial factor, Apoptosis-inducing factor or AIF, to the nucleus. It has been shown that PAR polymers bind to AIF in order to facilitate its release through the mitochondria, where it brings about chromatin condensation and large-scale nuclear fragmentation [116, 117]. Also, reports suggest the involvement of another critical factor for parthanatos i.e. Macrophage migration inhibitory factor (MIF), also called parthanatos-associated AIF nuclease (PAAN). AIF interaction with MIF promotes their translocation to the nucleus, where they contribute in catalysing DNA fragmentation [90, 116].

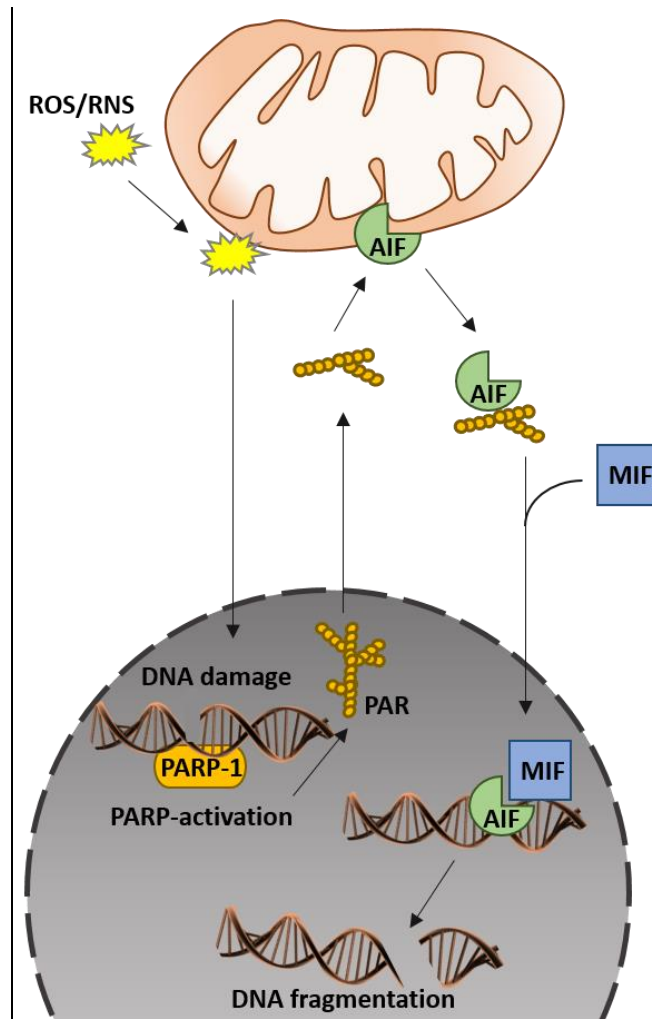


**Illustration 9. Schematic representation of parthanatos cell death pathway.** Peroxynitrite ( $\text{ONOO}^-$ ) along with excess ROS species causes DNA damage, leading to PARP-1 activation. Hyperactivation of PARP-1 leads to excessive PAR polymer formation and accumulation in nucleus. Consequently, PAR polymers exit the nucleus and facilitates the release of AIF from the mitochondria. AIF interacts with MIF in the cytosol and further, enter the nucleus leading to large-scale DNA fragmentation and subsequent cell death.

**1.3.7. Autophagy:** Autophagy is a cellular mechanism of self-eating, triggered to maintain cell's energy requirements by recycling the damaged organelles and protein aggregates. Therefore, autophagy under tightly regulated conditions is generally considered a cell survival mechanism with cytoprotective roles under nutrient deprivation, stressed or diseased conditions [118, 119]. However, autophagic molecular

machinery may promote cell death under specific pathophysiological or developmental settings [120, 121]. Autophagy starts with the formation of phagophores (vesicle nucleation) that engulf the damaged organelles or components. At the molecular level, autophagy involves a number of autophagy-related (Atg) proteins. During vesicle nucleation step, ULK/Atg1 complex recruits a series of Atg proteins to the isolated membrane. Next, vesicle elongation and completion take place, where a phagophore with loaded cargo turns into an autophagosome that requires the conjugation of Atg5 to Atg12 and LC3-I conversion to LC3-II. Next, the mature autophagosomes fuse with the lysosomes forming an autophagolysosome required for the degradation of the damaged contents by the lysosomal proteases [118, 120].

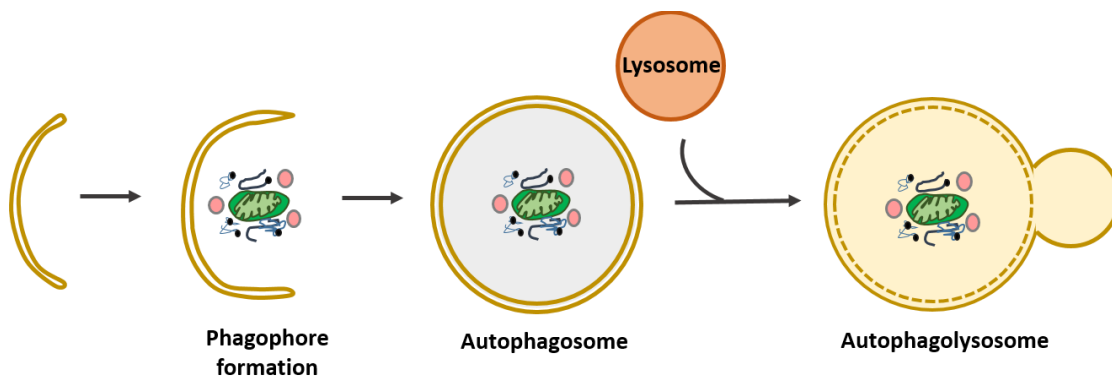


**Illustration 10. Schematic representing autophagy pathway.** Autophagy starts with vesicle nucleation or phagophore formation, where the isolated membranes engulf the damaged cellular cargo. The vesicle then grows and completes itself around the engulfed material turning into autophagosome. The mature autophagosome then fuses with lysosome, forming an autophagolysosome where the lysosomal hydrolytic enzymes degrade the cargo.

#### **1.4. *Vibrio parahaemolyticus***

*Vibrio parahaemolyticus* is a Gram-negative bacterium and a notable *Vibrio* species belonging to the family *Vibrionaceae*. It is a comma-shaped bacterium with a single polar flagellum for swimming and lateral flagella for swarming. *V. parahaemolyticus* is a halophilic bacterium that inhabits marine, estuarine and coastal environments [122]. This bacterium was first identified as a seafood-borne human pathogen by Tsunesaburo Fujino in the 1950s and held responsible for a severe food-poisoning outbreak in Japan. Ever since then, this bacterium has accounted for several cases of seafood-associated gastroenteritis globally [123]. *V. parahaemolyticus* strains are primarily classified into serotypes based on the antigenic properties of somatic (O) and capsular (K) antigens produced under different environmental conditions. Among most clinical isolates of *V. parahaemolyticus*, O3:K6 is the most predominant serotype [124].

##### **1.4.1. Pathophysiology**

*V. parahaemolyticus* is a causative agent of acute gastroenteritis in humans due to the consumption of raw or undercooked seafood [125]. The clinical manifestations include typical gastroenteritis-like symptoms such as abdominal cramping, nausea, vomiting, and fever with occasional episodes of bloody diarrhea. Although rare, this bacterium may lead to wound infections and septicemia, which could be life-threatening for the immunocompromised individuals [125].

##### **1.4.2. Pathogenicity**

The pathogenicity of *V. parahaemolyticus* is attributed to different virulence factors like adhesins, toxins like Thermostable Direct Hemolysin (TDH), TDH-Related Hemolysin (TRH) and Thermolabile Hemolysin (TLH), type III secretion system (T3SS1 and T3SS2), type VI secretion system, and iron acquisition system. Additionally, the bacterium harbors lipopolysaccharide, proteases and outer membrane proteins as virulence factors [126]. All these virulence arsenals collectively facilitate the pathogenesis of the bacterium and aid the process of colonization in human hosts and its survival in different environmental conditions [126]. Contributions of some essential and

established virulence factors in the pathogenesis process of *V. parahaemolyticus* are described as follows:

#### **a. Adhesins**

Adhesion of the bacteria to the host cells marks the initiation of the infection process. Multivalent Adhesion Molecule 7 or MAM7 is an adhesion protein widely conserved among Gram-negative bacteria [127]. It possesses an N-terminal domain required for its localization and anchoring in the outer membrane of the bacteria. It also contains mammalian cell entry (mce) domain that allows it to interact with fibronectin and membrane phosphatidic acid. Due to its constitutive expression in the bacteria, MAM7 enables the pathogen to contact the host cells immediately, thereon facilitating other host-pathogen interactions [128]. Other factors established for the adhesion process of *V. parahaemolyticus* are hemagglutinin, enolase and T6SS2 [126]. Mannose-sensitive hemagglutinin (MSHA) pilus exhibits affinity toward glycans which may serve as the receptors for the adhesion and, thus, facilitate efficient colonization of bacteria in the gastrointestinal tract. Enolase is a plasminogen-binding protein present as surface exposed protein on *V. parahaemolyticus*. Enolase has been reported to promote host-pathogen interaction, as observed in Hep-2 cells. T6SS2, via its effectors i.e. Hcp family proteins, help in the adhesion of this bacterium to the host intestinal epithelial cells.

#### **b. Toxins**

*V. parahaemolyticus* produces three toxins, namely, thermostable direct hemolysin (TDH), TDH-related hemolysin (TRH) and thermolabile hemolysin (TLH), which are encoded by *tdh*, *trh* and *tlh* genes, respectively [122]. Epidemiological data suggests that *tdh* and *trh* genes are found in most of the clinical isolates, while their occurrence in the environmental strains is sporadic. TDH is considered to be a critical virulence factor for the pathogenesis of this bacterium and an important factor to distinguish between the pathogenic and non-pathogenic strains. It has been characterized as a pore-forming toxin that forms pores on the erythrocyte membrane, thereby causing colloid-osmotic lysis of these cells. Other than its hemolytic activity, TDH has also been reported to exhibit enterotoxicity, cardiotoxicity and cytotoxicity [129]. At gene level, *trh* and *tdh* share 54.8-68.8% homology [130]. Like TDH, TRH contributes similarly to the pathogenesis of *V. parahaemolyticus*. TLH is characterised as a phospholipase that absolutely requires lecithin for its hemolytic activity. *tlh* is detected in both clinical and environmental

strains. The expression of *tlh* increases in the gut, however, its exact function remains unclear [126].

### **c. Type III secretion systems (T3SS)**

T3SS is a conserved bacterial virulence factor that injects the bacterial effector proteins directly into the host without any exposure to the external environment [126]. These effectors interfere with host's functioning like innate immune signaling, actin cytoskeleton or autophagy, to exert their virulence. T3SS is a syringe-like transmembrane device that is constituted of nearly 30 proteins categorised as: structural proteins, translocators, effectors and molecular chaperones. *V. parahaemolyticus* has two sets of T3SS: T3SS1 on chromosome 1 and T3SS2 on chromosome 2 [122].

T3SS1 is present in all clinical or environmental isolates of *V. parahaemolyticus* and mainly responsible for the biofilm formation, motility and cytotoxicity of the bacterium. Four major effector proteins are secreted by T3SS1: VopQ, VopS, VPA0450 and VopR (VP1683) [122]. VopQ imparts T3SS1-mediated eukaryotic cytotoxicity to the bacterium. VopQ causes lysosomal cleavage and autophagic vesicle formation that subsequently leads to host cell autophagy and cytotoxicity. VopQ is also reported to induce the production of IL-8 via the p38-mediated MAPK signaling pathway. VopS causes post-translational modifications (AMPylation) of Rho GTPase, preventing its binding and activation of downstream effectors that regulate the actin cytoskeleton. Therefore, VopS ultimately leads to the collapse of the actin cytoskeleton causing cell rounding and shrinkage. VPA0450 acts as a phosphatase that disrupts cellular integrity by detaching the plasma membrane from the actin cytoskeleton, thus, promotes membrane blebbing. VopR binds to phosphoinositide on the host cell membrane and acts as molecular chaperone for T3SS effectors in the host cell.

T3SS2 is encoded by the pathogenicity island (PAI) present on the chromosome 2 and is exclusive for the clinical isolates of *V. parahaemolyticus*. As observed in the rabbit ileal loop model, it is responsible for cytotoxicity of the colon epithelial cells and enterotoxicity in the host [126]. There are seven T3SS2 effectors (VopA, VopZ, VopT, VopC, VopV, VopL, and VPA1380) that have been characterized [122, 126]. VopA is an acetyltransferase that blocks MAPK signaling by acetylating Ser/Thr residues of the kinases, causing inhibition of cell growth and hence, cell death. Similarly, VopZ blocks MAPK signaling and also disrupts NF- $\kappa$ B signaling. VopT is an ADP ribosyltransferase

of Ras GTPase, responsible for T3SS2-mediated cell cytotoxicity. VopC is a deamidase that modulates the actin cytoskeleton and facilitates the invasion of the bacterium into host cells. VopV is a crucial effector that can bind both actin and filamin and lead to the accumulation of stress fibers, resulting in the host's enterotoxicity. However, the exact molecular mechanism of this enterotoxicity remains unclear. VopL causes actin filament nucleation and promotes the bacterial survival in the host by neutralizing reactive oxygen species (ROS). VPA1380 has a cysteine protease domain similar to large bacterial toxins and requires inositol hexose phosphate for its activation and cytotoxic function.

#### **d. Type VI secretion system (T6SS)**

T6SS is another secretory device which is functionally similar to T3SS. *V. parahaemolyticus* harbors two sets of it: T6SS1 and T6SS2 [131]. T6SS1 activity is favored under warm conditions and predominantly expressed in clinical strains. While T6SS2 expression is observed in both clinical and environmental strains and is most active under low-salt conditions. Both T6SSs play role in adhesion of the bacterium to the host cells and take part in intracellular trafficking and vesicular transport [122].

#### **e. Iron acquisition system**

Iron is considered indispensable for the growth and metabolism of pathogenic bacteria. These bacteria can acquire iron from the host mainly through red blood cells, lactoferrin and transferrin [131]. *V. parahaemolyticus* employs iron uptake system that either involves exotoxins to lyse blood cells and release haemoglobin or siderophores that can chelate iron from complexes [132]. Vibrioferrin is the iron carrier produced by *V. parahaemolyticus* that chelates iron from the host and transfers it to the bacterial cell for assimilation. The bacterial cell has vibrioferrin receptors like PvuA1 and PvuA2 on the outer membrane which in turn transfer the iron-vibrioferrin across inner membrane through ABC transporters in the inner membrane like PvuBCDE [126].

## 1.5. Thermostable Direct Hemolysin

Thermostable Direct Hemolysin or TDH is the major protein toxin secreted by *V. parahaemolyticus* [17, 123]. Most clinical strains of *V. parahaemolyticus* exhibited a hemolysis ring pattern on high-salt containing Wagatsuma blood agar called the Kanagawa phenomenon [133]. It was deduced that this phenomenon was imparted by the hemolytic activity of TDH [134]. Accordingly, TDH is recognized as the critical virulence factor of the pandemic strains of *V. parahaemolyticus*. Natural or non-clinical isolates were found negative for this phenomenon. However, the gene encoding TDH is also present in some of the non-clinical isolates of this bacterium [135]. TDH-related proteins are also documented in other *Vibrio* species, such as *V. cholerae*, *V. mimicus*, and *V. hollisae* [135]. Owing to its membrane-damaging activity, TDH has been characterized as a pore-forming toxin. The pore-formation by TDH allows unregulated flow of water and ions through the cell membrane [136]. The alterations in ion flux and TDH-associated cytotoxicity that destroys the intestinal epithelial cells, have been correlated with the bloody mucous diarrhoea observed during *V. parahaemolyticus* infection [137].

### 1.5.1. Regulation and secretion of TDH by *V. parahaemolyticus*

*V. parahaemolyticus* harbors two sets of *tdh* gene on its chromosomes: *tdh1* and *tdh2*. *tdh2* exhibits 97.2% homology with *tdh1* and is primarily responsible for the hemolytic activity phenotype [138, 139]. In the pandemic serovars, these two genes are designated as *tdhA* and *tdhS*. *tdhA* is the structural gene expressed and secreted by the Kanagawa-positive strain as the functional TDH hemolysin.

The expression of *tdh2* (and not *tdh1* gene) is under the regulation of *toxRS* operon that operates in a growth-medium dependent manner [140]. *ToxR* is an important protein of this operon which regulates the activation of *tdh* genes. *VtrA* and *VtrB* are two similar proteins regulating the expression of *tdh* and other genes on the pathogenicity island of *V. parahaemolyticus* [141]. The *tdh* expression is downregulated by another regulatory protein *CalR*, whose expression is itself regulated by *ToxR*. In a feedback loop, *CalR* inhibits *toxR* and its own gene expression [142]. Another study reports *luxM/luxS*-dependent regulation of *tdh* expression, where *LuxM* downregulates the

expression while LuxS upregulates the expression of *tdh* [143]. Also, HNS (nucleoid-associated DNA binding regulator) and Hfq (a global transcription regulator) have been shown to repress the production of TDH [144].

The expressed precursor form of TDH is composed of 189 amino acid residues with a 24 residues-long N-terminal signal peptide. TDH may take two distinct routes for its secretion through the bacterium [145]. The signal peptide in the precursor targets the toxin precursor towards the Sec machinery, where it is cleaved and mature TDH is generated and secreted through the type-2 secretion system (T2SS) as the exotoxin. After maturation, some fraction of TDH is transported back to the cytoplasm through the periplasmic space. Further with the aid of a chaperone VocC, TDH is exported via T3SS2 as an effector molecule. Both these modes of secretion of TDH appear to have varying functional implications. As an effector molecule, TDH leads to the fluid accumulation in the rabbit ileal-loop model. However, TDH as an exotoxin is reported to induce intra-peritoneal lethality in the murine model [145].

### **1.5.2. Structural and physicochemical properties of TDH**

The mature form of TDH is a 165 amino acids long polypeptide that takes up a  $\beta$ -sandwich core structure, wherein 10  $\beta$ -strands are packed between two short  $\alpha$ -helices ( $\alpha$ <sub>3-10</sub> helix and  $\alpha$ <sub>1</sub> helix) [17]. The biologically active form of TDH exists as homotetrameric assemblies. The crystal structure of the TDH tetramer depicts that each protomer faces another protomer with its C-terminal region at the inter-protomer interface, resulting into a central cavity of  $\sim 20$  Å in diameter and 50 Å in depth [17]. Disruption of the tetramers by disrupting the inter-protomer interactions hampers the membrane-damaging action of TDH, suggesting that TDH tetramers are indispensable for its functionality [17, 146].

TDH exhibits remarkable structural fold similarity with eukaryotic PFTs of the actinoporin family like Equinatoxin II, Fragaceatoxin C and Sticholysin II [17]. Interestingly, TDH has a crucial extended C-terminal region (CTR) (<sup>157</sup>SFFECKHQQ<sup>165</sup>) with a disulphide bond (between Cys151 and Cys161) that is absent in the actinoporins structure. CTR of each protomer is placed at the inter-protomer interface of TDH tetramer. The intra-protomer disulphide bond restrains the structural disposition of CTR

during the process of protein folding and assembly. Thus, the intra-disulphide bond mediates spatial locking of CTR at the inter-protomer interface and provides a regulatory mechanism responsible for the unique in-solution tetrameric assembly of TDH [146].

The N-terminal region or NTR (<sup>1</sup>FELPSVFPAP<sup>11</sup>) of TDH is a short stretch of 11-amino acids, which is immensely disordered than the rest of the protein. This region could not be modelled in the crystal structure presumably due to high conformational fluctuations. It has been documented that NTR and its flexibility play a necessary role in the membrane-binding and membrane-damaging action of TDH [147].

Another interesting physicochemical feature of TDH is its temperature-sensitive reversible amyloidogenic behaviour [148]. TDH shows the formation of amyloid-like structures at 60 °C that are functionally inactive. However, these structures become unfolded upon heating to 80-90 °C, and refold to their native structure and functionality when cooled down rapidly. This response to heat treatment is termed as the Arrhenius effect and is displayed by certain other PFTs from *Klebsiella pneumoniae*, *Staphylococcus aureus*, *Bacillus cereus* and *Pseudomonas aeruginosa* [148].

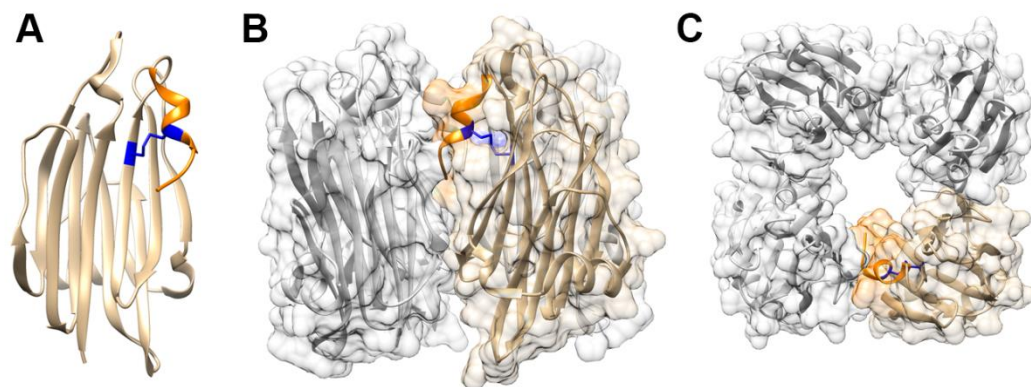


**Illustration 11. Structural features of TDH.** (A) TDH protomer exhibiting a  $\beta$ -sandwich core structure with a C-terminal region (highlighted in orange) which is linked through the intra-protomer disulphide bonds (depicted in blue). (B) Side view of TDH tetrameric assembly with one of the protomer highlighted as depicted in (A). (C) Top view of TDH tetramer showing the central pore-cavity. (Image source: Verma and Chattopadhyay, *Front. Mol. Biosci.* 2021 [129]) (PDB ID for structural coordinates: 3A57)

### **1.5.3. Pore-formation mechanism of TDH**

As described earlier, the pore-formation process by the PFTs is a highly orchestrated process involving the binding of the PFT to the host membrane, followed by subsequent steps of oligomerization and insertion, resulting in a functional trans-membrane pore. The structural basis of the pore-formation mechanism for TDH remains elusive at present. However, various studies have attempted to deduce the membrane-interaction step in the TDH's pore-formation process. GT1 and asialo-GM2 gangliosides have been suggested as putative TDH receptors on the cell surface [149, 150]. However, it still remains uncertain whether these gangliosides are the actual receptors, or whether they assist any accessory interactions of TDH. It has been reported that TDH can interact with detergent-resistant membrane fractions or the cholesterol and sphingomyelin-rich lipid-raft regions [151]. Membrane cholesterol depletion inhibited TDH-mediated cytotoxicity in the nucleated cells. In contrast, cholesterol depletion did not affect the pore-forming activity of TDH in erythrocytes. Depletion of sphingomyelin from the cells led to a compromised association with raft fractions and hampered cytotoxicity. However, the direct interaction of TDH with cholesterol and sphingomyelin has not been reported [151].

Altogether, the exact membrane surface receptors required for TDH binding yet remain unknown. Besides, a toroidal-pore model has been proposed for TDH, where the N-terminal domain of the toxin might be the putative membrane-inserting motif [129, 147].

### **1.5.4. Pathophysiological functions of TDH**

TDH has been characterized as a potent pore-forming toxin that causes the release of haemoglobin from the erythrocytes due to colloid osmotic lysis [152]. In addition, it evokes other pathophysiological effects in target hosts, like enterotoxicity, cardiotoxicity, and cytotoxicity [153-155]. Studies show that TDH intoxication triggers calcium influx in the target cells, where its cytotoxicity was observed to be independent of any calcium influx, while chloride ion secretion was found to be dependent on the calcium influx [156, 157]. Another report showed lysosomal disintegrity in response to the toxin and it was observed to be independent of the TDH-mediated calcium influx [156]. TDH is also shown to downregulate the proliferation of colon carcinoma cells in

a calcium-dependent manner [158]. TDH-mediated inflammatory responses involving inflammasome activation and caspase-1 activation have also been documented [159]. These observations, along with the history of *V. parahaemolyticus* outbreak and its association with TDH, emphasize upon the significance of TDH in the pathogenesis of the bacterium as its potent virulence factor. However, the mechanistic details for most of these TDH-elicited cell death responses are still obscure. Therefore, the underlying mechanism of TDH-mediated pathogenesis of *V. parahaemolyticus* in the context of host-pathogen interaction remain to be explored.

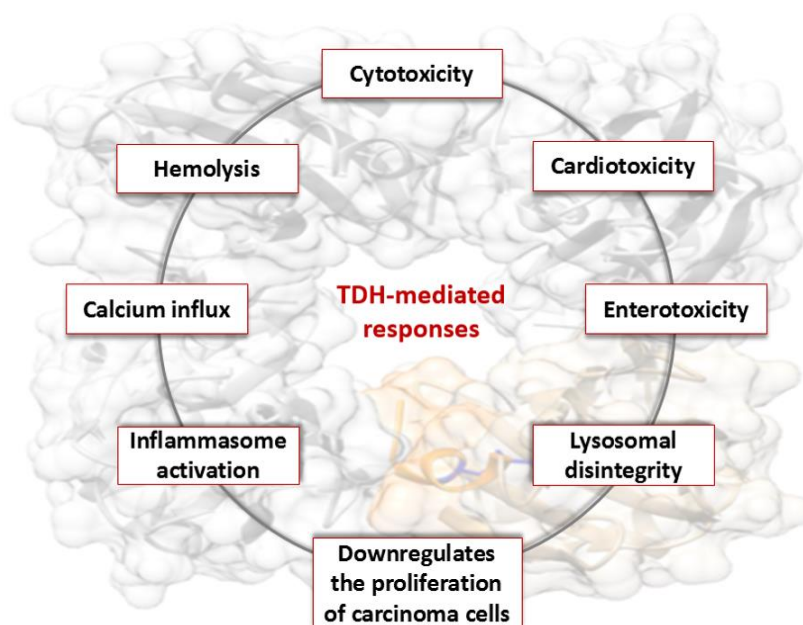


**Illustration 12. TDH-mediated pathophysiological responses.** TDH exhibits variety of cellular responses involving: (i) hemolysis as a result of its pore-formation activity causing colloid osmotic lysis in erythrocytes, (ii) cytotoxicity against various cell types, (iii) cardiotoxicity was confirmed via intravenous injection of toxin in rats and also in cultured mouse heart cells, (iv) enterotoxigenicity confirmed by chloride ion secretion and fluid accumulation in rabbit-ileal loop model, (v) influx of extracellular calcium in intestinal epithelial cells, (vi) compromised lysosomal integrity as detected in intestinal epithelial cells was found independent of calcium influx, (vii) downregulation of proliferation of colon carcinoma cells involves calcium sensing receptors, and (viii) activation of NLRP3 inflammasomes in macrophages.

The cytotoxicity of TDH has been observed against an array of nucleated mammalian cell types like FL cells, Intestine 407 cells, Caco-2 cells, HeLa cells, etc. The cytotoxic effects of a PFT could be suggestive of the direct consequences of its pore-forming ability. However, the process of cell death is fairly more intricate and complex in the nucleated mammalian cells than the colloid osmotic lysis of erythrocytes.

An earlier study showed that TDH could evoke some of the features of apoptosis-like programmed cell death, such as morphological changes, chromatin condensation, and DNA fragmentation in the target nucleated mammalian cells [160]. These features support that TDH-mediated cell death may involve intricate cellular processes. However, the molecular details of the cell death pathway evoked by TDH in mammalian cells remain fragmentary. As documented in the literature, apoptotic caspases are considered as key executioners of classical apoptosis [97]. However, the involvement of caspases in the TDH-mediated apoptosis-like cell death is unclear. In addition to the caspases, mitochondria are central to various programmed cell death pathways [107]. Therefore, it needs to be explored in more detail whether and how various such components operate to execute programmed cell death.

The present study attempts to elucidate the molecular details underlying the cell death response triggered by TDH in the target nucleated mammalian cells. In this direction, our work explores the pathophysiological role of TDH concerning bacterial pathogenesis and host-pathogen interaction processes.

## **1.6. Aim of the study**

To unravel the molecular mechanisms underlying the cell death pathway induced by Thermostable Direct Hemolysin (TDH), a major pore-forming toxin secreted by *Vibrio parahaemolyticus*.



# **Section-2**

## **Materials and methods**



## 2. Materials and Methods

### 2.1. Ethics statement

The use of human blood for the experiments was approved by the Bioethics Committee of the Indian Institute of Science Education and Research Mohali. Each donor provided written informed consent.

### 2.2. Expression and purification of TDH

TDH was recombinantly expressed and purified from *E. coli* Origami B cells as previously described by Kundu et al [146, 147]. Briefly, wild-type TDH nucleotide sequence (without the signal peptide) was cloned in the pET-14b vector and transformed in *E. coli* Origami B cells (Merck Millipore) for protein expression. Origami B cells harbouring TDH clone were grown in Luria Broth (LB) (Hi-media) media containing ampicillin (Hi-media) (50 µg/ml) at 37 °C, 180 rpm. At the mid-log phase ( $OD_{600\text{ nm}} \sim 0.4-0.6$ ), the protein expression was induced by adding 1 mM isopropyl β-D-1-thiogalactopyranoside (IPTG) (BR Biochem Life Sciences Pvt. Ltd.) to the culture and grown at 30 °C for 3 hours. Following incubation, the culture was pelleted down, and the harvested bacterial cells were resuspended in phosphate buffer saline (PBS) (10 mM  $Na_2HPO_4$ , 1.8 mM  $KH_2PO_4$ , 137 mM NaCl, 2.7 mM KCl, pH 7.4). The bacterial protease inhibitor cocktail (PI cocktail) (Sigma Aldrich) was added to the suspension. Next, the cell lysis was carried out by sonication (Mesonix Ultra-sonicator) at an amplitude of 20 for 20 minutes. The lysate was then centrifuged at 15,000 x g for 30 minutes at 4 °C. The extracted supernatant fraction containing the soluble protein was equilibrated with 20 mM imidazole (Hi-media) (prepared in PBS) and further subjected to Ni-NTA affinity chromatography-based purification. The supernatant was passed through the Ni-NTA column (Qiagen) and washed with 20 mM imidazole to remove the loosely bound non-specific proteins in the lysate. Next, the elution of the 6X-histidine tagged-TDH was carried out using 300 mM imidazole. The presence of protein in the eluted fractions was confirmed using Bradford's reagent (Sigma Aldrich).

Further, the eluted protein fraction was diluted four times with 10 mM Tris-Cl (pH 7.4) and loaded to the Q-sepharose anion exchange column (GE Healthcare Life Sciences). After loading the protein, the column was washed with 100 mM NaCl in 10 mM Tris-Cl, pH 7.4. The bound protein fraction was then eluted using 500 mM NaCl in 10 mM Tris-Cl, pH 7.4. Purified protein was further subjected to His-tag removal by thrombin treatment (1 unit of thrombin is required for 250 µg of protein) (Sigma-Aldrich) for 2 hours at 37 °C. Subsequently after His-tag cleavage, the protein underwent another round of purification through the Q-Sepharose Fast Flow chromatography. Finally, the purified protein fractions (with and without His-tag) were analyzed by sodium dodecyl sulfate-polyacrylamide gel electrophoresis (SDS-PAGE) and Coomassie staining. The protein concentration was calculated spectrophotometrically measuring the absorbance at 280 nm and using the theoretical extinction coefficient determined by its amino acid composition.

### **2.3. Hemolytic activity assay**

Membrane-damaging activity of TDH was quantitatively determined by measuring its hemolytic activity against human erythrocytes. The hemolytic activity assay monitors the change in turbidity of the erythrocytes in suspension spectrophotometrically at OD<sub>650 nm</sub> [13, 161]. The extent of lysis by the toxin is inversely proportional to the turbidity of the erythrocytes. Human erythrocytes were suspended in PBS buffer corresponding to ~0.9 OD<sub>650 nm</sub>. Upon TDH treatment (1 µM), the decrease in turbidity of erythrocytes was monitored every 5 minutes for a period of 1 hour. The percentage of hemolysis was calculated over buffer treated erythrocytes using the following formula:

$$\% \text{ Hemolysis} = (\text{OD}_{\text{max}} - \text{OD}) / (\text{OD}_{\text{max}} - \text{OD}_{\text{min}}) * 100$$

### **2.4. Cell culture conditions**

Caco-2 human intestinal epithelial cell line and THP-1 human monocytic cell line were used for the present study. Caco-2 cells were procured from the National Centre for Cell Science, Pune, India and were cultured in DMEM medium (Invitrogen) supplemented with 10% fetal bovine serum (FBS; Gibco, Thermofisher Scientific), 100 units/ml penicillin and 100 µg/ml streptomycin (Invitrogen). THP-1 cell line was procured from

the National Centre for Cell Science (NCCS), Pune, India. The cell line was cultured using RPMI 1640 medium (Invitrogen) supplemented with 10% FBS and 100 units/ml penicillin and 100 µg/ml streptomycin.

## **2.5. Lactate dehydrogenase release assay of cytotoxicity**

The cytotoxicity of TDH was measured against nucleated mammalian cells by employing lactate dehydrogenase (LDH) release assay. Caco-2 and THP-1 cells were seeded at a density of 0.1 million/100 µl, overnight at 37 °C. Following incubation, the cells were exposed to different concentrations of TDH (0.125 – 1.0 µM) for 24 hours at 37 °C. Also, for the time course experiment, cells were treated with 1 µM TDH for 2, 4, 8 and 24 hours. After the incubation period, the supernatant was collected and analysed for the presence of LDH using the CytoTox 96® Non-Radioactive Cytotoxicity Assay Kit (Promega) as per the manufacturer's protocol. Briefly, after treatments, the supernatants for each sample were collected separately and centrifuged for any residual cells at 250 x g for 5 minutes. Next, 50 µl of each sample is transferred to the wells of a 96-well plate and then added with 50 µl substrate provided in the kit and incubated roughly for 8-10 minutes to develop. After incubation, the reaction was stopped using 50 µl of the stop solution provided in the kit. The LDH release was measured spectrophotometrically by taking the absorbance (A) at 490 nm. Supernatant obtained from cells treated with lysis solution (provided in the assay kit) regarded as the positive control, corresponded to 100% LDH release ( $A_{max}$ ). Untreated (UT) cells were considered negative control for the experiment. Therefore, the percentage of cytotoxicity was calculated as follows:

$$\% \text{ LDH release or cytotoxicity} = (A - A_{UT}) / (A_{max} - A_{UT}) * 100$$

## **2.6. Analysis of morphological changes by flow cytometry**

Caco-2 and THP-1 cells were plated overnight at a density of  $1 \times 10^6$  cells/ml at 37 °C. Following incubation, the cells were treated with buffer (12 hours) or 1 µM TDH for 4 and 12 hours. Next, the cells were washed twice with PBS and acquired by BD FACSCalibur flow cytometer using BD FACSFlo<sup>TM</sup> Sheath Fluid. The scatter profiles of the cells with different treatments were monitored for the forward scatter (FSC; with

excitation at 488 nm, with filter 488/10) and side scatter (SSC; using excitation at 488 nm, with filter 488/10). The data were analysed using the FlowJo software and presented as dot plots (SSC vs. FSC) without any gating.

## **2.7. Analysis of morphological changes by phase contrast microscopy**

Caco-2 and THP-1 cells were plated overnight in a 24-well plate at a density of  $1 \times 10^6$  cells/ml overnight at 37 °C. Next, the cells were treated with TDH (1  $\mu$ M, for 2 and 4 hours) or buffer (4 hours). Following incubation, the cells were observed at 60x magnification under EVOS FL Imaging System (Thermo Fisher Scientific). A total of 10 images were taken for each treatment in each independent experiment. The images were processed in ImageJ software for representation.

## **2.8. Annexin V-FITC and propidium iodide staining**

Caco-2 and THP-1 cells were plated at a density of  $1 \times 10^6$  cells/ml, overnight at 37 °C. Next, the cells were treated with TDH (1  $\mu$ M, for 24 hours) or buffer (24 hours). Staurosporine (1  $\mu$ M, for 6 hours) (Sigma Aldrich), served as the positive control in THP-1 cells. *Vibrio cholerae* cytolysin or VCC (100 nM, 6 hours) served as the positive control in case of Caco-2 cells [22]. Following incubation, cells were harvested and washed twice with ice cold PBS. The samples were then subjected to staining using the Annexin V-FITC and propidium iodide (PI) staining kit (BD Biosciences) according to the manufacturer's protocol. Briefly, after washing, the cells were resuspended in 750  $\mu$ l of 1X binding buffer (provided in the kit). Further, 100  $\mu$ l of each sample was aliquoted in FACS tubes (BD Biosciences) and stained with 2.5  $\mu$ l of each Annexin V-FITC and PI for 15 minutes at room temperature. Single-stained controls of staurosporine or VCC treatments were kept, stained with 2.5  $\mu$ l of either Annexin V-FITC or PI. After 15 minutes incubation period, the samples were diluted using 400  $\mu$ l of 1X binding buffer and acquired on flow cytometer (BD FACSCalibur or BD Accuri C6 flow cytometer), where Annexin V-FITC and PI stained cells were acquired in FL-1 (excitation at 488 nm, with filter 530/30) and FL-2 (excitation at 488 nm, with filter 585/42) channels, respectively. During acquisition, the single stained staurosporine or VCC-treated control cells were used for compensation settings. The acquired data were further analysed using

the FlowJo software, where a pseudo-color plot (FL-2 vs. FL-1) was represented with the same quadrant gate settings applied to all the samples to segregate the differently stained populations.

For inhibitor-based studies, THP-1 cells were pre-treated with a pan-caspase inhibitor, ZVAD-fmk (40  $\mu$ M, 1 hour), which inhibits the catalytic function of caspases by binding irreversibly to their catalytic site. After the pre-treatment, the cells were treated with TDH (0.5  $\mu$ M, 24 hours) or buffer (24 hours). Staurosporine (1  $\mu$ M, for 6 hours) treated THP-1 cells with and without ZVAD-fmk pre-treatment served as the positive controls. Following incubation, the cells were subjected to Annexin V-FITC and PI staining, acquired and analysed in a similar manner as described above.

## **2.9. DNA fragmentation analysis by agarose gel electrophoresis**

Caco-2 cells ( $4 \times 10^6$ ) were plated overnight at 37 °C. Next, the cells were intoxicated with TDH (0.5  $\mu$ M, for 8 hours) or buffer (8 hours). Staurosporine (1  $\mu$ M, for 6 hours)-treated cells served as the positive control for the experiment. Following incubation, the cells were harvested and washed twice with PBS. The cell pellets were then resuspended in 50  $\mu$ l of lysis buffer (50 mM Tris-HCl buffer (pH 7.4), containing 20 mM EDTA, 1% NP-40) and mildly vortexed. Next, the cells were incubated on ice for 30 minutes with intermittent vortexing at every 10 minutes interval. The cells were then centrifuged at 1600 x g, at 4 °C for 5 minutes. Following centrifugation, the supernatant was collected and 50  $\mu$ l lysis buffer was added to the leftover pellet, heated at 65 °C for 5 minutes, and kept back in ice for 5 minutes. Then, the pellet was centrifuged again at 1600 x g, at 4 °C for 5 minutes. The supernatant recovered this time was combined with that from the previous step and the pellet was discarded. Subsequently, SDS was added to the collected supernatant fraction to a final concentration of 1% (weight/volume) and mixed. Then, RNase A (Qiagen) was added to a final concentration of 5  $\mu$ g/ml, and incubated for 2 hours at 56 °C. Following incubation, the supernatant was subjected to proteinase K (Invitrogen, Thermo Fisher Scientific) treatment (using a final protease concentration of 1  $\mu$ g/ $\mu$ l) at 37 °C for 2 hours. Subsequently, an equal volume of 5 M ammonium acetate (Hi-media) was added to the supernatant, and the DNA fragments were precipitated using 2.5-volumes of chilled absolute ethanol (Merck) for overnight at -20 °C. The precipitated DNA fragments were recovered by centrifugation at 12,000 x g for 15-20 minutes at 4

°C. The pellet was completely dried to get rid of any residual ethanol, and dissolved in 40 µl nuclease free water. The isolated DNA fragments were analysed for the laddering pattern on 1.5% agarose gel (1.5% agarose (BR Biochem Life Sciences Pvt. Ltd.) prepared in 50 ml of 1X Tris Acetate EDTA (TAE) buffer) by electrophoresis at 70 volt (V) for 1 hour.

## **2.10. Whole cell lysate preparation for cleaved caspase-3 detection**

5-6 x 10<sup>6</sup> Caco-2 or THP-1 cells were treated with 1 µM TDH for 2, 4 and 8 hours and buffer for 8 hours at 37 °C. Staurosporine-treated cells (2 µM for 6 hours) served positive control for the cleaved caspase detection. Following treatments, cells were harvested and washed twice with ice-cold 1X PBS. Subsequently, the cells were re-suspended in 200-250 µl of lysis buffer (comprising 50 mM Tris-HCl buffer, pH 8.0, containing 150 mM NaCl, 0.1% (w/v) sodium dodecyl sulfate (SDS), and 0.1% (v/v) Triton-X-100) supplemented with a mammalian protease inhibitor cocktail (Sigma-Aldrich) and subjected to sonication at 10 A for 6 seconds, thrice. The lysed cells were then centrifuged at 16,000 x g for 30 minutes at 4 °C. The supernatants, referred to as the whole cell lysates, were collected and resolved on 15% SDS-PAGE and transferred to methanol charged polyvinylidene difluoride (PVDF) (Bio-Rad Laboratories) membrane at 90 V for 90 minutes. After the transfer was complete, the PVDF membrane was blocked in 5% skimmed milk (Hi-media) prepared in 1X Tris-Buffer Saline with Tween-20 (TBST; 20 mM Tris (pH 7.6), 137 mM NaCl, 0.1% Tween-20) for 1 hour at room temperature. Following blocking, membrane was washed thrice every 5 minutes with 1X TBST and then, probed for cleaved caspase-3 using primary rabbit anti-cleaved caspase-3 monoclonal antibody (Cell Signaling Technology) (1:1000 dilution, volume/volume; prepared in 5% skimmed milk prepared in 1X TBST) with mild agitation overnight at 4 °C. Following incubation, membrane was washed thrice every 5 minutes with 1X TBST and incubated with secondary anti-rabbit HRP-linked IgG antibody (Sigma-Aldrich) (1:5000 dilution, volume/volume; prepared in 5% skimmed milk prepared in 1X TBST) for 1 hour at room temperature. After incubation, membrane was washed thrice every 5 minutes with 1X TBST and finally, developed and visualized using ImageQuant LAS 4010 (GE Healthcare Life sciences, Uppsala, Sweden).

### **2.11. Active caspase-3 detection by flow cytometry**

Caco-2 or THP-1 cells were seeded at a density of  $1 \times 10^6$  cells/ml in a 24-well plate overnight at 37 °C. Cells were then treated with TDH (0.5 and 1  $\mu$ M) for 8 hours at 37 °C. Buffer-treated cells served as the negative control, while treatment with staurosporine (1.5  $\mu$ M for Caco-2 cells and 2  $\mu$ M for THP-1 cells; for 6 hours) served as the positive control for the experiment. Following incubation, cells were harvested and subjected to staining, as per the manufacturer's protocol (BD Biosciences). Briefly, the harvested cells were washed with ice cold PBS (twice) and then resuspended in BD cytofix/cytoperm buffer provided in the kit (for  $1 \times 10^6$  cells, 0.5 ml buffer was used) and incubated for 20 minutes on ice. Next, the cells were washed twice using BD perm/wash buffer (1x) (for  $1 \times 10^6$  cells, 0.5 ml buffer was used). The cell pellet was then resuspended in 100  $\mu$ l BD perm/wash buffer (1x) containing FITC-conjugated anti-human active caspase-3 antibody (1:10 dilution; volume/volume) and incubated at room temperature for 30 minutes. After incubation, samples were washed with 1 ml of BD perm/wash buffer (1x) and finally, resuspended in 0.5 ml of the same buffer. The stained cells were acquired on a BD FACSCalibur flow cytometer in the FL-1 (excitation 488 nm, filter 530/30) channel. Data were further analysed with the FlowJo software where a density plot (SSC vs. FL-1) was represented and an oval-gate was marked for all the samples based on the positive control i.e. staurosporine-treated cells showing active-caspase-3 population.

### **2.12. JC-1 dye assay for Mitochondrial Membrane Permeability Transition**

Caco-2 or THP-1 cells were plated at a density of  $1 \times 10^6$  cells/ml overnight at 37 °C. Cells were then treated with TDH (1  $\mu$ M for 4 hours and 12 hours for Caco-2 cells; 0.5 and 1  $\mu$ M for 12 hours for THP-1 cells). Following incubations, cells were harvested and stained with JC-1 dye (Sigma-Aldrich) as per the manufacturer's protocol. Staining solution was added to media containing cells in the ratio 1:1 volume/volume and incubated for 20 minutes in CO<sub>2</sub> incubator at 37 °C. Cells were harvested and washed twice with ice cold 1X PBS. Finally samples were re-suspended in 500  $\mu$ l 1X PBS and acquired in flow cytometer. Valinomycin treatment (1  $\mu$ g/ml, for 20 minutes; provided in the kit; Sigma-Aldrich) which was provided along with the staining solution to the cells, served as the positive control for the experiment. Following staining, the cells were acquired in the FL-1 (excitation at 488 nm, with filter 530/30) and FL-2 (excitation at

488 nm, with filter 585/42) channels on a BD FACSCalibur flow cytometer. JC-1 monomers are detected at 530 nm emission wavelength, upon excitation at 490 nm, and JC-1 aggregates are detected at 590 nm emission wavelength, upon excitation at 525 nm. Valinomycin and buffer controls were used for the compensation settings. The data were analysed using the FlowJo software, and represented as the contour plots (FL-2 vs FL-1) with a rectangular gating applied according to the positive control for the FL-1 positive population.

### **2.13. ATP determination assay**

Caco-2 cells were plated at a density of  $1 \times 10^6$  cells/ml overnight at 37 °C. Cells were then treated with 1  $\mu$ M TDH or buffer for 1 hour. Following incubation, cells were harvested and the cell numbers were normalized for the viable cells by trypan blue dye exclusion method (of the non-viable cells) for both the TDH-treated and buffer-treated samples by counting the cells using a haemocytometer. Thus, equal numbers of viable cells were subjected to the determination of ATP levels in both the samples using the ATP Bioluminescence Assay Kit HSII (Roche Diagnostics, Merck), as per the manufacturer's instructions. Briefly, the cells were first washed with ice-cold PBS and then lysed using 50  $\mu$ l lysis reagent provided in the kit. The resulting cell lysates were then centrifuged at 8000 x g for 10 minutes at 4 °C, after which the supernatant was collected. Next, the obtained supernatant was diluted using 250  $\mu$ l of the dilution buffer provided in the kit. The samples were then developed by adding 50  $\mu$ l luciferase reagent, and the luminescence measurements were conducted on a 96-well plate-reader (POLARstar Omega, BMG Labtech). The ATP concentrations were determined for the samples using an ATP standard curve. The final data was represented as the fold change in the ATP levels relative to the buffer-treated sample.

### **2.14. Assay for the detection of loss of cytochrome c from mitochondria**

Caco-2 or THP-1 cells were seeded at a density of  $1 \times 10^6$  cells/ml, for overnight at 37 °C. Caco-2 cells were treated with TDH (0.5  $\mu$ M; for 4 hours) or valinomycin (Sigma-Aldrich) (1  $\mu$ g/ml; for 20 minutes). THP-1 cells were then treated with TDH (0.5 and 1  $\mu$ M) for 30 minutes at 37 °C. Buffer-treated cells were employed as the negative control

for the experiment. Subsequently, the cells were processed for the detection of cytochrome c release, following the method described in a prior report [162], with slight modifications as described in Gupta et al, 2015 [163]. In brief, the cells were harvested and washed twice with ice-cold PBS. Next, cells were selectively permeabilized using 100  $\mu$ l permeabilization buffer (containing 1% FBS, 0.05% saponin, 0.1% sodium azide in PBS) for 10 minutes on ice. The selective permeabilization of cells will allow the cytochrome c released into the cytosol due to the treatments (if any) to leak through the cell while that present in the intact mitochondria would still be present. The cells were then fixed using 4% paraformaldehyde for 15 minutes on ice. After fixation, the cells were washed twice with ice-cold PBS and incubated in 100  $\mu$ l blocking buffer (3% BSA + 0.5% saponin in PBS) for 30 minutes at room temperature. Following blocking, the cells were stained with rabbit anti-human cytochrome c antibody (Sigma-Aldrich) (1:50 dilution, volume/volume; prepared in the blocking buffer) overnight at 4 °C. After incubation, the cells were washed twice with ice-cold PBS, and stained with secondary FITC-conjugated goat anti-rabbit IgG antibody (Sigma-Aldrich) (1:100 dilution, volume/volume; prepared in blocking buffer) for 1 hour at room temperature. Cells were then washed twice with ice-cold PBS. Finally, the cells were resuspended in 500  $\mu$ l blocking buffer, and acquired on a BD FACSCalibur or BD Accuri C6 flow cytometer in the FL-1 channel (excitation at 488 nm, with filter 530/30) for the detection of FITC fluorescence. The data were analysed using the FlowJo software, represented as the density plot (SSC vs. FL-1), and an oval gate was applied on all the samples, marking the cell population showing loss of cytochrome c.

### **2.15. Mitochondrial fraction preparation for AIF, TDH and Bax translocation**

Caco-2 or THP-1 cells ( $\sim 10-12 \times 10^6$ ) were subjected to TDH treatment (1  $\mu$ M) for different time points. Untreated cells served as the control for the experiments. Mitochondrial fractions were isolated from the cells using the Mitochondrial Isolation kit (Sigma-Aldrich) as per the manufacturer's protocol. Briefly, following treatments, the cells were harvested and washed twice with ice-cold PBS. Subsequently, the cells were lysed using 200  $\mu$ l of detergent lysis buffer (prepared in 1X extraction buffer by adding 1:200 of the lysis detergent and 1:100 mammalian protease inhibitor, provided in the kit) and vortexed at an interval of a minute, for the next 5 minutes. After lysis, two-volume

extraction buffer (supplemented with mammalian protease inhibitor in the ratio 1:100) was added to these cells and incubated on ice for 10 minutes, with intermittent vortexing at every 3 minutes interval. Following incubation, lysed cells underwent centrifugation at 1000 x g for 10 minutes at 4 °C, twice to eliminate any debris. The resulting supernatant was then subjected to centrifugation at 8000 x g for 10 minutes at 4 °C. The pellet thus obtained was enriched in the mitochondrial fraction, while the supernatant was considered as the non-mitochondrial fraction. These fractions were resolved on 12.5% SDS-PAGE and further subjected to western blotting by transferring on methanol charged PVDF membrane at 90 V for 90 minutes. After transfer, the membrane was blocked using the blocking buffer (5% skimmed milk prepared in 1X TBST/PBST) for 1-2 hours at room temperature. After blocking the membrane was probed for the presence of TDH, AIF and Bax using rabbit anti-TDH antisera (1:1000 dilution, volume/volume, prepared in blocking buffer), rabbit anti-AIF antibody (1:2000 dilution, volume/volume, prepared in blocking buffer; Sigma-Aldrich), and mouse anti-active Bax (clone 6A7) antibody (1:1000 dilution, volume/volume, prepared in blocking buffer; BD Biosciences), respectively. TIM23 was probed as the marker of the mitochondrial fraction with mouse anti-TIM23 antibody (1:2000 dilution, volume/volume, prepared in blocking buffer; BD Biosciences). Following primary antibody staining, the membranes were washed 4-5 times every 5 minutes using 1X TBST/PBST. The non-mitochondrial/cytoplasmic load or the levels of cytoplasmic contamination in the mitochondrial fractions were determined using mouse anti-GAPDH antibody (1:1000 dilution, volume/volume; Santa Cruz Biotechnology, Inc.). The membrane was then stained for respective secondary antibodies (anti-rabbit or anti-mouse IgG; 1:5000 dilution; volume/volume in blocking buffer; Sigma-Aldrich) for 1 hour at room temperature. Next, the blots were washed thrice every 5 minutes with 1X TBST/PBST. Finally, the blots were developed and visualised using ImageQuant LAS 4010.

## **2.16. Nuclear fraction preparation for AIF and Endo G translocation**

Caco-2 or THP-1 cells (~10-12 x 10<sup>6</sup> cells) were treated with TDH (1 µM, for 1 and 2 hours). Untreated cells served as the control for the experiments. Following incubation, the cells were harvested and washed twice with ice-cold PBS. The cell pellet was then resuspended in 250 µl hypotonic buffer (10 mM HEPES (pH 7.9) containing 1.5 mM

MgCl<sub>2</sub> and 10 mM KCl), and centrifuged at 1850 x g for 5 minutes at 4 °C. The supernatant was discarded, and 150 µl hypotonic buffer, containing 1X mammalian protease inhibitor and 25 mM DTT, was added to the cell pellet, and incubated on ice for 10-15 minutes. Next, the cell pellet was sonicated thrice at 10 A for 6 seconds each, and then the pellet was separated by centrifugation at 3,300 x g for 15 min at 4 °C. The pellet was washed by adding 250 µl hypotonic buffer. Subsequently, 67 µl of low salt buffer (20 mM HEPES (pH 7.9), 25% glycerol, 1.5 mM MgCl<sub>2</sub>, 0.02 M KCl, 0.2 mM EDTA, mammalian protease inhibitor, and 25 mM DTT) was added to the obtained pellet, This was followed by the gradual (dropwise) addition of 33 µl of high salt buffer (20 mM HEPES (pH 7.9), 25% glycerol, 1.5 mM MgCl<sub>2</sub>, 0.8 M KCl, 0.2 mM EDTA) and incubated on ice for the next 10 minutes. Afterward, the pellet was sonicated twice at 10 A for 6 seconds, followed by 30 minutes incubation on ice. Finally, the pellet was centrifuged at 25,000 x g at 4 °C for 30 minutes, and the supernatant was collected. This collected supernatant fractions were enriched in the nuclear fraction and were resolved on 12.5% SDS-PAGE gel and subjected to immunoblotting similarly as mentioned in the section 2.15. PCNA or Lamin B1 were probed as the marker for the nuclear load, using mouse anti-PCNA antibody (1:2000 dilution, volume/volume; BioLegend) or rabbit anti-Lamin B1 antibody (1:1000 dilution, volume/volume; Santa Cruz Biotechnology). AIF and Endo G translocation were then probed in the nuclear fractions using rabbit anti-AIF antibody (1:2000 dilution, volume/volume; Sigma-Aldrich) and rabbit anti-endonuclease G antibody (1:1000 dilution, volume/volume; Cell Signaling Technology), respectively. The purity of the nuclear fractions was determined by checking for the cytoplasmic contamination using mouse anti-GAPDH antibody (1:1000 dilution, volume/volume; Santa Cruz Biotechnology, Inc.).

### **2.17. DCFDA fluorescence assay for the detection of intracellular ROS production**

Caco-2 cells ( $0.5 \times 10^6$ ) were plated overnight at 37 °C. Then, the cells were treated with 0.5 µM TDH for 2 hours at 37 °C. Buffer-treated cells served as the control for the experiment. Subsequent to treatments, cells were rinsed with serum-free DMEM medium, and then stained with 2', 7'-dichlorofluorescein diacetate (DCFDA, 10 µM; Sigma-Aldrich) for 30 minutes at 37 °C. Following incubation, the cells were washed twice and resuspended in 500 µl PBS. The stained cells were acquired on a BD

FACSCalibur or BD Accuri C6 flow cytometer in the FL-1 channel (excitation at 488 nm, with filter 530/30). The data were analysed with the FlowJo software, and represented either as a histogram plot (without any gating).

### **2.18. NAC-mediated inhibition studies**

Effect of ROS scavenger, N-acetyl-L-cysteine (NAC), were determined on the intracellular ROS production. For this, Caco-2 cells were treated with 5 and 10 mM NAC (Sigma-Aldrich) for 2 hours at 37 °C. Subsequent to NAC pre-treatment, the cells were treated with TDH (0.5 µM; for 2 hours at 37 °C), and further processed for the intracellular ROS detection by measuring the DCFDA fluorescence assay by flow cytometry as described above (section 2.17). The data were analysed with the FlowJo software, and finally, represented as a bar graph obtained from the quantification of the flow cytometry data, showing fold change in DCFDA fluorescence over buffer-treated control.

Effect of ROS scavenging on the cytotoxicity of TDH was also determined. Briefly, overnight plated Caco-2 cells were pre-treated with NAC (10 mM for 2 hours) and then subjected to TDH treatment (0.5 µM TDH for 2 hours). Following incubation, LDH-release assay was performed as described earlier in the section 2.5, with slight modifications in the calculation of %cytotoxicity. Since, NAC itself absorbs at the wavelengths used for the LDH-release assay, NAC absorbance values were subtracted from all the NAC-treated samples and then %cytotoxicity was calculated.

Effect of ROS scavenging on the calcium influx was assessed. For this, Caco-2 cells pre-treated with NAC (10 mM for 2 hours) were subjected to Fluo-4-AM-based detection assay for calcium and analysed as described later in the section 2.20, 'Calcium measurement assay'.

### **2.19. Mitochondrial ROS detection**

Fluorescence microscopy was employed to determine the production of mitochondrial ROS in TDH-treated cells. Coverslips were coated with Caco-2 cells ( $0.25 \times 10^6$ ) and incubated overnight at 37 °C. The cells were rinsed twice with serum-free medium and

subsequently loaded with 3  $\mu\text{M}$  MitoSOX (ThermoFisher Scientific) for 30 minutes at 37 °C in a serum-free medium. Further, the cells were washed twice with PBS and replenished with 10% FBS-containing DMEM. The cells were then treated with TDH (0.2  $\mu\text{M}$  for 30 minutes), or buffer. After treatment, the cells were washed twice using PBS and then, fixed with 4% paraformaldehyde for 15 minutes at room temperature. The nucleus were stained with DAPI (Sigma-Aldrich) which were used to count the number of cells per field for the fluorescence quantification. Finally, the coverslips were mounted using fluoromount and were observed under a 60X oil immersion objective of Olympus confocal laser scanning microscope (Model No. FV10i). A total of 30 images were captured for three independent sets (10 images each for both the treatments). The brightness and contrast settings were maintained identical for all treatments within a single set. The images were analysed and quantified using ImageJ software (National Institutes of Health, Bethesda, MD, USA), by calculating the percentage of integrated density (product of mean fluorescence intensity and area) per cell.

## **2.20. Calcium measurement assay**

To determine the calcium influx in response to TDH treatment,  $0.5 \times 10^6$  cells (Caco-2 or THP-1 cells) were loaded with Fluo-4-AM (ThermoFisher Scientific) (1.5  $\mu\text{M}$  prepared in HBSS (Hanks' balanced salt solution; Gibco) buffer without  $\text{Ca}^{2+}$  and  $\text{Mg}^{2+}$ , 2 mM probenecid and 0.02% (weight/volume) pluronic acid) for 1 hour at 37 °C. Fluo-4-AM is a calcium specific dye which becomes fluorescent only after its entry into the cell, where the cellular esterases remove the acetoxymethyl (AM) ester to release the free Fluo-4 which interacts with calcium [164]. Probenecid is an anion transporter inhibitor that improves the intracellular retention of free calcium indicator, while pluronic acid improves the solubilisation of Fluo-4-AM and improves its cell penetration [165].

Subsequent to cellular loading of the calcium indicator, the cells were washed once with PBS and then resuspended in 500  $\mu\text{l}$  of HBSS containing 1.5 mM  $\text{Ca}^{2+}$  and 1 mM  $\text{Mg}^{2+}$ . Calcium kinetics was then monitored on a BD FACSCalibur flow cytometer for 10-15 minutes (in the FL-1 channel; excitation at 488 nm, with filter 530/30), immediately after the specified treatment (0.5  $\mu\text{M}$  TDH) to the stained cells. The acquired data was plotted using the FlowJo software. Positive control treatment involved the use

of phorbol 12-myristate 13-acetate (PMA) plus ionomycin (0.5  $\mu\text{g/ml}$  each), while untreated cells served as the negative control for the experiment.

To investigate the role of extracellular  $\text{Ca}^{2+}$  and the contribution of intracellular calcium stores in calcium flux, Caco-2 cells were kept in HBSS devoid of any  $\text{Ca}^{2+}$  and  $\text{Mg}^{2+}$ . The rest of the protocol was followed similar to described above.

Additionally, the calcium chelation by BAPTA-AM was tested by loading THP-1 cells with BAPTA-AM (10  $\mu\text{M}$  for 1 hour) along with Fluo-4-AM dye. Moreover, the impact of BAPTA-AM on the cytotoxicity of TDH in Caco-2 cells was assessed. Following pre-treatment with BAPTA-AM (5 and 10  $\mu\text{M}$  for 1 hour), cells were treated TDH (0.5  $\mu\text{M}$ ) for 8 hours. Subsequently, %cytotoxicity was determined by employing LDH-release assay as described in the section 2.5.

## **2.21. Co-localization study using confocal microscopy**

Coverslips were coated with Caco-2 cells ( $0.3 \times 10^6$  cells) and incubated overnight at 37  $^{\circ}\text{C}$ . Subsequently, the cells were subjected to TDH (1  $\mu\text{M}$ ) or buffer treatments for 2 hours at 37  $^{\circ}\text{C}$ . After the incubation, cells were washed twice with PBS and then fixed with 4% paraformaldehyde for 15 minutes at room temperature. Following fixation, the cells were washed thrice with PBS. The cells were then treated with permeabilization buffer (0.1% saponin, 5% BSA, 1% FBS in PBS) for 1 hour at room temperature. After permeabilization, two washes with PBS were given and the coverslips were incubated in a blocking buffer (5% BSA and 1% FBS in PBS) for 1.5 hours at room temperature. Subsequently, the cells were stained with mouse anti-TDH antisera (1:200 dilution, volume/volume, prepared in permeabilization buffer; overnight at 4  $^{\circ}\text{C}$ ), followed by staining with rabbit anti-TOM20 antibody (1:300 dilution, volume/volume, prepared in permeabilization buffer; 1 hour at room temperature; Sigma-Aldrich). As a negative control for the overall co-localization assay, sodium potassium ATPase (a plasma membrane marker) and TOM20 (mitochondrial marker) were stained in both buffer and TDH-treated cells, using mouse anti-sodium potassium ATPase antibody (1:100 dilution, volume/volume, prepared in permeabilization buffer; Abcam) and rabbit anti-TOM20 antibody (1:300 dilution, volume/volume, prepared in permeabilization buffer; Sigma-Aldrich), respectively. Following incubation, the cells were washed thrice with PBS, and

then stained using anti-rabbit Alexa Fluor 488 and anti-mouse Alexa Fluor 568 (1:500 dilution, volume/volume, for both, prepared in permeabilization buffer; ThermoFisher Scientific) and DAPI (Sigma-Aldrich) for 1 hour at room temperature. After secondary antibody staining, cells were washed thrice with PBS, and the coverslips were mounted using fluoromount (Sigma-Aldrich). Next, the coverslips were observed under a Leica confocal microscope. To probe any co-localization of TDH or sodium potassium ATPase with the mitochondrial marker, ~10-13 random fields of each coverslips were captured under the identical parameters in individual experimental set up. To probe co-localization between TDH and TOM20, a total of 33 images were analyzed for the TDH treatment and 30 images for the corresponding buffer treatment, using ImageJ software. Similarly, to investigate any co-localization of sodium potassium ATPase and TOM20, 30 images were analysed for both the TDH and buffer treatments. All images within each set were processed with identical brightness and contrast settings. Pearson's correlation coefficients for co-localization were determined using the ImageJ software.

## **2.22. Effect of TDH on isolated mitochondria**

To examine the binding of TDH with isolated mitochondria, and any subsequent AIF release from them, mitochondria were isolated from approximately  $5 \times 10^6$  Caco-2 cells. The mitochondrial isolation was carried out as described above in the section 2.15. The obtained pellet fraction, enriched with intact mitochondria, was resuspended in 1X storage buffer provided in the Mitochondria Isolation kit (Sigma-Aldrich). The isolated mitochondria in suspension were subjected to TDH treatment (1  $\mu$ M) and incubated at 37 °C for 30 minutes. Following treatment, the mitochondria were washed twice properly using ice-cold PBS, to remove unbound TDH (if any). Next, the mitochondria were then fixed using 2% paraformaldehyde for 10 minutes on ice. After fixation, the mitochondria were washed thrice using ice-cold PBS. The mitochondria were then permeabilized using permeabilization buffer (PBS containing 0.05% saponin, 5% BSA, 1% FBS) for 10 minutes at room temperature. To determine TDH binding to the isolated mitochondria, mitochondria were stained with anti-TDH antisera (1:500 dilution, volume/volume; prepared in permeabilization buffer) for 30 minutes at room temperature. Following incubation, the mitochondria were washed thrice with ice-cold PBS. The mitochondria were subsequently stained with FITC-conjugated goat anti-rabbit antibody (1:100

dilution, volume/volume; prepared in permeabilization buffer) (Sigma-Aldrich) for 30 minutes at room temperature. After staining, the mitochondria were washed thrice and resuspended in ice-cold PBS. The binding of TDH was determined by detecting the FITC fluorescence on a BD FACSCalibur flow cytometer in the FL-1 channel (excitation at 488 nm, with filter 530/30). The acquired data was then processed with the FlowJo software, and represented as histogram plot.

As described above, similar method was followed to determine the release of AIF from the isolated mitochondria. Briefly, the isolated mitochondria were treated with TDH (1  $\mu$ M, 30 minutes), washed thoroughly, fixed and permeabilized. Next, the isolated mitochondria treated with TDH were stained with rabbit anti-AIF antibody (1:500 dilution, volume/volume; Sigma-Aldrich) and then with FITC-conjugated goat anti-rabbit antibody (1:100 dilution, volume/volume, prepared in permeabilization buffer; Sigma-Aldrich) for 30 minutes at room temperature. Isolated untreated mitochondria from untreated cells served as the negative control, while isolated mitochondria from the TDH-treated cells served as the positive control. The release of AIF from the isolated mitochondria was determined by monitoring the FITC fluorescence on a BD FACSCalibur flow cytometer in the FL-1 channel (excitation at 488 nm, with filter 530/30). The acquired data was then processed with the FlowJo software, and represented as density plots (SSC vs. FL-1). The oval gate in the density plots corresponded to the region of the positive control (isolated mitochondria from the TDH-treated cells), depicting the percentage of mitochondrial population showing loss of AIF.

For the western blot-based detection of TDH and AIF in the isolated mitochondria, mitochondria isolated from the Caco-2 cells were treated with TDH (1  $\mu$ M; for 1 and 2 hours) or OmpU (5  $\mu$ g/ml; for 2 hours) (*V. cholerae* OmpU served as the positive control for the experiment [163]). Following treatment, the fractions were resolved on 12.5% SDS-PAGE gel and further subjected to immunoblotting similarly as described in the section 2.10. The blot was probed for the presence of TDH and AIF using rabbit anti-TDH antisera (1:1000 dilution, volume/volume) and rabbit anti-AIF antibody (1:2000 dilution, volume/volume; Sigma-Aldrich). TIM23 was probed using mouse anti-TIM23 antibody (1:2000 dilution, volume/volume; BD Biosciences), as the mitochondrial marker. Cytoplasmic contamination was checked using mouse anti-GAPDH antibody (1:1000 dilution, volume/volume; Santa Cruz).

### 2.23. Semi-quantitative RT-PCR analysis for *bax* and *bcl-2*

Caco-2 or THP-1 cells ( $1 \times 10^6$  cells) were treated with 0.5  $\mu$ M TDH or buffer for 8 hours at 37 °C. After incubation, the cells were subjected to RNA isolation using TRIzol method [166]. Briefly, the cells were harvested by centrifugation at 300 x g for 5 minutes. The collected cell pellets were washed with ice-cold PBS. After washing, 0.5 ml TRIzol (Thermo Fisher Scientific) was added and passed through 1 ml syringe (26 G X 0.5 inch) at least 11-12 times. Next, 0.1 ml chloroform (Sigma-Aldrich) was added to each sample and vortexed for 15 seconds. Subsequently, the lysed cells were incubated at room temperature for 2-3 minutes and centrifuged at 12,000 x g for 15 minutes at 4 °C. The centrifugation resulted into the separation of phases into lower or phenol-chloroform phase (pink in color), an interphase and an upper colorless aqueous phase containing RNA. This upper phase was transferred in a fresh microcentrifuge tube. Further, the RNA was precipitated by adding 0.25 ml of ice-cold isopropyl alcohol (Sigma-Aldrich) and incubated for 10 minutes at room temperature. Following incubation, the samples were centrifuged at 12,000 x g for 10 minutes at 4 °C. The RNA precipitate was observed to form a transparent-gel like pellet on the side and bottom of the tube. The supernatant was completely removed and the pellet was washed with 0.5 ml of 75% ethanol (Merck). It was mixed by vortexing and then centrifuged at 7,500 x g for 5 minutes at 4 °C. The last washing step with ethanol was repeated and the ethanol was completely removed. Subsequently, the pellet was air dried or vacuum dried for 5-10 minutes to remove any residuals of the ethanol. Finally, the RNA pellet was dissolved in 30-40  $\mu$ l of RNase free water (Sigma-Aldrich) and the concentration of isolated RNA was quantified by nanodrop (Jenway).

Next, the cDNA was synthesized from the isolated mitochondria using the Verso cDNA synthesis kit (ThermoFisher Scientific). 0.5-1  $\mu$ g of the isolated RNA for each sample was used for cDNA synthesis following the manufacturer's instructions. The cDNA synthesis was carried out by following PCR cycle program: one cycle at 42 °C for 30 minutes and one cycle at 95 °C for 2 minutes performed on MyCycler thermocycler (Biorad).

The resulting 20  $\mu$ l of cDNA was diluted five-fold in nuclease-free water and then used as template for RT-qPCR (reaction volume 10  $\mu$ l). The gene expression analysis of *bax* and *bcl-2* was performed using a Maxima SYBR Green-qPCR master mix (Thermo

Fisher Scientific) based semiquantitative real-time PCR on Eppendorf Mastercycler EP Realplex Thermal Cycler (Eppendorf, Germany) according to the manufacturer's protocol. The RT-qPCR was performed for 40 cycles. The primer sequences were obtained from the Harvard primer bank. The primers were then synthesised by IDT Technologies, USA. All the sample values were normalised over the values of housekeeping control genes: *β-actin*, *hprt* and *hsp90*. The obtained values were analysed and expressed in terms of *bax/bcl-2* ratio.

For detection of active Bax levels in mitochondrial fractions of Caco-2 and THP-1 cells, the fractions were prepared and probed by immunoblotting as mentioned in the section 2.15.

#### **2.24. Detection of lysosomal membrane permeabilization**

Coverslips coated with Caco-2 cells ( $0.3 \times 10^6$ ) were incubated overnight at 37 °C. Subsequently, the cells were treated with TDH (0.5 μM; 1 hour) or buffer. Following incubation, the coverslips were washed twice with fresh media, then LysoTracker™ Deep Red (100 nM for 0.5 hour; prepared in DMEM supplemented with FBS and penicillin and streptomycin) (Invitrogen, ThermoFisher Scientific) was added to the cells. Next, the cells were washed twice with ice-cold PBS and fixed with 4% paraformaldehyde for 15 minutes at room temperature. After fixation, coverslips were washed thrice with ice-cold PBS, and then mounted using fluoromount. The coverslips were observed under a 60X oil immersion objective of Olympus confocal laser scanning microscope (Model No. FV10i). From three independent sets, a total of ~33-34 images were captured and analysed using the ImageJ software (National Institutes of Health, Bethesda, MD, USA), keeping the brightness and contrast settings identical for all the treatments in a single set. The images were quantified using ImageJ, by calculating the percentage of integrated density (product of mean fluorescence intensity and area) per cell corresponding to %lysotracker fluorescence intensity.

#### **2.25. Detection of cleaved PARP-1 in whole cell lysates**

Whole cell lysates of both Caco-2 and THP-1 cells were prepared as described above in the section 2.10. These lysates were then probed for the cleaved PARP-1 via western blot

(as described in the section 2.10), using rabbit anti-cleaved PARP-1 antibody (1:1000 dilution, volume/volume; Cell Signaling Technology).

## **2.26. Statistical analyses**

To perform the statistical analyses of the data where the comparisons were made between two groups, Student's unpaired t-test was performed using GraphPad/Quickcalc (available online). To compare three or more groups, one-way ANOVA followed by a post hoc test (Dunnett's or Tukey's Multiple comparison test) was performed using GraphPad Prism version 9.4.0, developed by GraphPad Software, San Diego, California, USA. The obtained *p*-values less than 0.05 were considered statistically significant, while those equal to or greater than 0.05 were considered non-significant (ns). The significance were denoted as follows: \**p* < 0.05, \*\* *p* < 0.01, \*\*\* *p* < 0.001.



# **Section-3**

## **Results**



### 3. Results

#### 3.1. Purification and hemolytic activity of TDH

TDH was recombinantly overexpressed in the *E.coli* Origami B cells. Subsequently, it was purified from the soluble fraction of bacterial cell lysate using Ni-NTA agarose affinity chromatography. This was followed by purification through anion-exchange chromatography. The 6X-His tag was removed from the protein using thrombin and then subjected to purification by anion-exchange chromatography. The purified protein fraction was analyzed using SDS-PAGE/Coomassie staining (Figure 1A). Next, the activity of purified TDH was confirmed by checking its hemolytic activity against the human erythrocytes. The hemolytic assay is considered as a signature assay for the PFTs to determine their pore-forming ability. TDH exhibited complete lysis of human erythrocytes in 60 minutes over buffer treatment, indicating its potent pore-forming efficacy (Figure 1B).

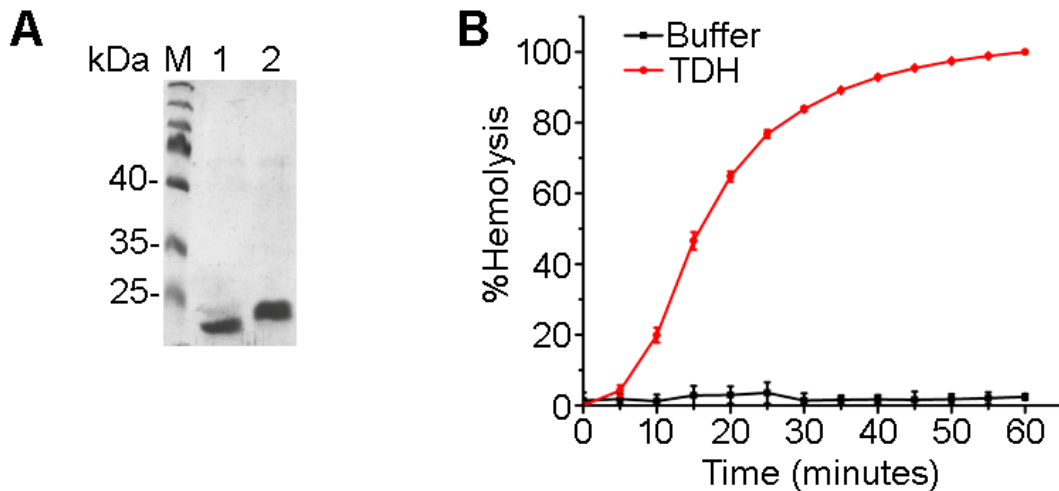


**Figure 1. SDS-PAGE/Coomassie staining profile and hemolytic activity of purified TDH.** (A) TDH was overexpressed in *E. coli* Origami B cells and purified using Ni-NTA affinity chromatography and Q-sepharose anion-exchange chromatography. Purified protein with His-tag and after cleavage of His-tag were subjected to SDS-PAGE/Coomassie staining. Lane M represents molecular weight markers, Lane 1 and 2

represent purified TDH without His-tag and with His-tag, respectively. (B) Purified TDH was assessed for its pore-forming activity on human erythrocytes. The %hemolysis for TDH (1  $\mu$ M) was monitored at every 5 minutes for over a period of 1 hour. TDH exhibited 100% hemolytic activity in 1 hour. Buffer-treated human erythrocytes served as the negative control for the experiment.

### **3.2. TDH displays potent cytotoxicity in the nucleated mammalian cells**

TDH has been characterized as a membrane-damaging pore-forming toxin [17]. Apart from its membrane-permeabilizing activity, TDH exhibits potent cytotoxicity against various nucleated mammalian cells [154, 156, 167]. To explore the underlying mechanism of TDH-mediated cytotoxic effects, we first examined the cytotoxicity of TDH in Caco-2 human intestinal epithelial cell line and THP-1 human monocytic cell line. We employed lactate dehydrogenase (LDH)-release assay to measure the extent of TDH-mediated cytotoxicity in these cell lines. LDH release assay measures the amount of LDH, a cytosolic enzyme, released from damaged cells into the surrounding medium. On addition of a substrate containing tetrazolium salts, LDH converts it to a colored product. The absorbance of this colored product is measured by a spectrophotometer which is proportional to the degree of LDH release due to cytotoxicity.

It was observed that different concentrations of TDH ranging from 0.125-1  $\mu$ M for 24 hours displayed ~60-67% cytotoxicity in Caco-2 cells and there was no dose-dependent cytotoxicity in these cells (Figure 2A). However, for the same range of concentrations and time point, a dose-dependent increase in cytotoxicity was observed against THP-1 cells. The cytotoxicity levels varied from ~36 to ~78% in THP-1 for the employed concentration range and time (Figure 2A). These data indicate that Caco-2 cells are possibly more susceptible toward the cytotoxicity of TDH than THP-1, at least for the concentration range and incubation time employed for the experiment.

Additionally, TDH-mediated cytotoxicity was checked for different time points (2, 4, 8 and 24 hours) in both, Caco-2 and THP-1 cells. A significantly high cytotoxicity (~70-80%) was observed upon 1  $\mu$ M TDH treatment for every time point against both the cell types (Figure 2B). A significant LDH release was observed for as low as 2 hours' time point. At 4 hours, there was a slight increase in the cytotoxicity and during later time

points, LDH release appeared to saturate. These data demonstrate that TDH exhibits potent cytotoxicity in both Caco-2 and THP-1 cells.

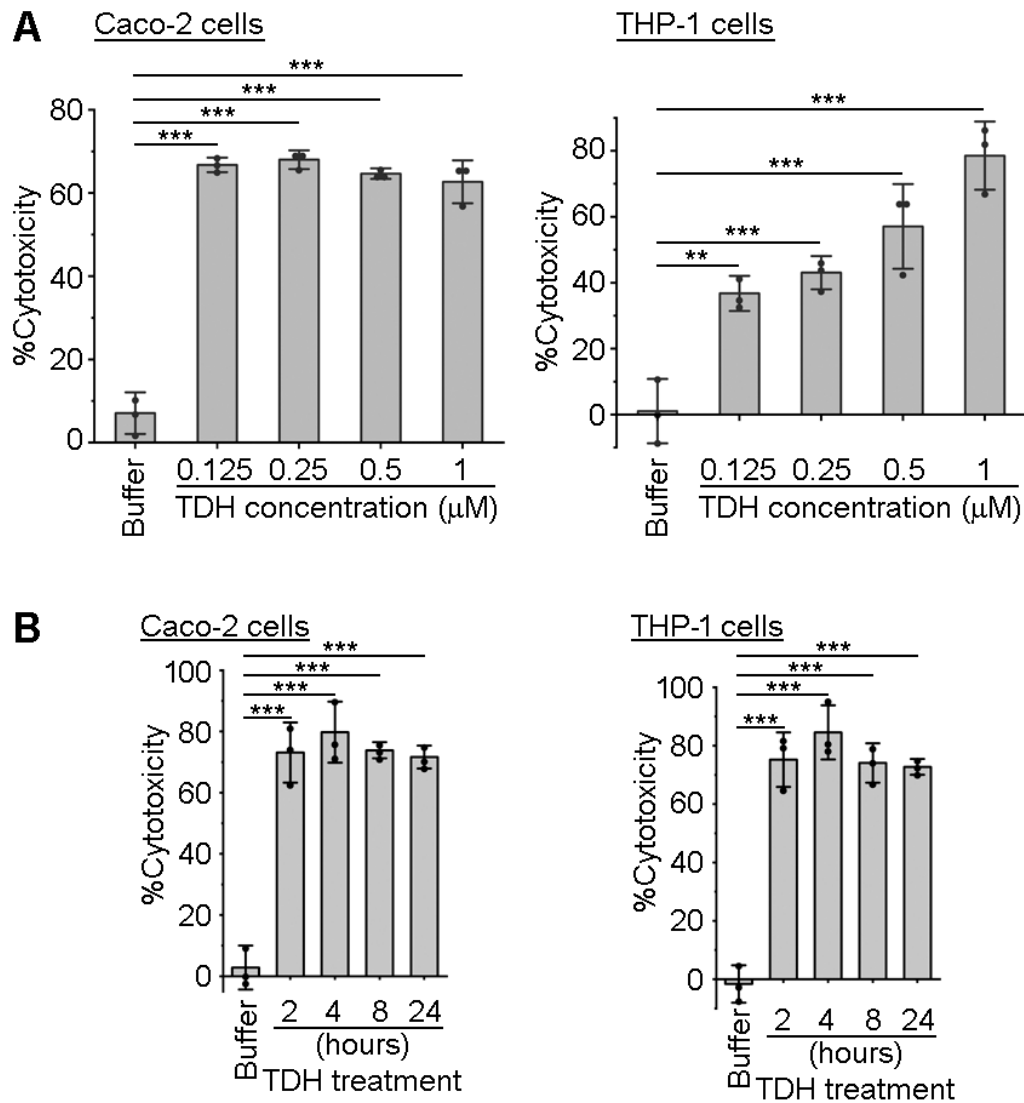


**Figure 2. TDH exhibits potent cytotoxicity in Caco-2 and THP-1 cells.** (A) Dose-dependent (0.125-1  $\mu$ M TDH for 24 hours) (upper panel) and (B) time-dependent (1  $\mu$ M TDH for 2, 4, 8 and 24 hours) (lower panel) changes in the cytotoxicity of TDH as monitored by LDH-release assay in Caco-2 (upper-left and lower-left panels) and THP-1 (upper-right and lower left panels) cells. Buffer-treated cells (for 24 hours) served as the negative control for the experiments. Data shown here are the averages  $\pm$  standard deviations from three independent experiments. \*\* $p < 0.01$ ; \*\*\* $p < 0.001$ ; one-way ANOVA with Dunnett's multiple comparison test.

### **3.3. TDH induces morphological alterations in target cells**

Toward exploring the pathophysiological effects of TDH on the nucleated mammalian cells, we examined the morphological changes induced by TDH in target cells, using flow cytometry and phase-contrast microscopy.

In flow cytometry, forward scatter (FSC) and side scatter (SSC) indicate the cell size and granularity, respectively [168]. This profile for a given cell type may change during cellular damage or cell death in response to certain stimuli. Increased cell granularity and cell shrinkage can be considered as the sign of apoptosis or other forms of cell death. The FSC-SSC profile of Caco-2 and THP-1 cells in response to TDH intoxication (1  $\mu$ M; for 4 and 12 hours) exhibited a decrease in FSC and an increase in SSC corresponding to TDH-mediated cell shrinkage and increased cell granularity, respectively (Figure 3A). This data indicates that TDH induces morphological changes in nucleated mammalian cells similar to apoptosis-like programmed cell death.

Additionally, the morphological changes were also recorded via phase-contrast microscopy in both Caco-2 and THP-1 cells. The microscopic images detected significant morphological alterations like membrane and organelle damage, perforation, shrinkage and increased granularity in both the cell types in response to TDH treatment (1 $\mu$ M; for 2 and 4 hours) (Figure 3B).

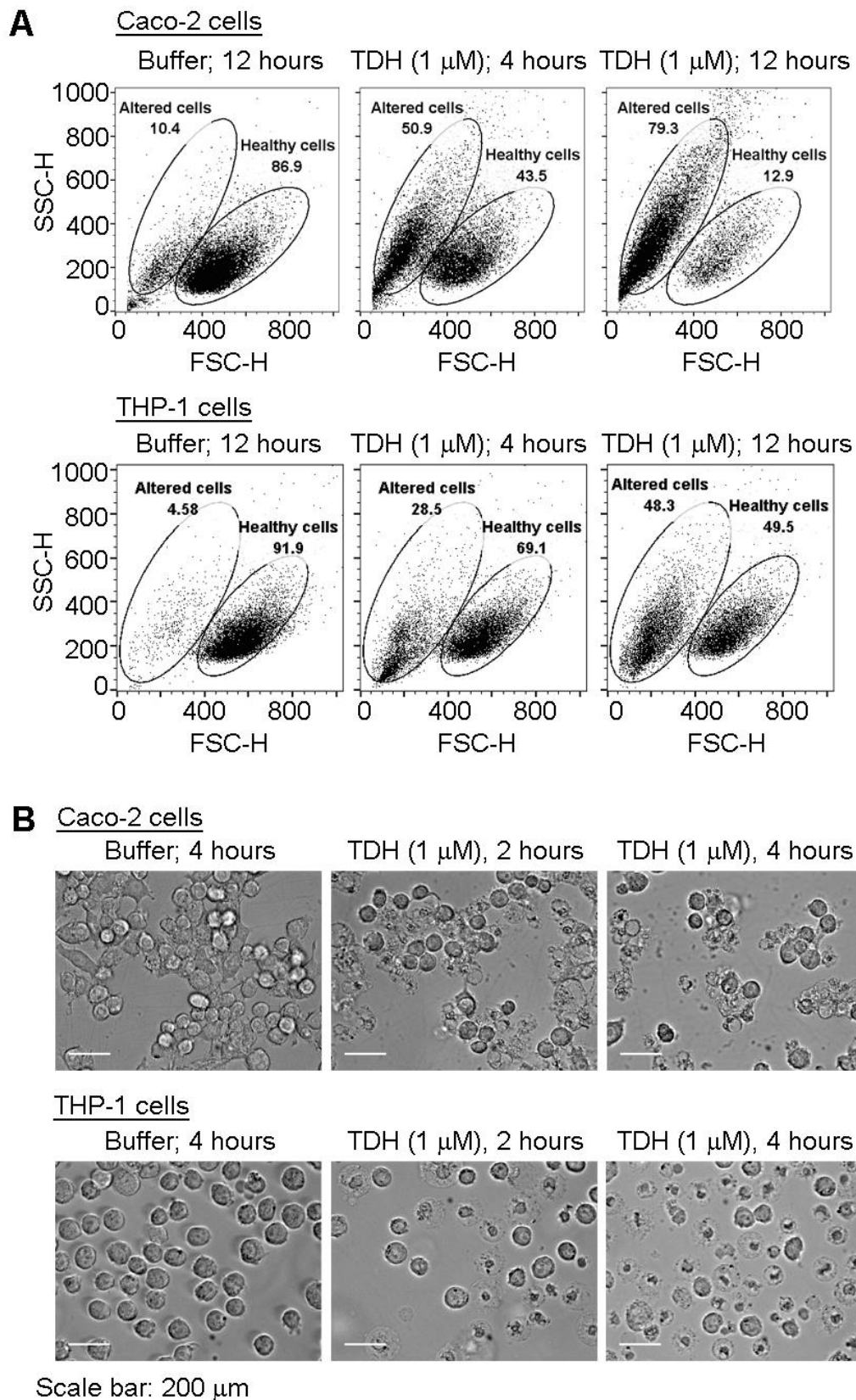


**Figure 3. TDH induces morphological changes in the target nucleated mammalian cells.** (A) Flow cytometry plots showing FSC-SSC profile of Caco-2 (upper panels) and

THP-1 (lower panels) cells treated with TDH (1  $\mu$ M; for 4 and 12 hours). Buffer (12 hours)-treated cells served as the negative control for the experiment. Oval gate marks the percentage of healthy and morphologically altered cells in each sample. Data shown here are the representatives of three independent experiments. (B) Phase-contrast micrographs of Caco-2 (upper panels) and THP-1 (lower panels) cells displaying morphological changes upon TDH intoxication (1  $\mu$ M; for 2 and 4 hours). Buffer (4 hours)-treated cells served as the negative control for the experiment. Images shown here are the representatives of two or more independent experiments.

### **3.4. TDH induces membrane phosphatidylserine flipping and DNA fragmentation resembling the features of apoptosis-like programmed cell death**

In order to investigate the biochemical effects of TDH-mediated cell death, we examined membrane phosphatidylserine flipping and DNA fragmentation in response to TDH treatment. In healthy cells, phosphatidylserine (PS), a negatively charged phospholipid, is present primarily on the inner leaflet of the plasma membrane. The onset of apoptosis or programmed cell death accompanies the flipping of PS on the outer leaflet of the bilayer, which can be detected by Annexin V-FITC staining in a flow cytometry-based assay [169]. The later stages of cell death involve plasma membrane and nuclear disintegration, thereby allowing propidium iodide (PI) intercalation within the DNA bases. Therefore, only Annexin V-FITC stained cells indicate the early stages of apoptosis while both Annexin V-FITC and PI stained cell population suggests late apoptotic cell death [169].

We observed that TDH treatment (1  $\mu$ M; 24 hours) exhibited a substantial Annexin V-FITC-positive population (~48%) in Caco-2 cells suggesting PS exposure on the cell surface. Also, a significant population (~22%) was observed to be both Annexin V-FITC and PI positive in Caco-2 cells corresponding to the late stages of cell death. Similarly, in THP-1 cells, ~28% and 67% cell populations correspond to the early and late stages of apoptosis. The total cell death considering early and late apoptotic population (Annexin V-FITC + Annexin V-FITC/PI positive cells) was in the range of ~70% and 80% for Caco-2 and THP-1 cells, respectively (Figure 4A & 4B). Therefore, these data revealed notable biochemical changes like PS flipping on the cell surface and

nuclear disintegration in target cells upon TDH treatment. *Vibrio cholerae* cytolysin (VCC) was used as the positive control for the experiment in Caco-2 cells (Figure 4A) [22]. Staurosporine served as positive control for the experiment in THP-1 cells (Figure 4B).

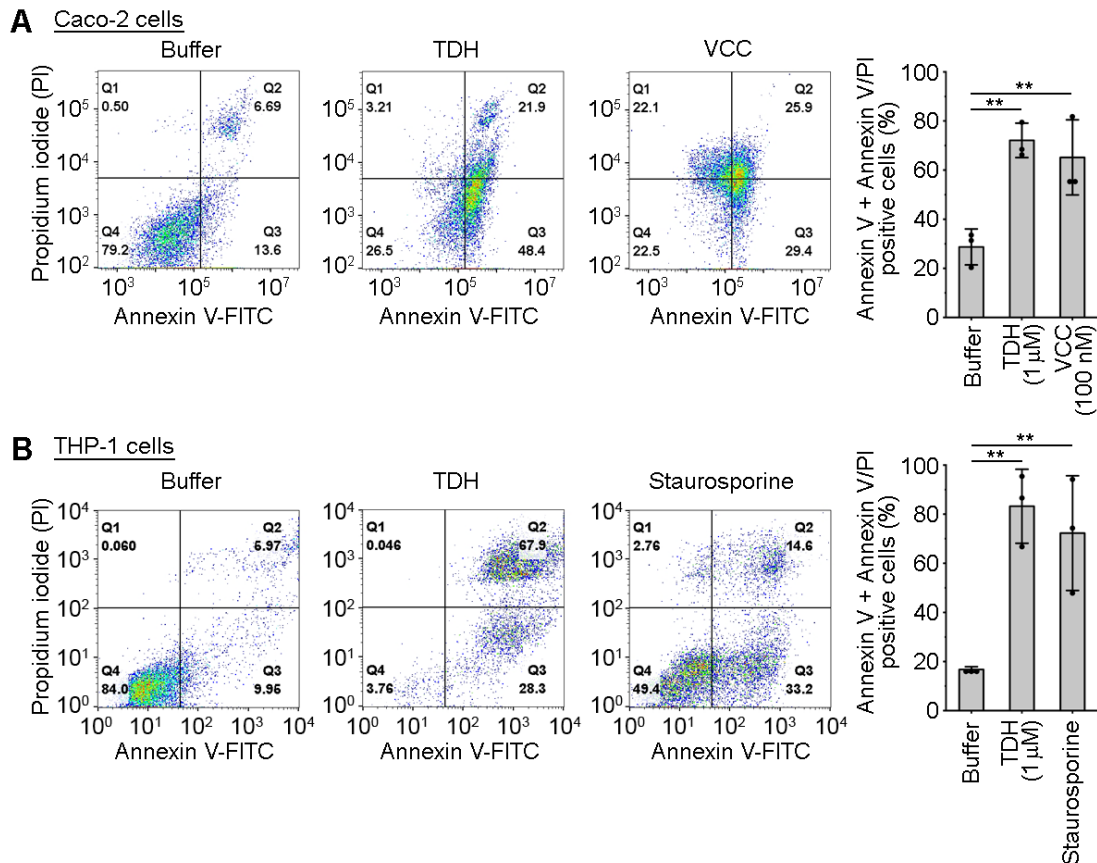


**Figure 4. TDH induces phosphatidylserine flipping and nuclear disintegration in target cells.** Flow cytometry profiles (left panels) showing an increase in Annexin V-FITC and PI staining in Caco-2 (A) and THP-1 (B) cells upon TDH treatment (1 μM; for 24 hours) over buffer treatment. VCC (100 nM; for 6 hours) and staurosporine (1 μM; for 6 hours) -treatments served as the positive control for the experiments in Caco-2 (A) and THP-1 (B) cells, respectively. Buffer-treated cells (for 24 hours) served as the negative control. Data shown here are the representatives of three independent experiments. Bar graph (right panel) represents the Annexin V + Annexin V/PI positive population (averages ± standard deviations of three independent experiments) corresponding to early + late apoptotic cell populations in both Caco-2 (A) and THP-1 (B) cells. \*\*p < 0.01; one-way ANOVA with Dunnett's multiple comparisons test.

Next, we analyzed the DNA damage in response to TDH intoxication, as DNA fragmentation is considered one of the peculiar features of any programmed cell death. In apoptosis, caspase-activated DNases (CADs) activation is responsible for the cleavage of nuclear DNA. The resulting DNA fragments are smaller in size (~100-200 base pairs) and mark a typical laddering pattern when visualized on the agarose gel [170, 171]. A characteristic DNA laddering pattern was observed in response to TDH treatment (0.5  $\mu$ M for 8 hours) in Caco-2 cells when analyzed by agarose gel electrophoresis (Figure 5). TDH-induced laddering pattern was found to be similar to that observed in response to staurosporine (1  $\mu$ M for 6 hours), thus, resembling the apoptotic cell death.

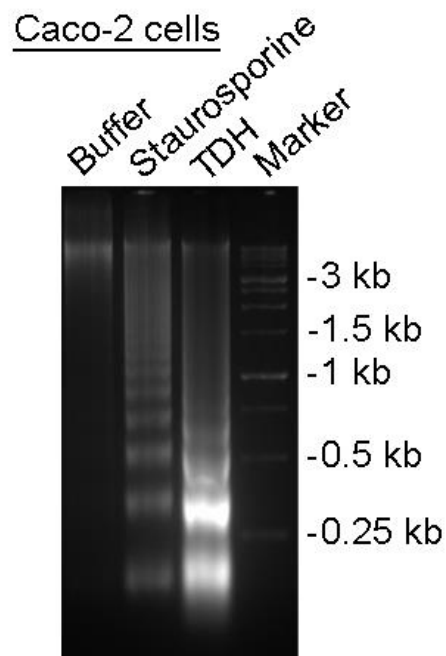


**Figure 5. TDH induces DNA fragmentation in Caco-2 cells, similar to that observed during apoptosis.** Agarose gel electrophoresis profile showing a laddering pattern of DNA fragmentation upon TDH treatment (0.5  $\mu$ M; for 8 hours) or buffer treatment (for 8 hours) in Caco-2 cells. DNA-laddering observed with staurosporine (1  $\mu$ M; for 6 hours) -treated Caco-2 cells served as the positive control. The data presented here is representative of three independent experiments.

Altogether, these results indicated the resemblance of TDH-induced biochemical changes in nucleated mammalian cells with that of apoptosis-like programmed cell death.

### **3.5. TDH-mediated cell death does not involve caspases as the key executioners**

Our findings thus far revealed that TDH induced various hallmark features of programmed apoptotic cell death in nucleated mammalian cells. However, to ascertain whether TDH could induce apoptosis in the target cells or not, we investigated the involvement of caspase(s). Caspases are considered as the key executioners and hallmark features of apoptosis. Both the extrinsic and intrinsic arms of apoptosis involves initiator caspases, which in turn activate the downstream executioner caspases [172]. Caspase-3 is considered the most active caspase during apoptosis and is processed into partially active p19 (larger subunit) and p12 (smaller subunit) forms by the initiator caspases. However, autoproteolytic cleavage of pro-domain from p19 subunit releases p17, a step necessary for complete catalytic activation of caspase-3 [173, 174].

Involvement of caspase-3 was examined using a flow cytometry-based assay to detect the levels of active caspase-3 in response to TDH treatment. Both THP-1 and Caco-2 cells were treated with TDH (0.5 and 1  $\mu$ M; for 8 hours) and further probed for active caspase-3 using FITC-conjugated anti-human active caspase-3 antibody. Cells treated with buffer and staurosporine served as the negative and positive control, for the experiment, respectively. Interestingly, any appreciable levels of active caspase-3 were not detected upon TDH intoxication in both Caco-2 and THP-1 cells (Figure 6A).

In addition to the flow cytometry assay, the activation of caspase-3 was probed using immunoblotting, in both Caco-2 and THP-1 cells upon TDH treatment (1  $\mu$ M; for 2, 4 and 8 hours) (These data were obtained in collaboration with Ms. Aakanksha Chauhan and Dr. Reena Thakur) [175]. Interestingly, the p19 subunit was found to be prominent while the p17 subunit was rather negligible in the immunoblots (Figure 6B). Staurosporine showed the processing of p19 to p17, serving as the positive control. These data suggest the partial processing of caspase-3 zymogen into the p19 form but the conversion from p19 to p17 form seems to be inhibited. Thus indicating that caspase-3 is not in its completely functional heterotetrameric form in TDH-mediated cell death. IAP (Inhibitor of Apoptosis) family proteins are known to inhibit the processing of

caspase-3 (and caspase-9 and -7) into p17 subunit by binding to the p19 subunit [174, 176, 177]. It is possible that in TDH-mediated cell death scenario, IAPs are possibly acting upon caspase-3 and hampering its catalytic activation.

The presence of partially active p19 form in immunoblots was in contrast to the flow-cytometry data, which failed to detect its presence along with the completely active p17 form, suggesting the inactive status of caspase-3. This could possibly be due to the differential sensitivity of antibodies for flow cytometry and immunoblots.

To confirm whether the catalytic activity of caspases is at all involved in the TDH-mediated cell death pathway, we employed ZVAD-fmk inhibitor-based study in THP-1 cells. ZVAD-fmk is a pan-caspase inhibitor that inhibits apoptotic caspases by irreversibly binding to their active site, thereby, blocking their catalytic function. THP-1 cells with and without ZVAD-fmk pre-treatment (40  $\mu$ M; 1 hour) were treated with TDH (0.5  $\mu$ M; 24 hours) and then subjected to flow cytometry-based Annexin V-FITC and PI staining to monitor the cell death. ZVAD-fmk pre-treatment did not show any reduction in early or late apoptotic populations in TDH-treated cells. Contrary to this, a marked decrease was observed upon ZVAD-fmk pre-treatment in early as well as late apoptotic populations of staurosporine-treated cells (Figure 6C).

Taken together, these data implied that TDH-mediated cell death response does not involve the participation of functional caspases and thus, TDH triggers a caspase-independent programmed cell death in target cells (Figure 6).

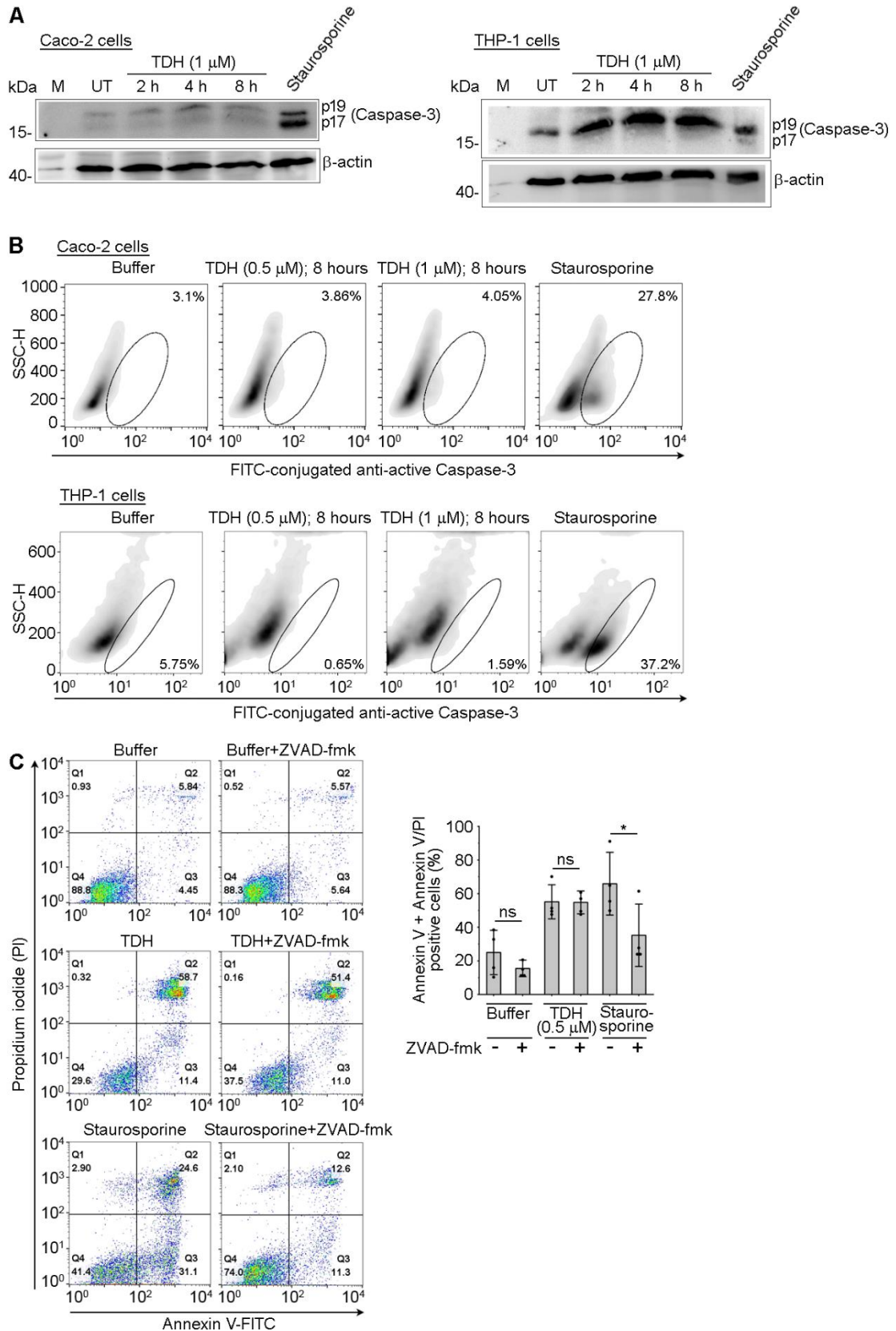


**Figure 6. TDH-mediated cell death is independent of caspase-activation.** (A) Flow cytometry-based density plots showing no appreciable levels of active caspase-3 in Caco-

2 (upper panels) and THP-1 cells (lower panels) upon TDH treatment (0.5  $\mu$ M; for 8 hours) suggesting inactive status of caspase-3. Buffer and staurosporine treated cells served as the negative and positive control, respectively for the experiments. Data presented here are the representatives of three independent experiments. (B) Western blot profiles showing absence of p17 subunit in Caco-2 (left panel) and THP-1 cells (right panel) upon TDH treatment (1  $\mu$ M; for 2, 4 and 8 hours) implying to the absence of active caspase-3. UT refers to untreated cells. Data shown here are the representatives of two or more independent experiments. (C) Flow cytometry profile showing effect of pan-caspase inhibitor ZVAD-fmk pre-treatment (40  $\mu$ M, for 1 hour) on programmed cell death response elicited by TDH (0.5  $\mu$ M, for 24 hours) in THP-1 cells. Buffer-treated cells were taken as the negative control. No decrease in Annexin V + Annexin V/PI positive populations was observed upon ZVAD-fmk pre-treatment for the TDH-intoxicated cells. Staurosporine (1  $\mu$ M, for 6 hours) treatment, with and without ZVAD-fmk pre-treatment served as the positive controls for the experiment. Bar graph shown in the right-most panel depicts Annexin V + Annexin V/PI positive cell populations upon buffer, TDH and staurosporine treatments, with or without ZVAD-fmk pre-treatment. Data shown here are the averages  $\pm$  standard deviations from four independent experiments. \* $p < 0.05$ ; ns, non-significant; one-way ANOVA with Tukey's multiple comparison test.

### **3.6. TDH induces mitochondrial membrane permeability transition (MMPT) in the target cells**

Mitochondria have been observed to be the central players in the execution of most of the programmed cell death pathways [107, 178, 179]. Mitochondrial membrane permeability transition (MMPT) and the accompanied mitochondrial damage may result in caspase-independent cell death [180]. Therefore, to explore the mechanistic details further, we examined the possible involvement of mitochondria in TDH-mediated programmed cell death. We probed for MMPT induction in response to TDH treatment in target cells by employing a flow cytometry-based JC-1 dye assay. In principle, JC-1 dye is a lipophilic cationic dye that tends to aggregate and exhibits red fluorescence in healthy mitochondria with intact membrane potential. In contrast, upon MMPT induction, JC-1 monomers leak out of the mitochondria resulting in a shift toward green

fluorescence. This transition from JC-1 aggregates to JC-1 monomers corresponds to a fluorescence shift from FL-2 to FL-1 channel in a flow cytometry plot [181]. Therefore, the JC-1 dye assay provides a quantitative measure of mitochondrial potential to detect mitochondrial damage. Both Caco-2 and THP-1 cells were intoxicated with TDH (1  $\mu$ M for 4 and 12 hours in Caco-2 cells; 0.5 and 1  $\mu$ M for 12 hours in THP-1 cells;) and subsequently, subjected to JC-1 dye assay. A substantial increase in JC-1 monomer-positive population was observed in response to TDH treatment (~71% of the Caco-2 cells and ~50% of the THP-1 cells when treated with 1  $\mu$ M TDH for 12 hours) over buffer-treated cells (Figure 7A & 7B). These data highlight that TDH intoxication disrupts the mitochondrial membrane potential in target cells, suggesting a potential role of mitochondria in TDH-mediated cell death.

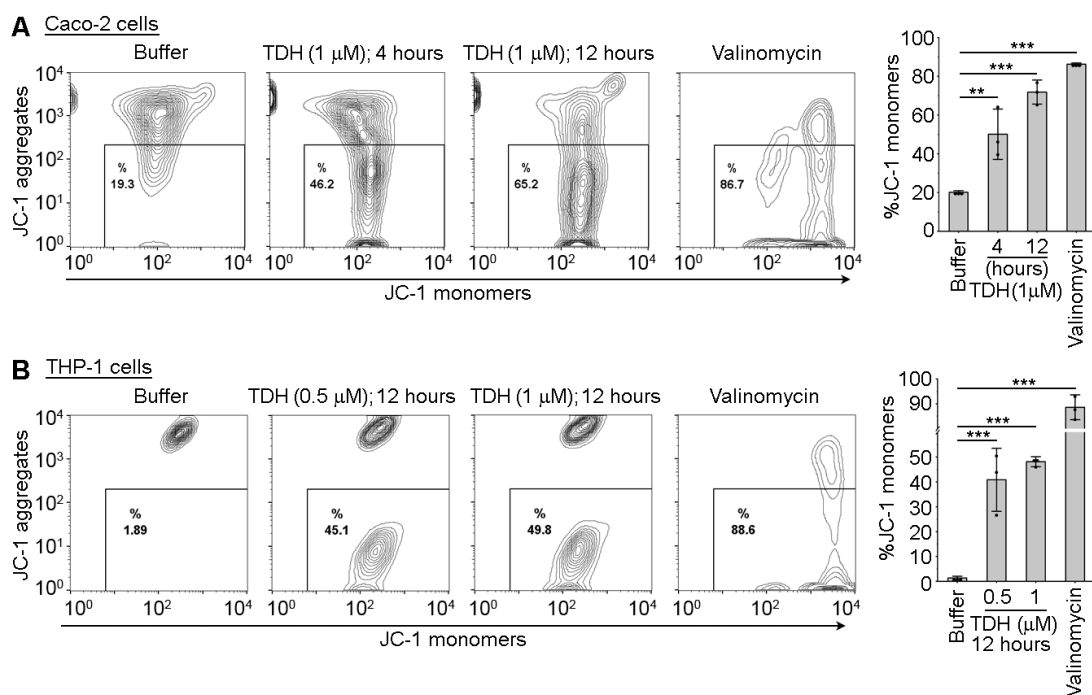


**Figure 7. TDH triggers mitochondrial membrane permeability transition (MMPT) in target cells.** Flow cytometry-based contour plots for (A) Caco-2 cells (upper panels) showing significant MMPT induction in response to TDH treatment (1  $\mu$ M; 4 and 12 hours) and (B) THP-1 cells (lower panels) showing significant MMPT induction upon TDH intoxication (0.5 and 1  $\mu$ M; for 12 hours). Buffer (12 hours) and valinomycin (1  $\mu$ g/ml, for 20 minutes) served as the negative and positive control for the experiments,

respectively. Data shown here are the representative of three independent experiments. Bar graphs (right-most panels of both A and B) displaying % JC-1 monomer positive cells for buffer, TDH and valinomycin treatments. Data plotted here are the averages  $\pm$  standard deviations from three independent experiments.  $**p < 0.01$ ;  $***p < 0.001$ ; one-way ANOVA with Dunnett's multiple comparison test.

### 3.7. TDH causes depletion of ATP pools in the target cells

To assess the consequences of TDH-mediated MMPT induction, we further checked ATP levels in Caco-2 levels. Since, mitochondria serve the powerhouse of the cell, its dysfunctioning may end up in diminished ATP levels. Also, PFTs are known to diminish the ATP pools in target cells [3, 182]. Therefore, it is possible that TDH being a potent PFT, may result in the depletion of ATP levels in the target cells. Interestingly, the levels of ATP in Caco-2 cells were indeed found diminished to a considerable extent upon TDH treatment (1  $\mu$ M; for 1 hour) over buffer-treated control cells (Figure 8).

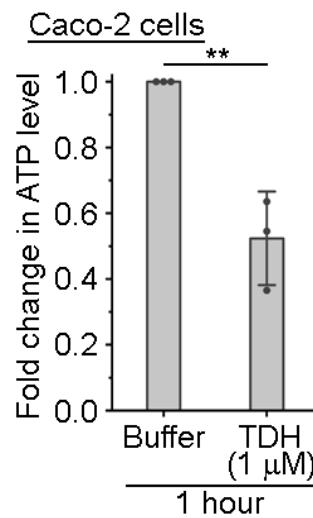


**Figure 8. TDH-mediated ATP depletion in Caco-2 cells.** Bar graph showing decrease in ATP levels of Caco-2 cells upon TDH treatment (1  $\mu$ M; for 1 hours) in comparison to buffer-treatment. Data represented here are the average  $\pm$  standard deviations from three independent experiments.  $**p < 0.01$ ; Student's unpaired *t*-test.

### 3.8. TDH triggers the release of cytochrome c from the mitochondria due to mitochondrial damage

Mitochondrial damage due to MMPT induction is accompanied by the release of various mitochondrial factors that may further take part in the execution of programmed cell death. Cytochrome c is one such mitochondrial factor that, under normal physiological conditions acts as an electron carrier of the electron transport chain in the mitochondria. During cell death induction, cytochrome c release into the cytoplasm eventually triggers the activation of caspases [101, 183]. Therefore, we probed for cytochrome c release as a potential outcome of MMPT induction by TDH intoxication. For this, Caco-2 and THP-1 cells were treated with TDH and probed for cytochrome c release using anti-cytochrome c antibody by following a flow cytometry-based assay as described in an earlier report [162], with slight modifications. It was observed that a significantly high percentage of the cell population (~70-75 % for both Caco-2 and THP-1 cells) showed loss of cytochrome c from their mitochondria over the buffer-treated control cells (Figure 9A & 9B). Thus, this data confirms that TDH causes mitochondrial damage that eventually results into the release of cytochrome c from the mitochondria of target cells.

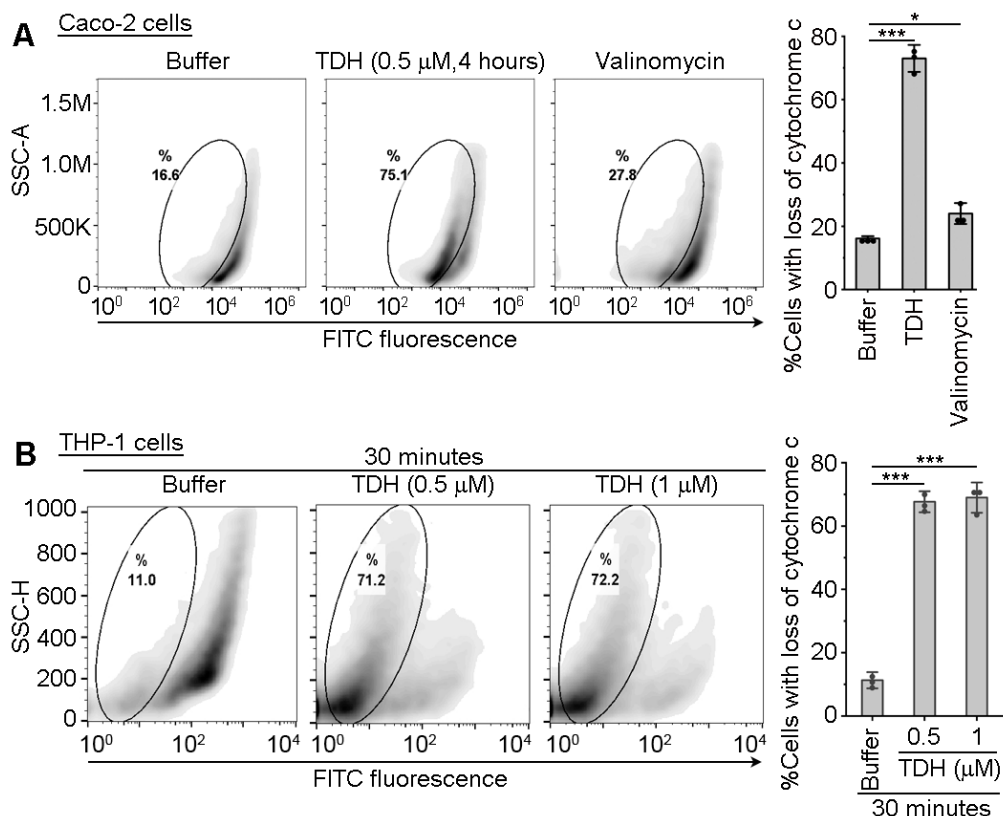


**Figure 9. TDH induces loss of cytochrome c in the target cells.** Flow cytometry profiles displaying (A) Caco-2 and (B) THP-1 cell populations with substantial loss of cytochrome c upon TDH treatment (0.5  $\mu$ M; for 4 hours in Caco-2 cells and 0.5 and 1  $\mu$ M; for 30 minutes in THP-1 cells). Buffer and valinomycin (1  $\mu$ g/ml for 20 minutes; for Caco-2 cells) served as the negative and positive control, respectively. Data shown here are the representative of three independent experiments. Bar graphs shown in the right-most showing percentage of cells exhibiting loss of cytochrome c upon respective treatments in (A) Caco-2 and (B) THP-1 cells. Data shown here are the averages  $\pm$  standard deviations from three independent experiments. \*\*\* $p < 0.001$ ; \* $p < 0.05$ ; one-way ANOVA with Dunnett's multiple comparison test.

### **3.9. TDH induces the translocation of apoptosis-inducing factor (AIF) from the mitochondria to the nucleus of target cells**

Another mitochondrial resident that is considered a critical executioner of the caspase-independent cell death is apoptosis-inducing factor (AIF). During normal conditions, AIF functions as an oxidoreductase in the mitochondria. However, AIF translocates to the nucleus upon mitochondrial damage, promoting chromatin condensation and DNA fragmentation [184, 185]. In order to examine the involvement of AIF in TDH-induced cell death, we probed for its migration from mitochondria to the nucleus in the target cells. The mitochondrial and nuclear fractions of Caco-2 cells treated with TDH (1  $\mu$ M; for 1 and 2 hours) were subjected to immunoblotting. AIF levels were observed to decrease from mitochondrial fractions, and at the same time, there was an increase in AIF levels in the nuclear fractions of Caco-2 cells in response to TDH treatment (Figure 10A & 10B). Similar observations were recorded for TDH-treated THP-1 cells (1  $\mu$ M; for 0.5, 1 and 2 hours) where, translocation of AIF from mitochondria to the non-mitochondrial fractions and then to the nucleus was observed (Figure 10C, 10D & 10E). Based on these observations, we inferred that TDH-mediated mitochondrial damage in target cells results in the release of AIF from the mitochondria and its subsequent translocation to the nucleus.

Nuclear translocation of AIF leads to peripheral chromatin condensation and DNA fragmentation. It is noteworthy that AIF usually cleaves DNA into larger fragments

(~50 kb) [186]. On the contrary, our observation showed that TDH treatment generates smaller oligonucleosomal fragments (~100-200 kb), displaying a laddering pattern on the agarose gel (as shown in Figure 5). Thus, a possible additional factor with nuclease activity might be responsible for smaller DNA fragmentation in the caspase-independent cell death scenario.

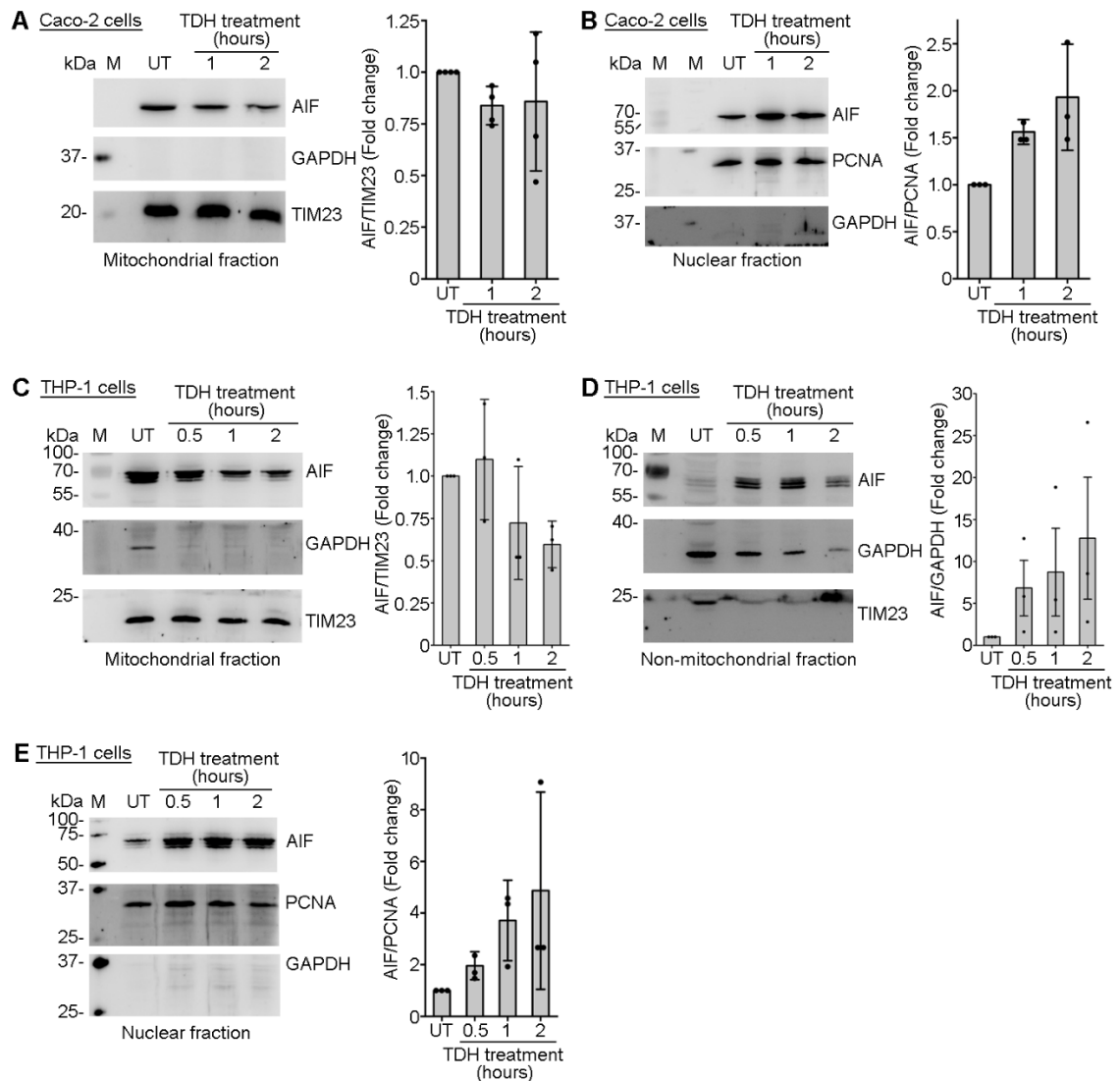


**Figure 10. TDH-induced MMPT causes the release of apoptosis inducing factor (AIF) from the mitochondria, which further translocates to the nucleus.** (A) Western blot profile showing loss of AIF from the mitochondrial fraction of Caco-2 cells upon TDH treatment (1  $\mu$ M; for 1 and 2 hours) in comparison to the mitochondrial fraction of untreated (UT) cells. TIM23 was probed as a mitochondrial marker while GAPDH, a

cytoplasmic marker was checked for cytoplasmic contamination in the mitochondrial fraction. (B) Western blot profile showing increase in AIF levels in the nuclear fraction of Caco-2 cells upon TDH treatment (1  $\mu$ M; for 1 and 2 hours) over the untreated (UT) cells. PCNA, a nuclear marker was probed to detect the nuclear load. GAPDH was probed for any cytoplasmic contamination in the nuclear fraction. (C) Western blot profile exhibiting the decreasing levels of AIF from the mitochondrial fractions of THP-1 cells upon TDH treatment (1  $\mu$ M; for 0.5, 1 and 2 hours) in comparison to the mitochondrial fractions of untreated (UT) cells. TIM23 served as the mitochondrial marker while GAPDH served as the marker for cytoplasmic contamination. (D) Western blot profiles showing the increasing levels of AIF in non-mitochondrial fractions (obtained during mitochondrial isolation) of THP-1 cells upon TDH treatment (1  $\mu$ M; for 0.5, 1 and 2 hours) over untreated (UT) cells. GAPDH, a cytoplasmic marker was probed for the load of the non-mitochondrial fraction while TIM23 was probed for mitochondrial contamination. (E) Western blot profile showing increased levels of AIF in the nuclear fractions of THP-1 cells in response to TDH intoxication (1  $\mu$ M; for 0.5, 1 and 2 hours) over untreated cells. PCNA was probed for nuclear load while GAPDH was probed for cytoplasmic contamination. Lane M stands for the molecular weight markers. Bar graph adjacent to the immunoblots shows the densitometric analysis of AIF calculated as fold change over normalized loading control in respective blots. Data shown here are representatives of three or more independent experiments.

### **3.10. TDH causes the translocation of endonuclease G to the nucleus of target cells, justifying the DNA-laddering pattern in caspase-independent cell death**

Endonuclease G (Endo G) is a mitochondrial resident protein required for mitochondrial DNA replication, recombination, and degradation [187]. Upon MMPT induction, it is released from the mitochondria into the cytoplasm and subsequently translocates to the nucleus. It breaks down the nuclear DNA into smaller fragments (~100-200 kb) in a caspase-independent manner. It has been documented that similar to CAD-mediated DNA cleavage, endo G also creates DNA fragments that generate a laddering pattern on agarose gel [188, 189]. Toward exploring the possible involvement of endo G in TDH-mediated cell death, we probed its migration into the nuclear fractions of Caco-2 and THP-1 cells treated with TDH (1  $\mu$ M; for 1 and 2 hours) ( Data for THP-1 cells were

obtained in collaboration with Ms. Aakanksha Chauhan and Dr. Reena Thakur) [175]. Immunoblots showed an increase in endo G levels in the nuclear fractions of both the cell types in response to TDH treatment, confirming its involvement in cell death induced by TDH (Figure 11A & 11B). Therefore, our data supported the possible justification for the caspase-independent DNA laddering pattern obtained in response to TDH (shown in Figure 5).

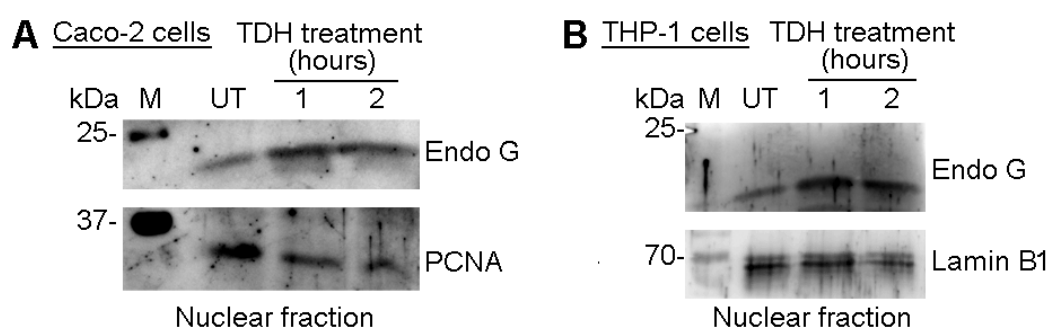


**Figure 11. TDH-induced MMPT leads to the nuclear translocation of endonuclease G (Endo G) in target cells.** Western blot profiles showing increased levels of endo G in the nuclear fractions of Caco-2 (A) and THP-1 (B) cells upon TDH treatment (1  $\mu$ M; for 1 and 2 hours) in comparison to the nuclear fractions of untreated (UT) cells. PCNA and Lamin B1 were used as nuclear markers in Caco-2 and THP-1 cells, respectively. Lane M stands for the molecular weight markers. Data presented here are the representative of three or more independent experiments.

### 3.11. TDH induces ROS production in the target cells

Reactive oxygen species (ROS) are critical signaling molecules contributing to various cellular processes such as cell differentiation, proliferation, immune responses, cell survival and cell death. Also, the generation of excessive oxidative stress may trigger the mitochondrial pathway of programmed cell death [190, 191]. Therefore, we further investigated the participation of ROS in TDH-associated mitochondrial damage or cell death. Firstly, intracellular ROS production was examined in Caco-2 cells in response to TDH intoxication (0.5  $\mu$ M for 2 hours) by monitoring DCFDA fluorescence as an indicator of ROS production. Flow cytometry profile showed a marked increase in

DCFDA fluorescence with TDH treatment over buffer, implying elevated intracellular ROS levels in response to TDH treatment (Figure 12A). Next, we checked whether TDH treatment could lead to the production of mitochondrial ROS/superoxide (mitoROS). We assessed the mitoROS generation in Caco-2 cells treated with TDH (0.2  $\mu$ M; for 30 minutes) and buffer using mitoSOX, a mitochondrial superoxide indicator. As observed through fluorescence microscopy, TDH-treated cells displayed significantly increased mitoSOX fluorescence intensity over buffer-treated cells, thus indicating mitoROS generation by TDH (Figure 12B).

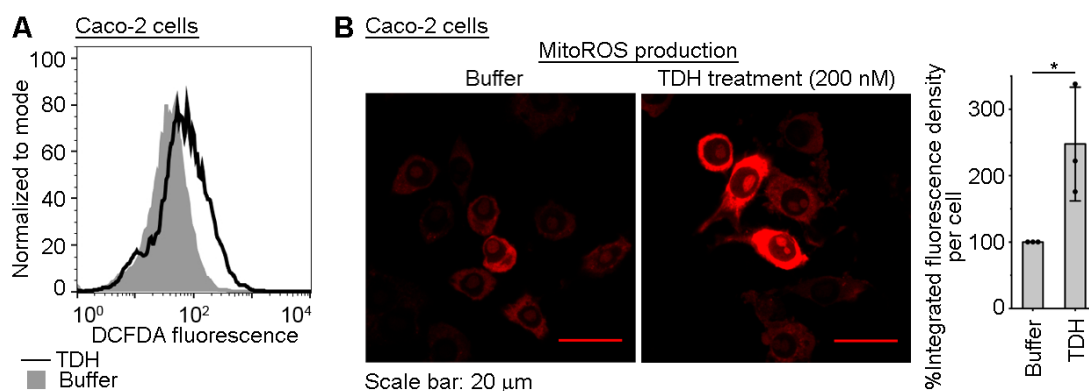


**Figure 12. TDH induces ROS production in Caco-2 cells.** (A) Flow cytometry-based histogram plot showing increased DCFDA fluorescence corresponding to an increased ROS production in Caco-2 cells upon TDH treatment (0.5  $\mu$ M; for 2 hours) over the buffer treatment. Data shown here are the representative of three independent experiments. (B) Fluorescence microscopy images showing increased mitoSOX fluorescence indicating increased mitochondrial ROS production in Caco-2 cells upon TDH treatment (0.2  $\mu$ M; for 30 minutes) in comparison to the buffer treatment. Images shown here are the representative of 30 images obtained from three independent experiments. Bar graph (right panel) representing quantification for micrographs showing mitoROS production. Higher mitoSOX fluorescence was observed in terms of percentage of integrated fluorescence density per cell observed for TDH-treated cells than buffer treatment. Data represented here are the averages  $\pm$  standard deviations from three independent experiments. \* $p$  < 0.05; Student's unpaired  $t$ -test.

Toward exploring whether ROS production has any critical role in TDH-mediated cell death, we checked the effect of ROS scavenging on TDH cytotoxicity. We observed that the pre-treatment of Caco-2 cells with a ROS scavenger, NAC (5 and 10 mM; for 2 hours), considerably reduced the intracellular ROS production by TDH treatment (0.5  $\mu$ M; for 2 hours) as observed by a decrease in DCFDA fluorescence with NAC pre-treatment (Figure 13A). In contrast, the NAC pre-treatment could only marginally affect/reduce the cytotoxicity levels of TDH (Figure 13B).

Considering these results, we inferred that TDH induces ROS generation in target cells; however, ROS might not be the only critical signaling mediator of the cell death pathway induced by TDH.

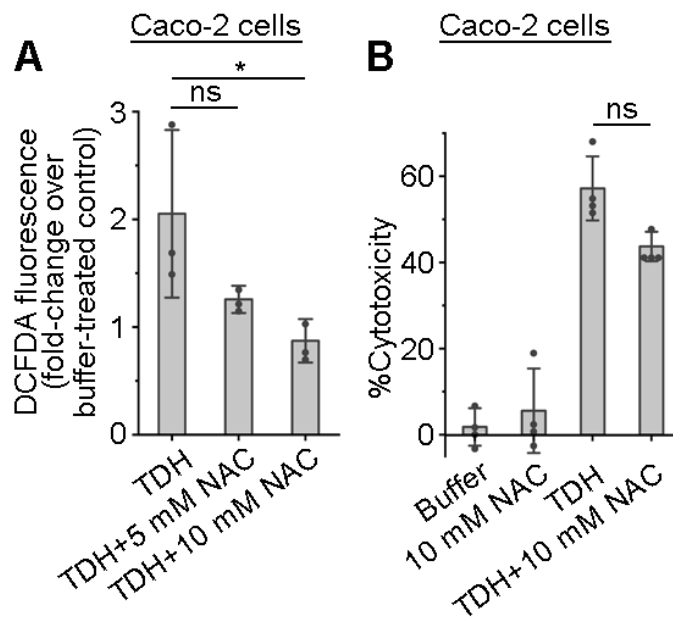


**Figure 13. ROS production does not appear to be the sole player of TDH-mediated cell death pathway.** (A) Bar graph depicting marked decrease in TDH-mediated ROS production (TDH treatment was 0.5  $\mu$ M; for 2 hours) in Caco-2 cells upon pre-treatment with NAC (5 and 10 mM; for 2 hours). DCFDA fluorescence of each sample was quantified as fold change over buffer treatment. Data shown here are the averages  $\pm$  standard deviations from three independent experiments. ns, non-significant; \* $p < 0.05$ ; one-way ANOVA with Dunnett's multiple comparison test. (B) Bar graph showing marginal decrease in the cytotoxicity of TDH (0.5  $\mu$ M; for 2 hours) in Caco-2 cells upon NAC-pre-treatment (10 mM; for 2 hours). Data shown here are the averages  $\pm$  standard

deviations from four independent experiments.  $^{**}p < 0.01$ ; ns, non-significant; one-way ANOVA with Tukey's multiple comparison test.

### **3.12. TDH induces ROS-mediated calcium influx in target cells**

Apart from ROS, calcium is another critical signaling molecule involved in various cellular processes, including cell death [192-194]. Excessive calcium overload in a cell can bring about mitochondrial and endoplasmic reticulum stress. In context to our results, we attempted to explore the implications of calcium in TDH-mediated cell death. We first checked whether TDH treatment (0.5  $\mu$ M) could induce calcium flux in THP-1 and Caco-2 cells, by monitoring Fluo-4-AM fluorescence for 10-15 min using flow cytometry. Fluo-4-AM is a cell-permeant probe that detects cytoplasmic calcium levels. A spike in the fluorescence intensity of Fluo-4 upon TDH treatment compared to buffer treatment suggested a calcium flux in both Caco-2 and THP-1 cells (Figure 14A). PMA + Ionomycin showed a striking increase in the fluorescence intensity and served as the positive control for the experiment. Next, calcium flux was examined without any extracellular calcium provided to the Caco-2 cells upon respective treatments. TDH-treated cells showed a basal fluorescence level similar to buffer-treated cells suggesting that TDH triggers an influx of extracellular calcium in target cells (Figure 14B). Toward exploring the interplay of ROS and calcium in TDH-mediated cell death, calcium influx was monitored in Caco-2 cells upon ROS scavenging by NAC. Pre-treatment of NAC scavenger (10 mM; for 2 hours) led to a noticeable decrease in the TDH-mediated calcium influx, suggesting a ROS-triggered calcium influx in the TDH-treated cells (Figure 14C). Next, to determine the direct impact of calcium on the cytotoxicity of TDH, cells were loaded with BAPTA-AM, a calcium chelator. BAPTA-AM pre-treatment (10  $\mu$ M; for 1 hour) resulted in a notable reduction in the fluorescence signal corresponding to calcium influx. However, BAPTA-AM-mediated calcium quenching led to only a marginal decrease in TDH cytotoxicity.

Altogether, these observations suggest that TDH induces prominent calcium influx in target cells, which might be linked to an enhanced ROS generation. However, based on our data, it appears calcium is not the sole mediator of the TDH-mediated cell death pathway.

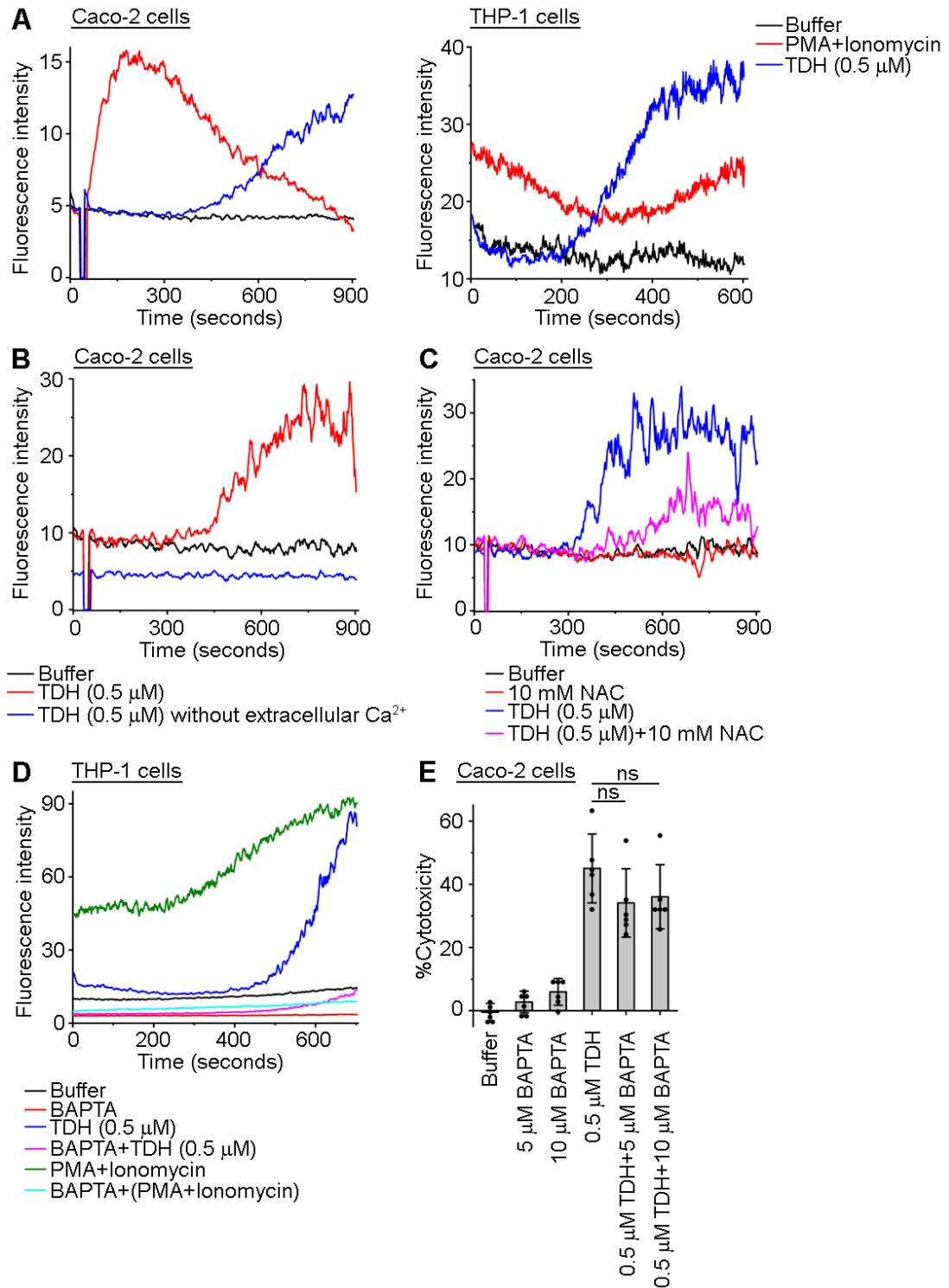


**Figure 14. TDH induces ROS-mediated calcium influx, while calcium chelation does not affect TDH-mediated cytotoxicity in the target cells.** (A) Flow cytometry-based data showing calcium kinetics in response to TDH treatment (0.5  $\mu$ M) in both Caco-2 (left panel) and THP-1 cells (right panel). Increased Fluo-4-AM intensities in presence

of extracellular calcium coresponded to the calcium surge upon TDH treatment in the cells. Buffer and PMA + Ionomycin served as negative and positive controls for the experiments, respectively. Data shown here are the representatives of three independent experiments. (B) Calcium kinetics plot showing that the absence of extracellular calcium resulted in the absence of any increased Fluo-4-AM intensity when monitored over 15 minutes, after TDH treatment (0.5  $\mu$ M) in Caco-2 cells. Buffer-treated cells served as the negative control, while TDH treatment in presence of extracellular calcium served as positive control for the experiment. Data shown here are the representatives of three independent experiments. (C) Calcium kinetics plot showing compromised calcium influx by TDH (0.5  $\mu$ M; monitored for 15 minutes) in Caco-2 cells, upon ROS scavenging by NAC pre-treatment (10 mM; for 2 hours). Data shown here are the representatives of three independent experiments. (D) Calcium kinetics plot showing compromised TDH-mediated (0.5  $\mu$ M) calcium influx in THP-1 cells upon calcium chelation by BAPTA-AM pre-treatment (10  $\mu$ M; for 1 hour). Data shown here are the representatives of three independent experiments. (E) Bar graph showing only a marginal decrease in TDH-mediated (0.5  $\mu$ M; for 8 hours) cytotoxicity levels upon calcium chelation by BAPTA-AM (5 and 10  $\mu$ M; pre-treatment for 1 hour) in Caco-2 cells. Data shown here are the averages  $\pm$  standard deviations from six independent experiments. *ns*, non-significant; one-way ANOVA with Tukey's multiple comparison test.

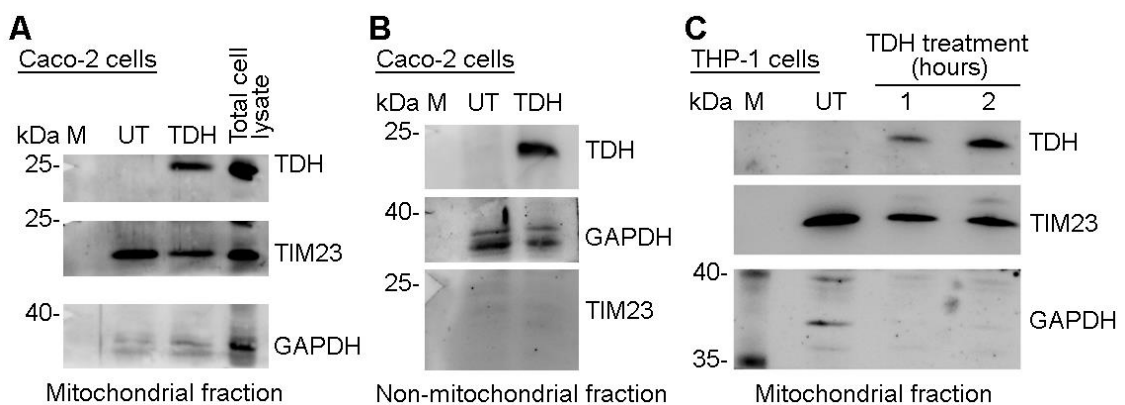
### **3.13. TDH translocates to the mitochondria of the target cells**

Bacterial virulence factors, including bacterial PFTs, have been documented to translocate to the mitochondria of host cells, where they may trigger mitochondrial dysfunctioning or damage [22, 67, 85, 163, 195-197]. Toward understanding the mechanistic details of TDH-mediated mitochondrial damage, we explore the possibility of migration of TDH to the mitochondria of target cells. Mitochondrial fractions isolated from TDH-treated Caco-2 and THP-1 cells (1  $\mu$ M; for 1 and 2 hours) were probed for the presence of TDH by immunoblotting (Data for Caco-2 cells was obtained in collaboration with Ms. Aakanksha Chauhan and Dr. Reena Thakur) [175]. Interestingly, the mitochondrial fractions of both Caco-2 and THP-1 cells exhibited the presence of TDH, implying the mitochondrial translocation of TDH (Figure 15A & 15C). Additionally, confocal microscopy data showed some detectable level of colocalization

of TDH with the mitochondrial marker TOM20 in Caco-2 cells (Figure 15D). We also checked for the colocalization between the plasma membrane marker sodium potassium ATPase (a negative control) and mitochondrial marker, TOM20 in Caco-2 cells and as expected, we did not find any colocalization between these two markers (Figure 15E) (In this section, the confocal microscopy-based experiments were performed by Ms. Kusum Lata) [175]. Therefore, sodium potassium ATPase colocalization with TOM20 served as an appropriate negative control confirming that our experimental setup, image acquisition and analysis can resolve the fluorescence signals for the plasma membrane marker and the mitochondrial marker.

It is noteworthy that apart from the presence of TDH in mitochondrial fractions, TDH was also detected in the non-mitochondrial fraction of Caco-2 cells (Figure 15B). Similarly, confocal microscopy data also showed only a detectable level of colocalization of TDH with the mitochondria (Figure 15D). Therefore, these observations clearly indicate that only a fraction of membrane-bound TDH translocates to the mitochondria of target cells.

Nevertheless, these data revealed that TDH exhibits a prominent propensity to translocate to the target cell mitochondria.



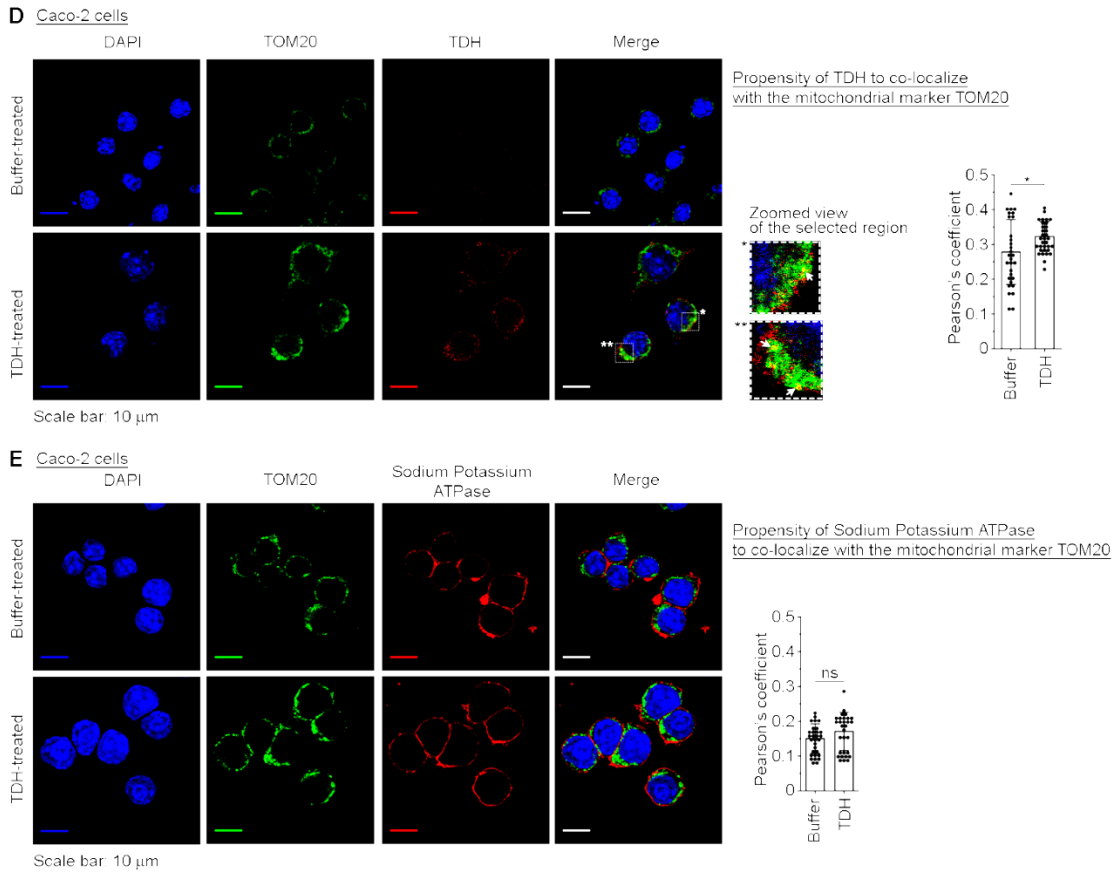


**Figure 15. TDH exhibits significant propensity to translocate to the mitochondria of target cells.** (A) Western blot profile showing presence of TDH in the isolated mitochondrial fractions of TDH-treated (1  $\mu$ M; for 2 hours) Caco-2 cells. (B) Western blot profile showing the presence of TDH in the non-mitochondrial fractions of Caco-2 cells treated with TDH (1  $\mu$ M; for 2 hours). (C) Western blot profile showing presence of TDH in the isolated mitochondrial fractions of TDH-treated (1  $\mu$ M; for 1 and 2 hours) THP-1 cells. TIM23 was probed as a mitochondrial marker while GAPDH was probed as cytoplasmic marker in these blots. Untreated cells (lane marked as UT) served as the controls. Lane M stands for molecular weight markers. (D) Confocal microscopy images showing detectable level of colocalization of TDH (red) with mitochondrial marker, TOM20 (green) in Caco-2 cells. Zoomed view of the selected regions (marked with \* and \*\*) shows some noticeable co-localization of TDH with TOM20 (yellow), and are indicated with arrows. Total 33 images for the TDH treatment (1  $\mu$ M; for 2 hours) and 30 images for the corresponding buffer treatment, from three independent experiments, were analysed and the representative images are shown here (left panels). (E) Confocal microscopy images showing no detectable levels of co-localization between sodium

potassium ATPase (red), a plasma membrane marker and TOM20 (green), serving as control for the specificity of colocalization signals. DAPI (blue) stained the nucleus of the cells. Buffer-treated cells served as the negative control. A total of 30 images, each for TDH and buffer-treated cells, from three independent experiments, were analysed, and representative images are shown here. Bar graph (right-most panel shown in D) depicts the Pearson's correlation coefficient values of colocalization between TDH and TOM20 indicating significant propensity of TDH to co-localize with the mitochondrial marker TOM20 in TDH-treated cells in comparison to the buffer-treated cells. Data shown here are the averages  $\pm$  standard deviations of 33 and 30 images for TDH and buffer treatments, respectively. \* $p < 0.05$ ; Student's unpaired t-test. Bar graph (right-most panel shown in E) depicts the Pearson's correlation coefficient values of colocalization between sodium potassium ATPase and TOM20 showing no significant levels of colocalization between the two in TDH-treated cells over corresponding buffer treatment. Data shown here are averages  $\pm$  standard deviations of 30 images for both TDH and buffer treatments. ns, non-significant; Student's unpaired t-test.

### **3.14. TDH association with the isolated mitochondria does not induce mitochondrial damage**

In the above section, we observed that TDH shows prominent ability to translocate to the mitochondria. Previously, we also observed that TDH could trigger MMPT induction in target cells. Therefore, as observed in case of other PFTs and bacterial virulence factors, it might be possible that the mitochondrial translocation of TDH itself can bring about mitochondrial damage [163, 195, 197, 198]. To explore such a possibility, we checked whether TDH could associate directly with the isolated mitochondria and induce mitochondrial damage. For this, isolated mitochondria from Caco-2 cells were treated with TDH (1  $\mu$ M; for 30 minutes) and probed for TDH binding using Anti-TDH antisera. The flow cytometry-based histogram profile showed that indeed TDH can associate with isolated mitochondria (Figure 16A). Immunoblotting also confirmed association of TDH with the isolated mitochondria (Figure 16B) (Immunoblot assays were performed in collaboration with Ms. Aakanksha Chauhan) [175]. Next, we examined the mitochondrial damage due to the direct association of TDH with the isolated mitochondria. Therefore, we probed the loss of AIF from the isolated mitochondria as a

signature of the mitochondrial damage. For this, isolated mitochondria from Caco-2 cells were treated with TDH (1  $\mu$ M; for 30 minutes) and probed for loss of AIF via flow cytometry using anti-AIF antibody. Untreated mitochondria isolated from untreated cells served as the negative control for the experiment. Since we have already observed that TDH induces AIF release from the mitochondria upon TDH treatment in target cells by immunoblotting in earlier sections, mitochondria isolated from the TDH-treated cells served as the positive control for the experiment. Interestingly, we did not observe AIF release upon direct TDH treatment to the isolated mitochondria over isolated untreated mitochondria (Figure 16C). However, a significant mitochondrial population showed the loss of AIF in the mitochondria isolated from the TDH-treated cells. Moreover, results obtained from immunoblotting confirmed that isolated mitochondria upon TDH treatment did not show any decrease in the AIF levels (Figure 16D) (Immunoblot assays were performed in collaboration with Ms. Aakanksha Chauhan) [175]. Therefore, these results highlighted that although TDH can interact directly with the isolated mitochondria, this interaction is not sufficient for inducing mitochondrial damage. TDH is capable of inducing MMPT only when administered to the cells. Thus, indicating the possible requirement of cytosolic component(s)/signal(s) to induce MMPT and TDH translocation alone is insufficient.

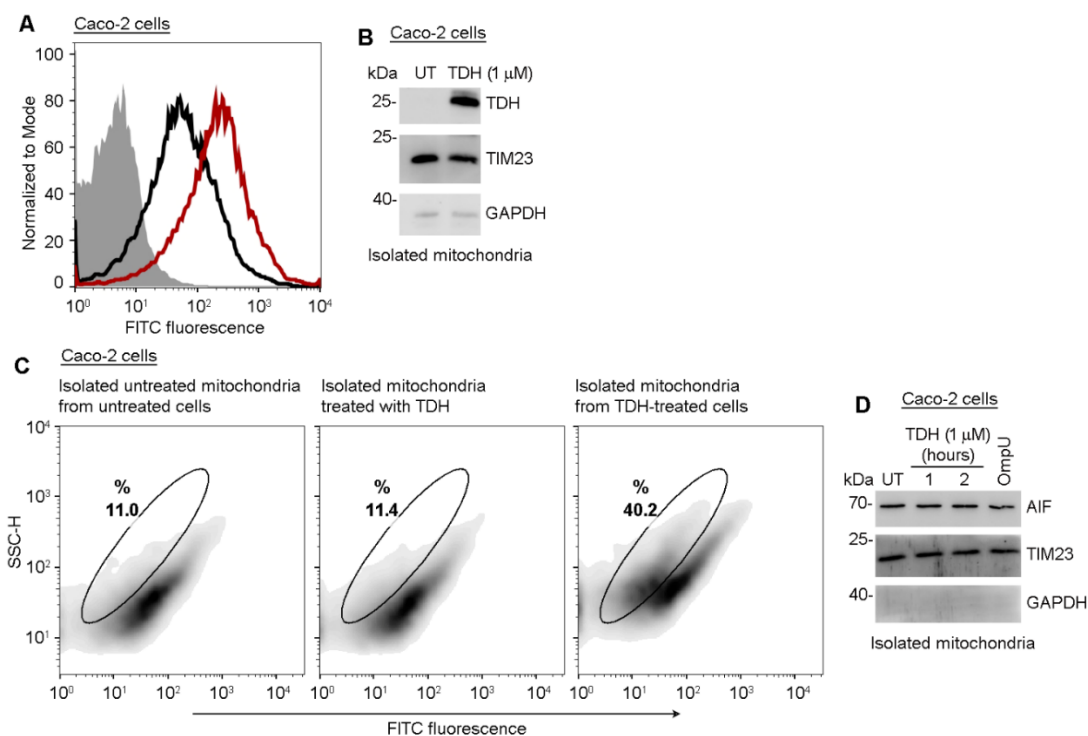


**Figure 16. TDH exhibits association with isolated mitochondria of Caco-2 cells without inducing AIF release from them.** (A) Flow cytometry-based histogram plots showing association of TDH with isolated mitochondria of Caco-2 cells. Isolated mitochondrial fraction from untreated Caco-2 cells were treated with TDH (1  $\mu$ M; for 30 minutes) and stained using anti-TDH antisera and FITC-conjugated secondary antibody (shown as red line). Buffer-treated isolated mitochondrial fraction stained with primary and secondary antibodies served as the control and is shown as black line. Unstained, buffer-treated isolated mitochondrial fraction (solid grey) is also shown. Data shown here are the representative of four independent experiments. (B) Western blot profile showing association of TDH with isolated mitochondria obtained from untreated Caco-2 cells and then, treated with TDH (1  $\mu$ M; for 1 hour). Untreated (UT) isolated mitochondrial fraction served as the negative control. TIM23 and GAPDH were probed for mitochondrial load and cytoplasmic contamination respectively. (C) Flow cytometry profiles showing no prominent AIF release from the isolated mitochondrial fractions of Caco-2 cells when treated with TDH (1  $\mu$ M for 30 minutes). Isolated untreated mitochondria from the untreated cells served as the negative control, while isolated mitochondria from the TDH-treated cells served as the positive control. Data presented here are the representatives of three independent experiments. (D) Western blot profile showing no loss of AIF from the isolated mitochondrial fractions of Caco-2 cells, upon direct TDH treatment (1  $\mu$ M; for 1 and 2 hours). Loss of AIF from the isolated mitochondria upon *V. cholerae* OmpU treatment (5  $\mu$ g/ml; for 2 hours) served as the positive control for the experiment [3]. Untreated (UT) isolated mitochondria from untreated cells served as the negative control. TIM23 and GAPDH were probed as the mitochondrial marker and cytoplasmic contamination in the isolated mitochondrial fraction, respectively. Data shown here are the representatives of three or more independent experiments.

### **3.15. TDH causes increased *bax/bcl-2* ratio along with mitochondrial recruitment of active bax molecules in the target cells**

In search for the cytosolic component or signal, we investigated the possible involvement of members of the Bcl-2 family. Reports suggest that members of the Bcl-2 family play significant roles in the programmed cell death pathways [199-201]. Under

pathophysiological conditions, cellular levels of pro-apoptotic molecules like bax may upregulate, while anti-apoptotic molecules like bcl-2 may undergo downregulation. Therefore, an overall increase in the bax/bcl-2 ratio can be seen in the damaged cells. This results in the recruitment of active bax molecules by displacing the bcl-2 molecules from the mitochondria. Subsequently, Bax molecules oligomerize and form Bax pores, resulting in mitochondrial outer membrane permeabilization (MOMP). This, in turn, may lead to loss of mitochondrial potential. To seek any potential interplay of the pro-apoptotic and anti-apoptotic molecules in TDH-mediated cell death, we estimated the bax/bcl-2 levels in TDH-treated THP-1 and Caco-2 cells. Semi-quantitative RT-PCR analysis data revealed ~3.5-fold and ~2-fold bax/bcl-2 ratio in Caco-2 and THP-1 cells, respectively (Figure 17A). This data led us toward the possible involvement of bax/bcl-2 in the TDH-mediated cell death pathway.

Next, we checked for the Bax recruitment to the mitochondria to confirm its involvement in mitochondrial damage in TDH-mediated cell death. Mitochondrial fractions isolated from Caco-2 and THP-1 cells treated with TDH (1  $\mu$ M; for 1 or 2 hours) were subjected to immunoblotting using an anti-active Bax monoclonal antibody (Immunoblot assays for THP-1 cells were performed in collaboration with Ms. Aakanksha Chauhan) [175]. The blots showed a substantial increase in the presence of active Bax in the mitochondrial fractions in response to TDH treatment (Figure 17B).

Overall, these results implied that Bax actively participates in the TDH-mediated cell death pathway. Our data demonstrated active-Bax association with mitochondria upon TDH intoxication in target cells. Increased recruitment of Bax on target cell mitochondria could induce mitochondrial damage, as observed in TDH-mediated cell death responses.

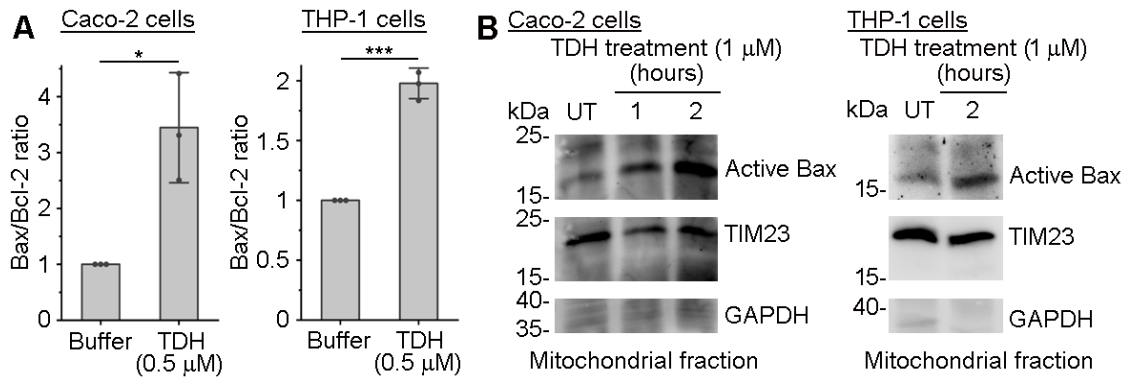


**Figure 17. TDH induces elevated bax/bcl-2 ratio and increased mitochondrial translocation of Bax in target cells.** (A) Semi-quantitative RT-PCR profiles of Caco-2 (left panel) and THP-1 cells (right panel) showing increased bax/bcl-2 gene expression levels upon TDH treatment (0.5 μM; for 8 hours) with respect to the buffer treatment. Data presented here are the averages ± standard deviations from three independent experiments. \* $p < 0.05$ ; \*\*\* $p < 0.001$ ; Student's unpaired  $t$ -test. (B) Western blot profiles showing an increased active Bax recruitment to the mitochondria of Caco-2 (left panel) and THP-1 cells (right panel) upon TDH treatment (1 μM). Mitochondrial fractions obtained from untreated cells (UT) served as the negative control for the experiment. TIM23 and GAPDH were probed as the mitochondrial marker and cytoplasmic contamination in the isolated mitochondrial fraction, respectively. Blots presented here are the representatives of two or more independent experiments.

### 3.16. TDH induces permeabilization of lysosomal membrane

Further, in order to check the effect of TDH on other organelles, we explored the impact of TDH intoxication on the lysosomes in target cells. Lysosomes are important organelles that harbours acidic hydrolases and some of the hydrolases upon lysosomal membrane permeabilization (LMP) may release into the cytosol and take part in caspase-independent cell death [202-204]. Therefore, we checked for LMP by employing lysotracker, a cell-permeable acidotropic dye that tend to accumulate in acidic organelles such as lysosomes. LMP can be detected using lysotracker by monitoring the decrease in its fluorescence. Using confocal microscopy, we observed that Caco-2 cells treated with TDH (0.5 μM; for 1 hour) displayed a substantial decrease in lysotracker fluorescence intensity in comparison to the buffer-treated cells (Figure 18) (This data has been

obtained in collaboration with Ms. Kusum Lata) [175]. This result clearly suggests that TDH intoxication in Caco-2 cells induces lysosomal membrane permeabilization.

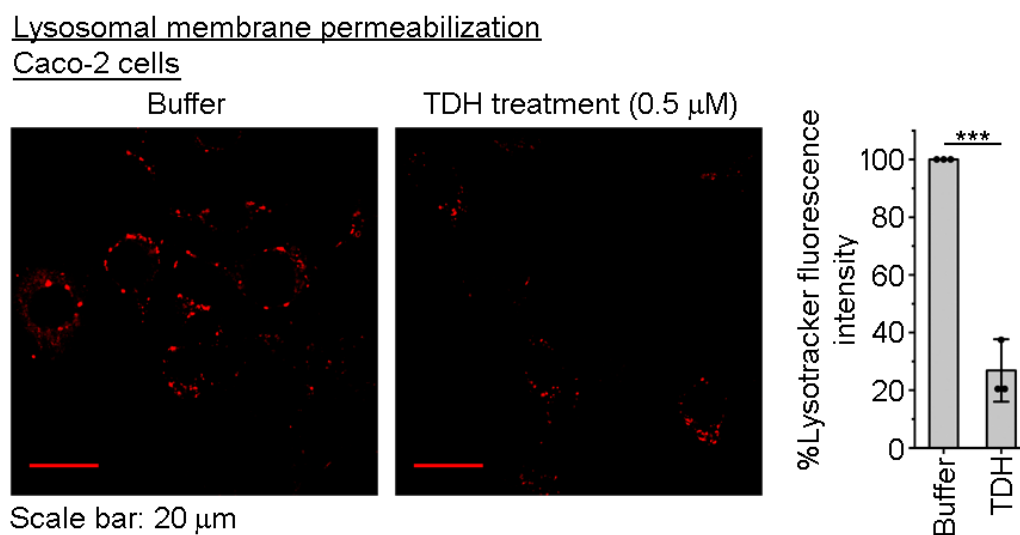


**Figure 18. TDH induces lysosomal membrane permeabilization in Caco-2 cells.**

Microscopy images showing lysosomal membrane permeabilization corresponding to the reduction in lysotracker fluorescence intensity in Caco-2 cells in response to TDH treatment (0.5  $\mu$ M; for 1 hour) in comparison to buffer-treated cells. Images shown here are the representative of ~33-34 images for each treatment obtained from three independent experiments. Bar graph (right-most panel) depicts the decrease in percentage of lysotracker fluorescence intensity in the TDH-treated cells over buffer-treated cells. Data shown here are the averages  $\pm$  standard deviations from three independent experiments. \*\*\* $p < 0.001$ ; Student's unpaired t-test.

### 3.17. TDH induces PARP-1 cleavage in target cells

Poly (ADP-ribose) polymerase-1 (PARP-1) is an enzyme that catalyses the transfer of poly ADP-ribosyl moieties (PARs) to specific proteins involved in DNA repair, by utilising  $\text{NAD}^+$  pools of cell. Upon excessive DNA damage, PARP-1 hyperactivation results in excessive PAR formation that migrates to cytosol and facilitates the translocation of AIF from the mitochondria to the nucleus of the cell, resulting into a unique type of programmed cell death, parthanatos [116, 117]. PARP-1 can be acted

upon by different cell death proteases including caspases, cathepsins, calpains, granzymes etc. The cleaved PARP-1 can also facilitate the mitochondrial release and nuclear translocation of AIF [205, 206]. Therefore, due to the involvement of AIF in TDH-mediated cell death, we explored whether PARP-1, at all, has any involvement (This data has been obtained in collaboration with Ms. Aakanksha Chauhan) [175]. Interestingly, in both Caco-2 and THP-1 cells, we observed cleaved PARP-1 in response to TDH treatment (1  $\mu$ M; for 2, 4 and 8 hours) suggesting that PARP-1 could be involved in TDH-mediated cell death (Figure 19). However, how exactly it could be involved during TDH intoxication remains to be explored further.

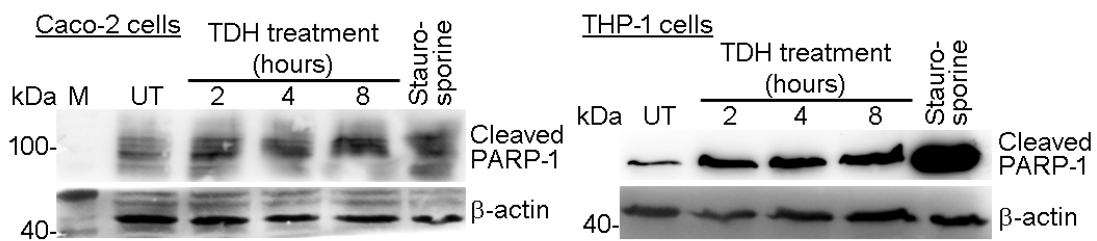


**Figure 19. TDH treatment augments PARP-1 cleavage in the target cells.** Western blot profiles showing increasing levels of cleaved PARP-1 in response to TDH treatment (1  $\mu$ M; for 2, 4 and 8 hours) in both Caco-2 (left panel) and THP-1 (right panel). Staurosporine treatment (2  $\mu$ M; for 6 hours) served as the positive control, while untreated cells (UT) served as the negative control for the experiment.  $\beta$ -actin was probed as the loading control for the whole cell lysates. Data shown here are representatives of three independent experiments.



# **Section-4**

## **Discussion & conclusion**



## 4. Discussion and conclusion

Pore-forming proteins/toxins (PFPs/PFTs) are the specialized class of protein toxins that can perforate the plasma membrane by forming pores on it, thus breaching the membrane barrier [2]. Assaults by PFTs may have impact on cell's physiology beyond the plasma membrane damage. Disruption of cellular homeostasis by PFTs leads to ionic imbalance, ATP depletion, subsequently inducing cascade(s) of cellular responses, including membrane remodelling, damage and repair, immunological and programmed cell death responses [4].

PFPs/PFTs serve varied functions in different organisms. For example; PFPs in higher vertebrates are utilized as the effectors of immunological or cell death responses mediating the elimination of infected cells and the clearance of the pathogen from the system [30-32]. On the other hand, bacterial PFTs serve as critical virulence factor required for the pathogenesis of the bacteria [45, 54, 69].

Interaction of bacterial PFTs with the host system may trigger diverse cellular responses, one of the critical responses being the cell death [8, 35, 70, 207]. Host cell death is one such mechanism that can be exploited by the host and the pathogen for their advantage. PFTs may induce cell death either for nutrient retrieval from target cells for the pathogen or enabling the dissemination of the pathogen to spread infection inside host. Conversely, from host's perspective, cell death may serve as a defense mechanism that can prevent spread of the infection by eradicating infected cells from the system. Several distinct cell death responses have been observed in association with various PFTs (see Table 2 in the Introduction section). These responses may vary depending on the type of PFT in question, its dose and time of administration and the type of target cells. Mostly, it appears that the pore-forming activity of a PFT is crucial for initiating cell death responses. However, in a recent documentation, pore-formation-independent apoptotic cell death has been observed for *Vibrio cholerae* cytolysin (VCC) in intestinal epithelial cells [22]. In certain cases, mechanistic cues such as ionic imbalance and activation of the stress kinases may also play pivotal roles in determining the type of cell death [24-26]. Considering the distinct cell death responses and the intricate molecular mechanisms triggered by various PFTs, the assessment of PFTs becomes a critical aspect within the context of bacterial pathogenesis and host-pathogen interactions.

Thermostable Direct Hemolysin (TDH) is recognised as a significant virulence determinant of the pandemic strains of the marine bacterium *Vibrio parahaemolyticus* [134]. Earlier studies have characterised TDH as a membrane-damaging potent pore-forming toxin that exhibits numerous pathophysiological functionalities in target cells [153-155, 208]. The pore-formation activity of TDH results in free diffusion of ions, water and small molecules across the damaged plasma membrane, potentially leading to colloid-osmotic lysis [136]. The hemolytic activity against erythrocytes by TDH appears to be a straight-forward outcome of its pore-forming ability. However, the pathophysiological effects exerted by TDH in nucleated mammalian cells seem to involve much more intricate and complex mechanism. TDH has been shown to elicit potent cytotoxicity against nucleated mammalian cells, thus incurring tissue damage during bacterial pathogenesis. The ionic imbalance and TDH-mediated cytotoxicity have been associated with the development of bloody mucous diarrhea observed during *V. parahaemolyticus* infections [137]. In an earlier report, TDH has been shown to induce features of apoptosis-like cell death [160]. However, the molecular details to such a programmed cell death induced by TDH remain poorly understood.

Therefore, the present thesis work aimed to understand the cytotoxic effects and attempted to elucidate the molecular mechanism governing the cell death pathway triggered by TDH in the nucleated mammalian cells.

Being a bacterial exotoxin, TDH is typically secreted in the extracellular milieu by the bacteria [145]. Recombinantly expressed and purified TDH with its His-tag removed was used for the current study (Figure 1A), to ensure that its effects would closely mimic those during the actual infection scenario. The purified protein was examined for the hemolytic activity against the human erythrocytes, a signature property used to test the pore-forming efficacy of the PFTs. The purified TDH was observed to be functionally active exhibiting complete lysis of human erythrocytes within an hour at 1  $\mu$ M concentration (Figure 1B).

To study the cytotoxic effects of TDH, the present study was conducted in two distinct cell types i.e. Caco-2, a human intestinal epithelial cell lines and THP-1, a human monocytic cell line. *V. parahaemolyticus* infection primarily leads to gastroenteritis, marked by the inflammation and damage to the intestinal epithelium [131]. Therefore, an intestinal epithelial cell line like Caco-2 is highly suitable for investigating TDH-

mediated cell death, as these cells represent the initial targets encountered by the bacterium or its virulence determinants during infection. Hence, a detailed investigation of TDH-mediated cell death processes was conducted in Caco-2 cells. Additionally, THP-1 cells were employed to validate certain key observations of TDH-induced programmed cell death responses. This facilitated in exploring the potential variations (if any) in the intricate details of these processes between the two distinct cell types.

TDH exhibits potent cytotoxicity against various cell types such as FL cells, Intestine 407 cells, Caco-2 cells, HeLa cells, etc. [153, 154, 156, 167, 208]. Consistent with earlier reports, potent cytotoxicity (by monitoring LDH release assay) of TDH was observed against Caco-2 and THP-1 cells for a range of concentrations (0.125 -1  $\mu$ M) and time points (2, 4, 8 and 24 hours). Interestingly, within the TDH concentration range and incubation time used in this study, Caco-2 cells exhibited a higher susceptibility to TDH compared to THP-1 cells (Figure 2A). Even at the lowest TDH concentration, Caco-2 cells showed saturation in LDH release (~65% cytotoxicity). This disparity may be attributed to the physiological relevance of Caco-2 cells as intestinal epithelial cells, which makes them a more relevant target for TDH. Furthermore, in the time course study of TDH's cytotoxicity at a concentration of 1  $\mu$ M, notably high levels of cytotoxicity (~70-80%) were consistently observed at all time points for both the cell types (Figure 2B). This observation implies that the concentration used may have resulted in the release of saturating levels of LDH even at earlier time points, and the slight decrease in cytotoxicity beyond 8 hours might be attributed to the degradation of the LDH enzyme.

Apoptosis is a classical form of programmed cell death characterized by a series of orchestrated events that induces distinct morphological and biochemical changes in cells [94]. The morphological features includes cell shrinkage and increased cellular granularity due to organelle damage, membrane blebbing and formation of apoptotic bodies [91, 168]. Phosphatidylserine flipping on the outer leaflet of the plasma membrane from its inner leaflet is one of the characteristic features and considered as onset of apoptosis [169]. The late stages of apoptosis are accompanied with plasma membrane and nuclear disintegration along with characteristic DNA laddering pattern on an agarose gel. This pattern arises from small-scale DNA fragmentation, typically consisting of fragments around 180-200 base pairs. The process of DNA cleavage is predominantly carried out by specific endonucleases known as Caspase-Activated DNases (CADs), which are activated by caspases [170, 171].

Therefore, the cytotoxic impacts of TDH on the target cells were assessed for the features of apoptotic programmed cell death. TDH-treated Caco-2 and THP-1 cells were examined for the morphological and biochemical changes. The flow cytometry-based FSC-SSC profile and microscopic analysis methods indicated morphological alterations in target cells (Figure 3). Exposure to TDH resulted in cell shrinkage and an increase in cell granularity. Furthermore, the cells exhibited signs of membrane perforation and damage.

Upon investigating TDH-mediated biochemical changes in target cells, phosphatidylserine flipping on outer leaflet of the membrane bilayer and nuclear disintegration were observed using Annexin V-FITC and PI staining (Figure 4). Furthermore, a characteristic DNA laddering pattern was evident in Caco-2 cells in response to TDH. This pattern implied fragmentation of DNA into small pieces, which appeared as a ladder when subjected to agarose gel electrophoresis (Figure 5).

These findings clearly indicate that TDH has significant cytotoxic effects on target cells and the observed morphological and biochemical characteristics closely resemble to those typically observed during apoptosis-like programmed cell death. This suggests that TDH-mediated programmed cell death could possibly be a form of apoptosis.

Caspases (cysteine-dependent aspartate-specific proteases) are the key executioners of apoptosis and their activation is considered a hallmark feature of apoptotic programmed cell death [97, 172]. These proteases are integral to both extrinsic and intrinsic arms of apoptosis. Each apoptotic pathway features specific initiator caspases: caspase-8 in extrinsic pathway and caspase-9 in intrinsic pathway, which, upon activation subsequently activate downstream executioner caspases i.e. Caspase-3, -7 and -6. Notably, among these, caspase-3 stands out as the dominant and most activated executioner caspase for both extrinsic and intrinsic pathway [209]. Caspase-3 is a 32 kDa zymogen that is processed by the initiator caspases, yielding a partially active heterotetrameric form with p19 and p12 subunits. However, complete catalytic activation of caspase-3 requires autoproteolytic cleavage of the pro-domain converting p19 to p17 subunit [173, 210].

In order to ascertain previously observed apoptosis-like features in TDH-mediated cell death, involvement of caspases as hallmark of apoptosis was also verified.

In a flow cytometry-based assay for the detection of active caspase-3, no appreciable levels of active caspase-3 were detected in either of the cell types. Unlike the flow cytometry-based assay, immunoblotting both partially active p19 and fully active p17 form (in case of staurosporine) were detected, possibly due to the differential sensitivity of the antibodies used for flow-cytometry and immunoblotting assay. Interestingly, the immunoblotting data revealed that the conversion of p19 subunit to p17 was hampered in response to TDH treatment (Figure 6A). Therefore, it is possible that due to partial processing of caspase-3, it is not present in its completely functional form in TDH-treated cells. These findings strongly indicated that TDH-mediated cell death pathway does not involve functional activity of caspase-3.

The IAP (Inhibitors of Apoptosis) family, including XIAP (X-linked Inhibitor of Apoptosis) or cIAPs (Cellular Inhibitor of Apoptosis), can regulate the activation of caspases by binding to the processed forms of caspases and inhibiting their catalytic function [176, 177]. IAPs possess BIR (Baculovirus IAP Repeats) domains: BIR1, BIR2 and BIR3, which selectively target caspases to hinder their activity. BIR1 and BIR2 targets catalytic site of caspase-3 and -7 impeding their catalytic function, while BIR3 binds and inhibits caspase-9 activation. Earlier it has been documented that IAPs may inhibit the conversion of p19 to p17 subunit, thereby, restraining the activity of caspase-3 [174, 211]. Therefore, our results suggest that IAPs might be involved in TDH-induced cell death, potentially preventing caspase-3 from becoming active. Indeed, IAPs were found to be involved in TDH-mediated cell death, which has been shown in our lab by Ms. Aakanksha Chauhan [175].

In addition to the observed inactive status of caspase-3 in TDH-mediated cell death, ZVAD-fmk-based study in THP-1 cells (Figure 6C), showed no reduction in cell death upon caspase inhibitor pre-treatment. These data imply that despite partial caspase activation, caspases does not execute the TDH-mediated cell death. Therefore, it was concluded that TDH induces caspase-independent cell death in nucleated mammalian cells.

Next, to decipher the molecular mechanism underlying the TDH-induced caspase independent cell death pathway, literature suggested that caspase-independent programmed cell death may include the involvement of various organelles such as mitochondria, lysosomes, endoplasmic reticulum etc. [212, 213]. Mitochondria are

central to various cell death pathways including apoptosis and caspase-independent cell death [178, 180, 194, 214]. Disruption of mitochondrial functioning, often due to factors like calcium overload and oxidative stress, can lead to the opening of the mitochondrial permeability transition pore (MPTP). Prolonged opening of this pore results in the dissipation of mitochondrial membrane potential, loss of oxidative phosphorylation causing a decrease in ATP levels and mitochondrial membrane permeability transition (MMPT), that subsequently, resulted into the release of mitochondrial factors from the inter-membrane space to the cytosol [107, 180]. Therefore, the involvement of mitochondria in TDH-mediated caspase-independent cell death and whether TDH is capable of inducing such changes to the mitochondria were investigated. It was observed that TDH is capable of substantial MMPT induction in both Caco-2 and THP-1 cells as observed by JC-1 dye assay (Figure 7). Moreover, depleted ATP levels and release of cytochrome c, a mitochondrial factor into the cytosol of target cells (Figure 8 & 9), strongly imply toward mitochondrial damage and dysfunctioning by TDH intoxication.

Cytochrome c is a heme-containing protein found in mitochondria, where it helps in energy production by acting as an electron carrier [215]. Another role of cytochrome c has been implicated during intrinsic pathway of apoptosis, where it is released from the mitochondria into the cytosol. It joins Apaf-1 in the cytosol to form a complex called apoptosome that triggers activation of caspase-9 [104, 216]. The release of cytochrome c has been observed in other forms of cell death as well but it may not always end up in caspase activation. Factors like ATP-depletion or IAPs-mediated inhibition of processed/activated caspases could be the probable reasons due to which release of cytochrome c could not lead to caspase-activation in TDH-mediated cell death [101, 217-219]. However, its release was checked as a sign of MMPT induction by TDH (Figure 9).

Mitochondrial involvement or MMPT induction in TDH-mediated cell death pathway implied toward the plausible involvement of AIF (Apoptosis Inducing Factor), a critical mitochondrial factor implicated in caspase-independent cell death. AIF is a mitochondrial NADH-dependent oxidoreductase present in the mitochondrial intermembrane space. During MMPT induction, it is released from the mitochondria into the cytosol and further translocates to the nucleus. Nuclear translocation of AIF results into peripheral chromatin condensation and DNA fragmentation [184, 220]. Therefore, to examine the role of AIF in TDH-mediated cell death, release of AIF from the

mitochondria and its translocation to the nucleus were probed in both Caco-2 and THP-1 cells (Figure 10). Indeed, AIF was found to migrate from mitochondria to the nucleus of TDH-treated cells, confirming its involvement in TDH induced caspase-independent cell death.

Nuclear translocation of AIF is known to induce peripheral chromatin condensation and extensive fragmentation of the genetic material. Importantly, AIF generates relatively larger fragments of DNA, approximately 50 kb in size [186]. However, in the context of TDH-induced cell death, a distinct pattern of DNA fragmentation emerged. This pattern was characterized by smaller oligonucleosomal DNA fragmentation (~100-200 bases) (Figure 5). This divergence from the larger fragments produced by AIF suggests the involvement of a nuclease enzyme other than CADs (Caspase-Activated DNases) in TDH-mediated caspase-independent cell death.

Studies revealed an intriguing companion to AIF during its nuclear translocation, Endonuclease G (Endo G) [188]. Endo G is normally present in the mitochondrial intermembrane space where it participates in the mitochondrial DNA replication. However, in response to mitochondrial damage, Endo G relocates to the nucleus. Within nucleus it generates oligonucleosomal DNA fragments which exhibit DNA laddering pattern on agarose gel electrophoresis [187, 189]. To investigate the role of Endo G in TDH-induced cell death, its nuclear translocation was probed in both Caco-2 and THP-1 cells (Figure 11). Remarkably, nuclear translocation of Endo G was indeed observed in these cells. Thus, providing evidence for its involvement in TDH-mediated caspase-independent cell death and justifying the observed laddering pattern independently of caspases (Figure 5).

Reactive oxygen species (ROS) are considered as the crucial signaling molecules having importance in both physiological and pathological processes [191]. These species are natural byproducts of the cell's oxygen metabolism and are typically regulated by the cell's respiratory metabolism. However, impaired mitochondrial function could be one of the causes for excessively high amounts of ROS production. This heightened oxidative stress can have detrimental effects on cellular health, potentially leading to cell death. Overload of ROS is known to trigger the mitochondrial pathway of programmed cell death by disrupting the mitochondrial potential and causes mitochondrial damage, which in turn leads to the release of mitochondrial factors [190, 192, 193]. Since, the

mitochondrial damage and release of mitochondrial factors has already been observed, it would be intriguing to investigate whether ROS production is involved in TDH-mediated cell death pathway. Indeed, substantial intracellular ROS production was observed in Caco-2 cells following TDH intoxication (Figure 12A). Notably, significant amount of mitochondrial ROS was also detected in response to TDH (Figure 12B). Further, to check whether ROS production plays any role in TDH-induced cell death, the effect of N-acetyl cysteine, a ROS scavenger was assessed on the production of intracellular ROS and TDH's cytotoxicity. NAC effectively scavenged intracellular ROS, reducing the ROS levels (Figure 13A). However, it could not decrease the TDH-mediated cytotoxicity to considerable levels (Figure 13B). These findings suggested ROS production may not be the sole mediator of cell death by TDH, rather it could be an outcome of mitochondrial damage.

Another critical molecule in both cell's physiological and pathological signaling is calcium. Dysregulation of calcium levels may disrupt the normal functioning of the cellular organelles such as the endoplasmic reticulum and mitochondria, potentially leading to cell death [25, 221]. Additionally, the mutual interplay between calcium and ROS may affect mitochondrial functioning. Calcium and ROS may signal to induce the release of cytochrome c from the mitochondria as observed during apoptosis [192, 193, 221, 222]. Overload of calcium and oxidative stress may trigger prolonged MPTP opening, causing mitochondrial swelling and rupture as observed in MPT-driven necrosis (see introduction section 1.3.2). Therefore, role of calcium was examined in the context of TDH-mediated cell death responses. Interestingly, calcium influx mediated by ROS production was observed in target cells in response to TDH intoxication (Figure 14). However, the cytotoxicity of TDH appeared to be independent of calcium influx, as calcium chelation by BAPTA-AM did not result in any significant reduction in cytotoxicity of TDH (Figure 14E). These results were found in corroboration to the previously reported data that TDH's cytotoxicity is independent of calcium influx [156]. However, in addition to the previous report, these findings provide evidence for a plausible ROS and calcium mutual interplay in TDH-mediated cell death, and the precise role of this interplay remains ambiguous at present.

To gain deeper insights into the mitochondrial damage, the possibility of translocation of TDH to the target cell mitochondria was also examined. Previous research has indicated that various bacterial virulence factors including pore-forming

toxins (PFTs) are able to invade the mitochondria within target cells and induce mitochondrial damage. For instance, *Helicobacter pylori*'s vacuolating-cytolysin, VacA exhibits mitochondrial localization followed by the loss of mitochondrial potential and cyt c release, ultimately triggering apoptosis [55, 196, 198]. Similarly, Panton-Valentine Leukocidin (PVL), a PFT from *Staphylococcus aureus* induces apoptosis in target cells by translocating to the mitochondria and causing the release of apoptotic factors such as cytochrome c, Smac/DIABLO [67]. Enterohemorrhagic *Escherichia coli* Hemolysin (EHEC-Hly) has also been found to translocate to the mitochondria of epithelial and endothelial cells leading to mitochondrial damage and eventual apoptotic cell death [85]. Pneumolysin, a cholesterol-dependent cytolysin from *Streptococcus pneumoniae* was also observed to localize with mitochondria of target cell, bringing about the mitochondrial damage [195]. In a recent study, *Vibrio cholerae* cytolysin (VCC) was also observed to translocate to the target cell mitochondria, although further investigation is needed to understand the precise consequences of mitochondrial translocation of the toxin [22]. Interestingly, TDH exhibited a remarkable propensity to translocate to the mitochondria of both Caco-2 and THP-1 cells (Figure 15). This observation is intriguing, considering that TDH is primarily recognised as a pore-forming exotoxin that targets plasma membrane [145].

To better understand the impact of TDH's interaction with the mitochondria of target cells, an investigation was conducted to determine whether TDH could directly create pores in the mitochondrial membrane or induce damage independently, resulting in the release of mitochondrial factors. These experiments were conducted in isolated mitochondria. Interestingly, TDH exhibited prominent association with mitochondria, even under cell free conditions. However, it is important to note that this interaction with TDH did not lead to mitochondrial damage, as there was no significant reduction in AIF levels detected in the isolated mitochondria following exposure to TDH. These findings implied that induction of mitochondrial damage in TDH-mediated programmed cell death may require cytosolic factor(s)/signal(s) in addition to TDH itself.

In the quest to identify the cytosolic factor responsible for mitochondrial damage, contribution of the Bcl-2 family of proteins was examined. These proteins have been implicated in programmed cell death processes, including apoptosis and necrosis-type cell death [199-201, 223]. Under normal physiological conditions, cells maintain low levels of pro-apoptotic molecules like Bax and Bak, while anti-apoptotic molecules such

as Bcl-2 are abundant to restrain the pro-apoptotic proteins. However, adverse conditions can trigger the upregulation of pro-apoptotic molecules and downregulation of anti-apoptotic molecules. These levels can be translated to bax/bcl-2 ratio and a higher bax/bcl-2 ratio in damaged cells is indicative of the involvement of the pro-apoptotic molecules. This shift in bax/bcl-2 ratio allows active Bax molecules to displace the pre-existing Bcl-2 molecules on the mitochondrial membrane. Consequently, Bax molecules oligomerize and form functional pores on the mitochondrial outer membrane, leading to the mitochondrial outer membrane permeabilization (MOMP). This event in turn triggers MMPT, ultimately resulting in the release of mitochondrial factors required for the execution of cell death [200, 224].

Notably, an increased bax/bcl-2 ratio was observed in both Caco-2 and THP-1 cells, suggesting the possible interplay of Bcl-2 family members in response to TDH (Figure 17A). Furthermore, the increased recruitment of active bax molecules in the mitochondrial fractions clearly indicated the participation of pro-apoptotic molecules in mitochondrial damage (Figure 17B). Therefore, it is evident that Bax serves as the cytosolic factor responsible for damaging the mitochondria. However, future work in this direction will determine whether Bax alone is sufficient for the mitochondrial damage or if it requires the assistance of additional cytosolic factor(s) or signal(s).

Recent research on the porin protein PorB from the pathogenic bacterium *Neisseria gonorrhoeae* has shown its ability to translocate to the mitochondrial inner membrane, resulting in the loss of mitochondrial potential and changes in the mitochondrial cristae structure [225]. In addition to PorB, the pro-apoptotic molecule Bak gets activated in the apoptotic cell death process, leading to the permeabilization of outer mitochondrial membrane and the release of cytochrome c [225]. Hence, in TDH-mediated caspase-independent cell death such a possibility may exist, wherein the mitochondrial translocation of TDH and the cytosolic factor, Bax may work synergistically to induce mitochondrial damage and release of the mitochondrial factors.

To explore the impact of TDH on cellular organelles beyond mitochondria and their possible involvement in TDH-mediated caspase-independent cell death, focus was directed toward lysosomes. The status of lysosomal stress was examined in terms of lysosomal membrane permeabilization, a marker of lysosomal damage during pathological conditions [203, 204]. Indeed, TDH was observed to induce lysosomal

membrane permeabilization in target cells (Figure 18), suggesting that lysosomes could be the critical players of TDH-mediated caspase-independent cell death pathway. Lysosomes are acidic organelles that harbour several proteases essential for intracellular protein degradation and recycling. Among these enzymes, cathepsins are the most abundant and typically require lysosomal acidification for their activity. However, certain lysosomal cathepsins may release upon lysosomal rupture and function at ambient pH of the cytosol. Cathepsins can serve different roles in programmed cell death pathways [202, 204, 226]. They can act upstream to the mitochondria, inducing MMPT and the release of mitochondrial factors. Simultaneously, they can operate downstream of the mitochondria, by activating certain effectors that promote cell death. Therefore, the involvement of lysosomal cathepsins can be speculated in cell death pathway induced by TDH.

Another hypothesis originated from the findings regarding the involvement of lysosomes in TDH-mediated cell death is that TDH might accumulate within the lysosomes, ultimately leading to lysosomal rupture. This could potentially serve as an escape to the mitochondria via the lysosomal route. Further studies in this direction will provide critical insights into the precise role of lysosomes in TDH-mediated caspase-independent cell death.

In addition to these findings, Poly (ADP-ribose) polymerase-1 (PARP-1) cleavage was also observed in response to TDH treatment in both Caco-2 and THP-1 cells. PARP-1 is a nuclear enzyme which primarily functions to repair DNA damage. It synthesizes poly ADP-ribosyl (PAR) moieties by utilising the cellular pool of  $\text{NAD}^+$ , thus, signaling the recruitment of the DNA repairing factors at the site of DNA damage [227].

PARP-1 plays a multifaceted role in regulating different forms of cell death processes. Excessive DNA damage can trigger hyperactivation of PARP-1, resulting into overproduction of PAR polymers. This, in turn, consumes large amounts of  $\text{NAD}^+$  and ATP, leading to energy depletion within the cell. The surplus PAR chains move from nucleus to cytosol, facilitating the translocation of AIF from mitochondria to nucleus. Therefore, PARP-1 triggers a unique form of cell death called parthanatos [116, 117]. Moreover, PARP-1 can be targeted and cleaved by distinct cell death proteases like caspases, cathepsins, calpains, granzymes and others, yielding various fragments.

Notably, the 89 kDa fragment, primarily generated either by caspases or independently of caspases, by cathepsins, retains the catalytic domain and has been shown to promote the translocation of AIF from mitochondria to nucleus [205, 206]. Future studies in this direction will reveal the exact role of PARP-1 cleavage and its association with TDH-induced caspase independent cell death. This will help in understanding whether the observed nuclear translocation of AIF is triggered by PARP-1 and whether its cleavage is mediated by cathepsins in the TDH-mediated caspase-independent cell death pathway.

In conclusion, the present thesis work demonstrates TDH-induced cytotoxicity and its consequential effects in the target cells. These effects encompass morphological changes, phosphatidylserine relocation on the outer membrane of the lipid bilayer, nuclear disintegration and DNA fragmentation. This underscores TDH's role as a potent cytolytic pore-forming toxin and a significant contributor in the pathogenesis process of the pathogenic bacterium *Vibrio parahaemolyticus*. The current research reveals that TDH triggers a caspase-independent programmed cell death in two distinct type of cells, involving mitochondrial damage as a pivotal trigger for cell death execution. Additionally, this study unravels key participants responsible for the execution of the cell death in a caspase-independent manner, including AIF and Endo G which contribute to the characteristic DNA fragmentation observed in response to TDH. While the study identifies TDH's ability to trigger ROS generation and calcium influx in the target cells, their impact on TDH's cytotoxicity appears limited. Intriguingly, TDH, being a bacterial exotoxin, exhibits an unexpected ability to translocate to target cell's mitochondria. This observation, in conjunction with the recruitment of active Bax to mitochondria, suggests a potential synergistic action of TDH and Bax in causing mitochondrial damage. Moreover, the study attempts to explore the involvement of organelles beyond mitochondria, such as lysosomes and observed lysosomal membrane permeabilization induced by TDH. Additionally, PARP-1 cleavage is detected in TDH-mediated cell death, indicating its potential role in the process.

### Caspase-independent programmed cell death induced by TDH

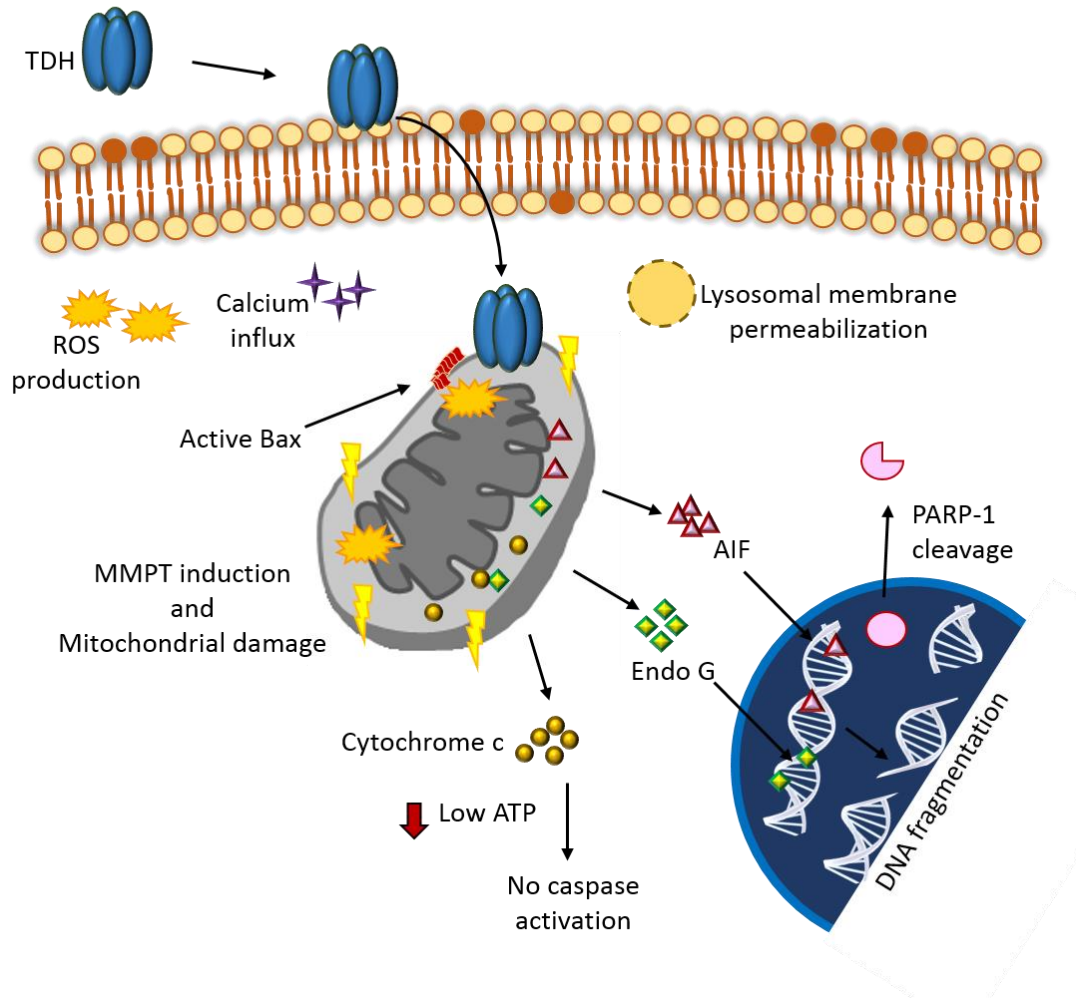


**Illustration 13. Diagrammatic representation of TDH-mediated caspase-independent cell death in target cells.**

These findings pose several new queries that would require further exploration. For example, the exact implications of ROS and calcium remain ambiguous in the context of TDH-mediated cell death scenario. The mechanism of TDH translocation to the target cell mitochondria remains to be deciphered. Also, it is not clear at present that how exactly Bax gets activated upon TDH intoxication of the target cells. The potential role of lysosomes and PARP-1 in mediating caspase-independent cell death still remains uncharted. Also, this question needs to be addressed whether the TDH-mediated cell death can be categorised as PARP-1 and AIF-mediated cell death, ‘parthanatos’. It would be of particular interest in the field of pore-forming toxin’s biology to investigate whether

TDH's ability to induce programmed cell death is intricately linked to the toxin's pore-forming functionality. Consequently, future investigations are essential to comprehensively explore and address these unresolved questions.

Taken together, the present thesis work elucidates the intricate molecular mechanism governing the cell death response triggered by TDH in nucleated mammalian cells. It is noteworthy that TDH, a prototype bacterial PFT, extends its pathophysiological effects beyond the target cell's plasma membrane. Current work deduced that TDH induces caspase-independent cell death in nucleated mammalian cells, characterized by mitochondrial damage, AIF and Endo G-mediated chromatin condensation and DNA fragmentation, toxin's translocation to the mitochondria, involvement of Bax, lysosomal stress, and potential participation of PARP-1. Therefore, this research sheds light on the various essential molecules operating in the pathway and opens up exciting new avenues for future exploration. In sum, this work puts forth critical new insights into the significance of the pathophysiological effects of TDH concerning bacterial pathogenesis and its implications in the host-pathogen interaction processes. Moreover, being an atypical pore-forming toxin, TDH-mediated cellular responses expand our existing knowledge about cellular responses by pore-forming toxins. Further investigations are required to fully elucidate the roles of various organelles and molecular factors in TDH-induced cell death, offering potential targets for therapeutic intervention in *V. parahaemolyticus* infections.

# References



1. Blazek, A.D., B.J. Paleo, and N. Weisleder, *Plasma Membrane Repair: A Central Process for Maintaining Cellular Homeostasis*. Physiology (Bethesda), 2015. **30**(6): p. 438-48.
2. Mondal, A.K. and K. Chattopadhyay, *Structures and functions of the membrane-damaging pore-forming proteins*. Adv Protein Chem Struct Biol, 2022. **128**: p. 241-288.
3. Dal Peraro, M. and F.G. van der Goot, *Pore-forming toxins: ancient, but never really out of fashion*. Nat Rev Microbiol, 2016. **14**(2): p. 77-92.
4. Verma, P., et al., *Pore-forming toxins in infection and immunity*. Biochem Soc Trans, 2021. **49**(1): p. 455-465.
5. Lakey, J.H., F.G. van der Goot, and F. Pattus, *All in the family: the toxic activity of pore-forming colicins*. Toxicology, 1994. **87**(1-3): p. 85-108.
6. Jiang, J., et al., *Atomic structure of anthrax protective antigen pore elucidates toxin translocation*. Nature, 2015. **521**(7553): p. 545-9.
7. Seike, S., et al., *Delta-toxin from Clostridium perfringens perturbs intestinal epithelial barrier function in Caco-2 cell monolayers*. Biochim Biophys Acta Biomembr, 2018. **1860**(2): p. 428-433.
8. Nguyen, B.N., B.N. Peterson, and D.A. Portnoy, *Listeriolysin O: A phagosome-specific cytolysin revisited*. Cell Microbiol, 2019. **21**(3): p. e12988.
9. Bischofberger, M., I. Iacovache, and F.G. van der Goot, *Pathogenic pore-forming proteins: function and host response*. Cell Host Microbe, 2012. **12**(3): p. 266-75.
10. Mondal, A.K., et al., *Sequence Diversity in the Pore-Forming Motifs of the Membrane-Damaging Protein Toxins*. J Membr Biol, 2020. **253**(5): p. 469-478.
11. Heuck, A.P., R.K. Tweten, and A.E. Johnson, *Beta-barrel pore-forming toxins: intriguing dimorphic proteins*. Biochemistry, 2001. **40**(31): p. 9065-73.
12. Mondal, A.K. and K. Chattopadhyay, *Taking Toll on Membranes: Curious Cases of Bacterial beta-Barrel Pore-Forming Toxins*. Biochemistry, 2020. **59**(2): p. 163-170.

13. Mondal, A.K., et al., *Tyrosine in the hinge region of the pore-forming motif regulates oligomeric beta-barrel pore formation by Vibrio cholerae cytolysin*. Mol Microbiol, 2021. **115**(4): p. 508-525.
14. Martner, A., et al., *Pneumolysin released during Streptococcus pneumoniae autolysis is a potent activator of intracellular oxygen radical production in neutrophils*. Infect Immun, 2008. **76**(9): p. 4079-87.
15. Elluri, S., et al., *Outer membrane vesicles mediate transport of biologically active Vibrio cholerae cytolysin (VCC) from V. cholerae strains*. PLoS One, 2014. **9**(9): p. e106731.
16. Hamada, D., et al., *Tetrameric structure of thermostable direct hemolysin from vibrio parahaemolyticus revealed by ultracentrifugation, small-angle X-ray scattering and electron microscopy*. J Mol Biol, 2007. **365**(1): p. 187-95.
17. Yanagihara, I., et al., *Structure and functional characterization of Vibrio parahaemolyticus thermostable direct hemolysin*. J Biol Chem, 2010. **285**(21): p. 16267-74.
18. Mondal, A.K., et al., *Structural Basis and Functional Implications of the Membrane Pore-Formation Mechanisms of Bacterial Pore-Forming Toxins*. Adv Exp Med Biol, 2018. **1112**: p. 281-291.
19. Margheritis, E., S. Kappelhoff, and K. Cosentino, *Pore-Forming Proteins: From Pore Assembly to Structure by Quantitative Single-Molecule Imaging*. Int J Mol Sci, 2023. **24**(5).
20. Gilbert, R.J., et al., *Membrane pore formation at protein-lipid interfaces*. Trends Biochem Sci, 2014. **39**(11): p. 510-6.
21. Olivier, F.A.B., et al., *The escape of Candida albicans from macrophages is enabled by the fungal toxin candidalysin and two host cell death pathways*. Cell Rep, 2022. **40**(12): p. 111374.
22. Kaur, D., et al., *Pore formation-independent cell death induced by a beta-barrel pore-forming toxin*. FASEB J, 2022. **36**(10): p. e22557.

23. Babiychuk, E.B., et al., *Intracellular Ca(2+) operates a switch between repair and lysis of streptolysin O-perforated cells*. *Cell Death Differ*, 2009. **16**(8): p. 1126-34.
24. Khilwani, B., A. Mukhopadhaya, and K. Chattopadhyay, *Transmembrane oligomeric form of Vibrio cholerae cytolysin triggers TLR2/TLR6-dependent proinflammatory responses in monocytes and macrophages*. *Biochem J*, 2015. **466**(1): p. 147-61.
25. Bouillot, S., E. Reboud, and P. Huber, *Functional Consequences of Calcium Influx Promoted by Bacterial Pore-Forming Toxins*. *Toxins (Basel)*, 2018. **10**(10).
26. Cabezas, S., et al., *Damage of eukaryotic cells by the pore-forming toxin sticholysin II: Consequences of the potassium efflux*. *Biochim Biophys Acta Biomembr*, 2017. **1859**(5): p. 982-992.
27. Brito, C., et al., *Mechanisms protecting host cells against bacterial pore-forming toxins*. *Cell Mol Life Sci*, 2019. **76**(7): p. 1319-1339.
28. Fennessey, C.M., S.E. Ivie, and M.S. McClain, *Coenzyme depletion by members of the aerolysin family of pore-forming toxins leads to diminished ATP levels and cell death*. *Mol Biosyst*, 2012. **8**(8): p. 2097-105.
29. Voskoboinik, I., J.C. Whisstock, and J.A. Trapani, *Perforin and granzymes: function, dysfunction and human pathology*. *Nat Rev Immunol*, 2015. **15**(6): p. 388-400.
30. Bayly-Jones, C., D. Bubeck, and M.A. Dunstone, *The mystery behind membrane insertion: a review of the complement membrane attack complex*. *Philos Trans R Soc Lond B Biol Sci*, 2017. **372**(1726).
31. Samson, A.L., et al., *MLKL trafficking and accumulation at the plasma membrane control the kinetics and threshold for necroptosis*. *Nat Commun*, 2020. **11**(1): p. 3151.
32. Shi, J., W. Gao, and F. Shao, *Pyroptosis: Gasdermin-Mediated Programmed Necrotic Cell Death*. *Trends Biochem Sci*, 2017. **42**(4): p. 245-254.

33. Chipuk, J.E., L. Bouchier-Hayes, and D.R. Green, *Mitochondrial outer membrane permeabilization during apoptosis: the innocent bystander scenario*. Cell Death Differ, 2006. **13**(8): p. 1396-402.
34. Yoo, I.H., et al., *Role of pneumococcal pneumolysin in the induction of an inflammatory response in human epithelial cells*. FEMS Immunol Med Microbiol, 2010. **60**(1): p. 28-35.
35. Alcantara, R.B., L.C. Preheim, and M.J. Gentry, *Role of Pneumolysin's complement-activating activity during pneumococcal bacteremia in cirrhotic rats*. Infect Immun, 1999. **67**(6): p. 2862-6.
36. Karmakar, M., et al., *Neutrophil IL-1beta processing induced by pneumolysin is mediated by the NLRP3/ASC inflammasome and caspase-1 activation and is dependent on K<sup>+</sup> efflux*. J Immunol, 2015. **194**(4): p. 1763-75.
37. Zysk, G., et al., *Pneumolysin is the main inducer of cytotoxicity to brain microvascular endothelial cells caused by Streptococcus pneumoniae*. Infect Immun, 2001. **69**(2): p. 845-52.
38. Hupp, S., et al., *Pneumolysin boosts the neuroinflammatory response to Streptococcus pneumoniae through enhanced endocytosis*. Nat Commun, 2022. **13**(1): p. 5032.
39. Diep, B.A., et al., *Polymorphonuclear leukocytes mediate Staphylococcus aureus Panton-Valentine leukocidin-induced lung inflammation and injury*. Proc Natl Acad Sci U S A, 2010. **107**(12): p. 5587-92.
40. Ma, X., et al., *Staphylococcal Panton-Valentine leukocidin induces pro-inflammatory cytokine production and nuclear factor-kappa B activation in neutrophils*. PLoS One, 2012. **7**(4): p. e34970.
41. Tseng, C.W., et al., *Staphylococcus aureus Panton-Valentine leukocidin contributes to inflammation and muscle tissue injury*. PLoS One, 2009. **4**(7): p. e6387.
42. Lubkin, A. and V.J. Torres, *The ever-emerging complexity of alpha-toxin's interaction with host cells*. Proc Natl Acad Sci U S A, 2015. **112**(46): p. 14123-4.

43. Brito, C., et al., *Perfringolysin O-Induced Plasma Membrane Pores Trigger Actomyosin Remodeling and Endoplasmic Reticulum Redistribution*. *Toxins (Basel)*, 2019. **11**(7).
44. O'Brien, D.K. and S.B. Melville, *Effects of Clostridium perfringens alpha-toxin (PLC) and perfringolysin O (PFO) on cytotoxicity to macrophages, on escape from the phagosomes of macrophages, and on persistence of C. perfringens in host tissues*. *Infect Immun*, 2004. **72**(9): p. 5204-15.
45. Los, F.C., et al., *Role of pore-forming toxins in bacterial infectious diseases*. *Microbiol Mol Biol Rev*, 2013. **77**(2): p. 173-207.
46. Hernandez-Flores, K.G. and H. Vivanco-Cid, *Biological effects of listeriolysin O: implications for vaccination*. *Biomed Res Int*, 2015. **2015**: p. 360741.
47. Dhakal, B.K. and M.A. Mulvey, *The UPEC pore-forming toxin alpha-hemolysin triggers proteolysis of host proteins to disrupt cell adhesion, inflammatory, and survival pathways*. *Cell Host Microbe*, 2012. **11**(1): p. 58-69.
48. Wang, C., et al., *Alpha-hemolysin of uropathogenic Escherichia coli induces GM-CSF-mediated acute kidney injury*. *Mucosal Immunol*, 2020. **13**(1): p. 22-33.
49. Khilwani, B. and K. Chattopadhyay, *Signaling beyond Punching Holes: Modulation of Cellular Responses by Vibrio cholerae Cytolysin*. *Toxins (Basel)*, 2015. **7**(8): p. 3344-58.
50. Toh, E., et al., *Bacterial protein MakA causes suppression of tumour cell proliferation via inhibition of PIP5K1alpha/Akt signalling*. *Cell Death Dis*, 2022. **13**(12): p. 1024.
51. Corkery, D.P., et al., *Vibrio cholerae cytotoxin MakA induces noncanonical autophagy resulting in the spatial inhibition of canonical autophagy*. *J Cell Sci*, 2021. **134**(5).
52. Refai, A., et al., *Mycobacterium tuberculosis Virulent Factor ESAT-6 Drives Macrophage Differentiation Toward the Pro-inflammatory M1 Phenotype and Subsequently Switches It to the Anti-inflammatory M2 Phenotype*. *Front Cell Infect Microbiol*, 2018. **8**: p. 327.

53. Grover, A. and A.A. Izzo, *BAT3 regulates Mycobacterium tuberculosis protein ESAT-6-mediated apoptosis of macrophages*. PLoS One, 2012. **7**(7): p. e40836.
54. Peng, X. and J. Sun, *Mechanism of ESAT-6 membrane interaction and its roles in pathogenesis of Mycobacterium tuberculosis*. Toxicon, 2016. **116**: p. 29-34.
55. Palframan, S.L., T. Kwok, and K. Gabriel, *Vacuolating cytotoxin A (VacA), a key toxin for Helicobacter pylori pathogenesis*. Front Cell Infect Microbiol, 2012. **2**: p. 92.
56. Zhu, P., et al., *Helicobacter pylori VacA induces autophagic cell death in gastric epithelial cells via the endoplasmic reticulum stress pathway*. Cell Death Dis, 2017. **8**(12): p. 3207.
57. Yahiro, K., et al., *Helicobacter pylori VacA toxin causes cell death by inducing accumulation of cytoplasmic connexin 43*. Cell Death Dis, 2015. **6**(11): p. e1971.
58. Ponmalar, II, et al., *Correlated protein conformational states and membrane dynamics during attack by pore-forming toxins*. Proc Natl Acad Sci U S A, 2019. **116**(26): p. 12839-12844.
59. Etxaniz, A., et al., *Membrane Repair Mechanisms against Permeabilization by Pore-Forming Toxins*. Toxins (Basel), 2018. **10**(6).
60. Romero, M., et al., *Intrinsic repair protects cells from pore-forming toxins by microvesicle shedding*. Cell Death Differ, 2017. **24**(5): p. 798-808.
61. Husmann, M., et al., *Elimination of a bacterial pore-forming toxin by sequential endocytosis and exocytosis*. FEBS Lett, 2009. **583**(2): p. 337-44.
62. Pleckaityte, M., *Cholesterol-Dependent Cytolysins Produced by Vaginal Bacteria: Certainties and Controversies*. Front Cell Infect Microbiol, 2019. **9**: p. 452.
63. Yue, J. and J.M. Lopez, *Understanding MAPK Signaling Pathways in Apoptosis*. Int J Mol Sci, 2020. **21**(7).
64. Adams, C.J., et al., *Structure and Molecular Mechanism of ER Stress Signaling by the Unfolded Protein Response Signal Activator IRE1*. Front Mol Biosci, 2019. **6**: p. 11.

65. Bischof, L.J., et al., *Activation of the unfolded protein response is required for defenses against bacterial pore-forming toxin in vivo*. PLoS Pathog, 2008. **4**(10): p. e1000176.
66. Hetz, C., *The unfolded protein response: controlling cell fate decisions under ER stress and beyond*. Nat Rev Mol Cell Biol, 2012. **13**(2): p. 89-102.
67. Genestier, A.L., et al., *Staphylococcus aureus Panton-Valentine leukocidin directly targets mitochondria and induces Bax-independent apoptosis of human neutrophils*. J Clin Invest, 2005. **115**(11): p. 3117-27.
68. Thapa, R., S. Ray, and P.A. Keyel, *Interaction of Macrophages and Cholesterol-Dependent Cytolysins: The Impact on Immune Response and Cellular Survival*. Toxins (Basel), 2020. **12**(9).
69. Berends, E.T.M., et al., *Staphylococcus aureus Impairs the Function of and Kills Human Dendritic Cells via the LukAB Toxin*. mBio, 2019. **10**(1).
70. Melehani, J.H., et al., *Staphylococcus aureus Leukocidin A/B (LukAB) Kills Human Monocytes via Host NLRP3 and ASC when Extracellular, but Not Intracellular*. PLoS Pathog, 2015. **11**(6): p. e1004970.
71. Yap, W.Y. and J.S. Hwang, *Response of Cellular Innate Immunity to Cnidarian Pore-Forming Toxins*. Molecules, 2018. **23**(10).
72. Nishimoto, A.T., J.W. Rosch, and E.I. Tuomanen, *Pneumolysin: Pathogenesis and Therapeutic Target*. Front Microbiol, 2020. **11**: p. 1543.
73. Koffel, R., et al., *Host-Derived Microvesicles Carrying Bacterial Pore-Forming Toxins Deliver Signals to Macrophages: A Novel Mechanism of Shaping Immune Responses*. Front Immunol, 2018. **9**: p. 1688.
74. Verma, V., et al., *alpha-Hemolysin of uropathogenic E. coli regulates NLRP3 inflammasome activation and mitochondrial dysfunction in THP-1 macrophages*. Sci Rep, 2020. **10**(1): p. 12653.
75. Svedova, M., et al., *Pore-formation by adenylate cyclase toxoid activates dendritic cells to prime CD8+ and CD4+ T cells*. Immunol Cell Biol, 2016. **94**(4): p. 322-33.

76. Gekara, N.O., et al., *Listeria monocytogenes induces T cell receptor unresponsiveness through pore-forming toxin listeriolysin O*. J Infect Dis, 2010. **202**(11): p. 1698-707.
77. Subramanian, K., et al., *Pneumolysin binds to the mannose receptor C type 1 (MRC-1) leading to anti-inflammatory responses and enhanced pneumococcal survival*. Nat Microbiol, 2019. **4**(1): p. 62-70.
78. Pereira, J.M., et al., *The Yin and Yang of Pneumolysin During Pneumococcal Infection*. Front Immunol, 2022. **13**: p. 878244.
79. Kitur, K., et al., *Toxin-induced necroptosis is a major mechanism of Staphylococcus aureus lung damage*. PLoS Pathog, 2015. **11**(4): p. e1004820.
80. Haslinger, B., et al., *Staphylococcus aureus alpha-toxin induces apoptosis in peripheral blood mononuclear cells: role of endogenous tumour necrosis factor-alpha and the mitochondrial death pathway*. Cell Microbiol, 2003. **5**(10): p. 729-41.
81. Menzies, B.E. and I. Kourteva, *Staphylococcus aureus alpha-toxin induces apoptosis in endothelial cells*. FEMS Immunol Med Microbiol, 2000. **29**(1): p. 39-45.
82. Powers, M.E. and J. Bubeck Wardenburg, *Host autophagy combating S. aureus: alpha-toxin will be tolerated*. Cell Host Microbe, 2015. **17**(4): p. 419-20.
83. Carrero, J.A., H. Vivanco-Cid, and E.R. Unanue, *Granzymes drive a rapid listeriolysin O-induced T cell apoptosis*. J Immunol, 2008. **181**(2): p. 1365-74.
84. Sauer, J.D., et al., *Listeria monocytogenes triggers AIM2-mediated pyroptosis upon infrequent bacteriolysis in the macrophage cytosol*. Cell Host Microbe, 2010. **7**(5): p. 412-9.
85. Bielaszewska, M., et al., *Enterohemorrhagic Escherichia coli hemolysin employs outer membrane vesicles to target mitochondria and cause endothelial and epithelial apoptosis*. PLoS Pathog, 2013. **9**(12): p. e1003797.
86. Soong, G., et al., *Staphylococcus aureus activation of caspase 1/calpain signaling mediates invasion through human keratinocytes*. J Infect Dis, 2012. **205**(10): p. 1571-9.

87. Gutierrez, M.G., et al., *Protective role of autophagy against Vibrio cholerae cytotoxin, a pore-forming toxin from V. cholerae*. Proc Natl Acad Sci U S A, 2007. **104**(6): p. 1829-34.
88. Rassow, J., *Helicobacter pylori vacuolating toxin A and apoptosis*. Cell Commun Signal, 2011. **9**: p. 26.
89. Goldmann, O., et al., *Streptococcus pyogenes induces oncosis in macrophages through the activation of an inflammatory programmed cell death pathway*. Cell Microbiol, 2009. **11**(1): p. 138-55.
90. Galluzzi, L., et al., *Molecular mechanisms of cell death: recommendations of the Nomenclature Committee on Cell Death 2018*. Cell Death Differ, 2018. **25**(3): p. 486-541.
91. Elmore, S., *Apoptosis: a review of programmed cell death*. Toxicol Pathol, 2007. **35**(4): p. 495-516.
92. Vitale, I., et al., *Apoptotic cell death in disease-Current understanding of the NCCD 2023*. Cell Death Differ, 2023. **30**(5): p. 1097-1154.
93. Kerr, J.F., A.H. Wyllie, and A.R. Currie, *Apoptosis: a basic biological phenomenon with wide-ranging implications in tissue kinetics*. Br J Cancer, 1972. **26**(4): p. 239-57.
94. Saraste, A. and K. Pulkki, *Morphologic and biochemical hallmarks of apoptosis*. Cardiovasc Res, 2000. **45**(3): p. 528-37.
95. Ge, Y., M. Huang, and Y.M. Yao, *Efferocytosis and Its Role in Inflammatory Disorders*. Front Cell Dev Biol, 2022. **10**: p. 839248.
96. Kesavardhana, S., R.K.S. Malireddi, and T.D. Kanneganti, *Caspases in Cell Death, Inflammation, and Pyroptosis*. Annu Rev Immunol, 2020. **38**: p. 567-595.
97. Denault, J.B. and G.S. Salvesen, *Caspases: keys in the ignition of cell death*. Chem Rev, 2002. **102**(12): p. 4489-500.
98. Shi, Y., *Caspase activation, inhibition, and reactivation: a mechanistic view*. Protein Sci, 2004. **13**(8): p. 1979-87.

99. Timmer, J.C. and G.S. Salvesen, *Caspase substrates*. Cell Death Differ, 2007. **14**(1): p. 66-72.
100. Tait, S.W. and D.R. Green, *Mitochondria and cell death: outer membrane permeabilization and beyond*. Nat Rev Mol Cell Biol, 2010. **11**(9): p. 621-32.
101. Liu, X., et al., *Induction of apoptotic program in cell-free extracts: requirement for dATP and cytochrome c*. Cell, 1996. **86**(1): p. 147-57.
102. Du, C., et al., *Smac, a mitochondrial protein that promotes cytochrome c-dependent caspase activation by eliminating IAP inhibition*. Cell, 2000. **102**(1): p. 33-42.
103. Yang, Q.H., et al., *Omi/HtrA2 catalytic cleavage of inhibitor of apoptosis (IAP) irreversibly inactivates IAPs and facilitates caspase activity in apoptosis*. Genes Dev, 2003. **17**(12): p. 1487-96.
104. Hu, Q., et al., *Molecular determinants of caspase-9 activation by the Apaf-1 apoptosome*. Proc Natl Acad Sci U S A, 2014. **111**(46): p. 16254-61.
105. Ashkenazi, A. and V.M. Dixit, *Death receptors: signaling and modulation*. Science, 1998. **281**(5381): p. 1305-8.
106. Li, H., et al., *Cleavage of BID by caspase 8 mediates the mitochondrial damage in the Fas pathway of apoptosis*. Cell, 1998. **94**(4): p. 491-501.
107. Izzo, V., et al., *Mitochondrial Permeability Transition: New Findings and Persisting Uncertainties*. Trends Cell Biol, 2016. **26**(9): p. 655-667.
108. Vanden Berghe, T., et al., *Regulated necrosis: the expanding network of non-apoptotic cell death pathways*. Nat Rev Mol Cell Biol, 2014. **15**(2): p. 135-47.
109. Baines, C.P., et al., *Loss of cyclophilin D reveals a critical role for mitochondrial permeability transition in cell death*. Nature, 2005. **434**(7033): p. 658-62.
110. Dhuriya, Y.K. and D. Sharma, *Necroptosis: a regulated inflammatory mode of cell death*. J Neuroinflammation, 2018. **15**(1): p. 199.
111. Galluzzi, L., et al., *Necroptosis: Mechanisms and Relevance to Disease*. Annu Rev Pathol, 2017. **12**: p. 103-130.

112. Yu, P., et al., *Pyroptosis: mechanisms and diseases*. Signal Transduct Target Ther, 2021. **6**(1): p. 128.
113. Ding, J. and F. Shao, *SnapShot: The Noncanonical Inflammasome*. Cell, 2017. **168**(3): p. 544-544 e1.
114. Li, J., et al., *Ferroptosis: past, present and future*. Cell Death Dis, 2020. **11**(2): p. 88.
115. Jiang, X., B.R. Stockwell, and M. Conrad, *Ferroptosis: mechanisms, biology and role in disease*. Nat Rev Mol Cell Biol, 2021. **22**(4): p. 266-282.
116. Fatokun, A.A., V.L. Dawson, and T.M. Dawson, *Parthanatos: mitochondrial-linked mechanisms and therapeutic opportunities*. Br J Pharmacol, 2014. **171**(8): p. 2000-16.
117. Koehler, R.C., V.L. Dawson, and T.M. Dawson, *Targeting Parthanatos in Ischemic Stroke*. Front Neurol, 2021. **12**: p. 662034.
118. D'Arcy, M.S., *Cell death: a review of the major forms of apoptosis, necrosis and autophagy*. Cell Biol Int, 2019. **43**(6): p. 582-592.
119. Galluzzi, L., et al., *Molecular definitions of autophagy and related processes*. EMBO J, 2017. **36**(13): p. 1811-1836.
120. Das, G., B.V. Shrivage, and E.H. Baehrecke, *Regulation and function of autophagy during cell survival and cell death*. Cold Spring Harb Perspect Biol, 2012. **4**(6).
121. Sharma, K., et al., *Cytotoxic autophagy in cancer therapy*. Int J Mol Sci, 2014. **15**(6): p. 10034-51.
122. Letchumanan, V., K.G. Chan, and L.H. Lee, *Vibrio parahaemolyticus: a review on the pathogenesis, prevalence, and advance molecular identification techniques*. Front Microbiol, 2014. **5**: p. 705.
123. Wang, R., et al., *The pathogenesis, detection, and prevention of Vibrio parahaemolyticus*. Front Microbiol, 2015. **6**: p. 144.
124. Nair, G.B., et al., *Global dissemination of Vibrio parahaemolyticus serotype O3:K6 and its serovariants*. Clin Microbiol Rev, 2007. **20**(1): p. 39-48.

125. Yeung, P.S. and K.J. Boor, *Epidemiology, pathogenesis, and prevention of foodborne Vibrio parahaemolyticus infections*. Foodborne Pathog Dis, 2004. **1**(2): p. 74-88.
126. Li, L., et al., *Molecular mechanisms of Vibrio parahaemolyticus pathogenesis*. Microbiol Res, 2019. **222**: p. 43-51.
127. Krachler, A.M., H. Ham, and K. Orth, *Outer membrane adhesion factor multivalent adhesion molecule 7 initiates host cell binding during infection by gram-negative pathogens*. Proc Natl Acad Sci U S A, 2011. **108**(28): p. 11614-9.
128. Krachler, A.M. and K. Orth, *Functional characterization of the interaction between bacterial adhesin multivalent adhesion molecule 7 (MAM7) protein and its host cell ligands*. J Biol Chem, 2011. **286**(45): p. 38939-47.
129. Verma, P. and K. Chattopadhyay, *Current Perspective on the Membrane-Damaging Action of Thermostable Direct Hemolysin, an Atypical Bacterial Pore-forming Toxin*. Front Mol Biosci, 2021. **8**: p. 717147.
130. Bhowmik, S.K., G.P. Pazhani, and T. Ramamurthy, *Phylogenetic and in silico functional analyses of thermostable-direct hemolysin and tdh-related encoding genes in Vibrio parahaemolyticus and other Gram-negative bacteria*. Biomed Res Int, 2014. **2014**: p. 576528.
131. Broberg, C.A., T.J. Calder, and K. Orth, *Vibrio parahaemolyticus cell biology and pathogenicity determinants*. Microbes Infect, 2011. **13**(12-13): p. 992-1001.
132. Wang, J., et al., *Regulation of Virulence Factors Expression During the Intestinal Colonization of Vibrio parahaemolyticus*. Foodborne Pathog Dis, 2022. **19**(3): p. 169-178.
133. Chun, D., et al., *Nature of the Kanagawa phenomenon of Vibrio parahaemolyticus*. Infect Immun, 1975. **12**(1): p. 81-7.
134. Nishibuchi, M., K. Kumagai, and J.B. Kaper, *Contribution of the tdh1 gene of Kanagawa phenomenon-positive Vibrio parahaemolyticus to production of extracellular thermostable direct hemolysin*. Microb Pathog, 1991. **11**(6): p. 453-60.

135. Raghunath, P., *Roles of thermostable direct hemolysin (TDH) and TDH-related hemolysin (TRH) in Vibrio parahaemolyticus*. *Front Microbiol*, 2014. **5**: p. 805.
136. Honda, T., et al., *The thermostable direct hemolysin of Vibrio parahaemolyticus is a pore-forming toxin*. *Can J Microbiol*, 1992. **38**(11): p. 1175-80.
137. Honda, T. and T. Iida, *The pathogenicity of Vibrio parahaemolyticus and the role of the thermostable direct haemolysin and related haemolysins*. 1993. **4**(2): p. 106-113.
138. Nishibuchi, M. and J.B. Kaper, *Duplication and variation of the thermostable direct haemolysin (tdh) gene in Vibrio parahaemolyticus*. *Mol Microbiol*, 1990. **4**(1): p. 87-99.
139. Nishibuchi, M. and J.B. Kaper, *Thermostable direct hemolysin gene of Vibrio parahaemolyticus: a virulence gene acquired by a marine bacterium*. *Infect Immun*, 1995. **63**(6): p. 2093-9.
140. Lin, Z., et al., *Vibrio parahaemolyticus has a homolog of the Vibrio cholerae toxRS operon that mediates environmentally induced regulation of the thermostable direct hemolysin gene*. *J Bacteriol*, 1993. **175**(12): p. 3844-55.
141. Kodama, T., et al., *Two regulators of Vibrio parahaemolyticus play important roles in enterotoxicity by controlling the expression of genes in the Vp-PAI region*. *PLoS One*, 2010. **5**(1): p. e8678.
142. Zhang, Y., et al., *Vibrio parahaemolyticus CalR down regulates the thermostable direct hemolysin (TDH) gene transcription and thereby inhibits hemolytic activity*. *Gene*, 2017. **613**: p. 39-44.
143. Guo, M., et al., *Regulation of Thermostable Direct Hemolysin and Biofilm Formation of Vibrio parahaemolyticus by Quorum-Sensing Genes luxM and luxS*. *Curr Microbiol*, 2018. **75**(9): p. 1190-1197.
144. Nakano, M., et al., *Hfq regulates the expression of the thermostable direct hemolysin gene in Vibrio parahaemolyticus*. *BMC Microbiol*, 2008. **8**: p. 155.
145. Matsuda, S., et al., *Export of a Vibrio parahaemolyticus toxin by the Sec and type III secretion machineries in tandem*. *Nat Microbiol*, 2019. **4**(5): p. 781-788.

146. Kundu, N., et al., *Disulphide bond restrains the C-terminal region of thermostable direct hemolysin during folding to promote oligomerization*. *Biochem J*, 2017. **474**(2): p. 317-331.
147. Kundu, N., et al., *N-Terminal Region of Vibrio parahemolyticus Thermostable Direct Hemolysin Regulates the Membrane-Damaging Action of the Toxin*. *Biochemistry*, 2020. **59**(4): p. 605-614.
148. Fukui, T., et al., *Thermostable direct hemolysin of Vibrio parahaemolyticus is a bacterial reversible amyloid toxin*. *Biochemistry*, 2005. **44**(29): p. 9825-32.
149. Takeda, Y., et al., *Inactivation of the biological activities of the thermostable direct hemolysin of Vibrio parahaemolyticus by ganglioside Gt1*. *Infect Immun*, 1976. **14**(1): p. 1-5.
150. Douet, J.P., et al., *Study of the haemolytic process and receptors of thermostable direct haemolysin from Vibrio parahaemolyticus*. *Res Microbiol*, 1996. **147**(9): p. 687-96.
151. Matsuda, S., et al., *Association of Vibrio parahaemolyticus thermostable direct hemolysin with lipid rafts is essential for cytotoxicity but not hemolytic activity*. *Infect Immun*, 2010. **78**(2): p. 603-10.
152. Sakurai, J., et al., *Interaction of thermostable direct hemolysin of Vibrio parahaemolyticus with human erythrocytes*. *Biken J*, 1975. **18**(4): p. 187-92.
153. Sakurai, J., et al., *Cytotoxic effect of the thermostable direct hemolysin produced by Vibrio parahaemolyticus on FL cells*. *Infect Immun*, 1976. **13**(3): p. 876-83.
154. Raimondi, F., et al., *Enterotoxicity and cytotoxicity of Vibrio parahaemolyticus thermostable direct hemolysin in in vitro systems*. *Infect Immun*, 2000. **68**(6): p. 3180-5.
155. Honda, T., et al., *Demonstration of the cardiotoxicity of the thermostable direct hemolysin (lethal toxin) produced by Vibrio parahaemolyticus*. *Infect Immun*, 1976. **13**(1): p. 163-71.
156. Tang, G.Q., et al., *Ca(2+)-independent cytotoxicity of Vibrio parahaemolyticus thermostable direct hemolysin (TDH) on Intestine 407, a cell line derived from human embryonic intestine*. *FEMS Microbiol Lett*, 1995. **134**(2-3): p. 233-8.

157. Takahashi, A., et al., *Mechanisms of chloride secretion induced by thermostable direct haemolysin of Vibrio parahaemolyticus in human colonic tissue and a human intestinal epithelial cell line*. J Med Microbiol, 2000. **49**(9): p. 801-810.
158. Chowdhury, P., et al., *Thermostable direct hemolysin downregulates human colon carcinoma cell proliferation with the involvement of E-cadherin, and beta-catenin/Tcf-4 signaling*. PLoS One, 2011. **6**(5): p. e20098.
159. Higa, N., et al., *Vibrio parahaemolyticus effector proteins suppress inflammasome activation by interfering with host autophagy signaling*. PLoS Pathog, 2013. **9**(1): p. e1003142.
160. Naim, R., et al., *Vibrio parahaemolyticus thermostable direct hemolysin can induce an apoptotic cell death in Rat-1 cells from inside and outside of the cells*. FEMS Microbiol Lett, 2001. **195**(2): p. 237-44.
161. Saha, N. and K.K. Banerjee, *Carbohydrate-mediated regulation of interaction of Vibrio cholerae hemolysin with erythrocyte and phospholipid vesicle*. J Biol Chem, 1997. **272**(1): p. 162-7.
162. Waterhouse, N.J. and J.A. Trapani, *A new quantitative assay for cytochrome c release in apoptotic cells*. Cell Death Differ, 2003. **10**(7): p. 853-5.
163. Gupta, S., G.V. Prasad, and A. Mukhopadhaya, *Vibrio cholerae Porin OmpU Induces Caspase-independent Programmed Cell Death upon Translocation to the Host Cell Mitochondria*. J Biol Chem, 2015. **290**(52): p. 31051-68.
164. Vines, A., G.J. McBean, and A. Blanco-Fernandez, *A flow-cytometric method for continuous measurement of intracellular Ca(2+) concentration*. Cytometry A, 2010. **77**(11): p. 1091-7.
165. Rossi, A.M. and C.W. Taylor, *Reliable measurement of free Ca(2+) concentrations in the ER lumen using Mag-Fluo-4*. Cell Calcium, 2020. **87**: p. 102188.
166. Rio, D.C., et al., *Purification of RNA using TRIzol (TRI reagent)*. Cold Spring Harb Protoc, 2010. **2010**(6): p. pdb prot5439.

167. Park, K.S., et al., *Cytotoxicity and enterotoxicity of the thermostable direct hemolysin-deletion mutants of Vibrio parahaemolyticus*. *Microbiol Immunol*, 2004. **48**(4): p. 313-8.
168. Bortner, C.D. and J.A. Cidlowski, *Flow cytometric analysis of cell shrinkage and monovalent ions during apoptosis*. *Methods Cell Biol*, 2001. **66**: p. 49-67.
169. Marino, G. and G. Kroemer, *Mechanisms of apoptotic phosphatidylserine exposure*. *Cell Res*, 2013. **23**(11): p. 1247-8.
170. Enari, M., et al., *A caspase-activated DNase that degrades DNA during apoptosis, and its inhibitor ICAD*. *Nature*, 1998. **391**(6662): p. 43-50.
171. Iglesias-Guimaraes, V., et al., *Apoptotic DNA degradation into oligonucleosomal fragments, but not apoptotic nuclear morphology, relies on a cytosolic pool of DFF40/CAD endonuclease*. *J Biol Chem*, 2012. **287**(10): p. 7766-79.
172. Cohen, G.M., *Caspases: the executioners of apoptosis*. *Biochem J*, 1997. **326** (Pt 1)(Pt 1): p. 1-16.
173. Han, Z., et al., *A sequential two-step mechanism for the production of the mature p17:p12 form of caspase-3 in vitro*. *J Biol Chem*, 1997. **272**(20): p. 13432-6.
174. Kavanagh, E., et al., *Regulation of caspase-3 processing by cIAP2 controls the switch between pro-inflammatory activation and cell death in microglia*. *Cell Death Dis*, 2014. **5**(12): p. e1565.
175. Verma, P., et al., *Vibrio parahaemolyticus thermostable direct haemolysin induces non-classical programmed cell death despite caspase activation*. *Mol Microbiol*, 2023.
176. Hay, B.A., *Understanding IAP function and regulation: a view from Drosophila*. *Cell Death Differ*, 2000. **7**(11): p. 1045-56.
177. Deveraux, Q.L. and J.C. Reed, *IAP family proteins--suppressors of apoptosis*. *Genes Dev*, 1999. **13**(3): p. 239-52.
178. Ravagnan, L., T. Roumier, and G. Kroemer, *Mitochondria, the killer organelles and their weapons*. *J Cell Physiol*, 2002. **192**(2): p. 131-7.

179. Neitemeier, S., et al., *BID links ferroptosis to mitochondrial cell death pathways*. Redox Biol, 2017. **12**: p. 558-570.
180. Lorenzo, H.K. and S.A. Susin, *Mitochondrial effectors in caspase-independent cell death*. FEBS Lett, 2004. **557**(1-3): p. 14-20.
181. Smiley, S.T., et al., *Intracellular heterogeneity in mitochondrial membrane potentials revealed by a J-aggregate-forming lipophilic cation JC-1*. Proc Natl Acad Sci U S A, 1991. **88**(9): p. 3671-5.
182. Chassin, C., et al., *Pore-forming epsilon toxin causes membrane permeabilization and rapid ATP depletion-mediated cell death in renal collecting duct cells*. Am J Physiol Renal Physiol, 2007. **293**(3): p. F927-37.
183. Garrido, C., et al., *Mechanisms of cytochrome c release from mitochondria*. Cell Death Differ, 2006. **13**(9): p. 1423-33.
184. Bano, D. and J.H.M. Prehn, *Apoptosis-Inducing Factor (AIF) in Physiology and Disease: The Tale of a Repented Natural Born Killer*. EBioMedicine, 2018. **30**: p. 29-37.
185. Cande, C., et al., *Apoptosis-inducing factor (AIF): key to the conserved caspase-independent pathways of cell death?* J Cell Sci, 2002. **115**(Pt 24): p. 4727-34.
186. Susin, S.A., et al., *Two distinct pathways leading to nuclear apoptosis*. J Exp Med, 2000. **192**(4): p. 571-80.
187. van Loo, G., et al., *Endonuclease G: a mitochondrial protein released in apoptosis and involved in caspase-independent DNA degradation*. Cell Death Differ, 2001. **8**(12): p. 1136-42.
188. Benitez-Guzman, A., et al., *Endonuclease G takes part in AIF-mediated caspase-independent apoptosis in Mycobacterium bovis-infected bovine macrophages*. Vet Res, 2018. **49**(1): p. 69.
189. Li, L.Y., X. Luo, and X. Wang, *Endonuclease G is an apoptotic DNase when released from mitochondria*. Nature, 2001. **412**(6842): p. 95-9.
190. Ott, M., et al., *Mitochondria, oxidative stress and cell death*. Apoptosis, 2007. **12**(5): p. 913-22.

191. Villalpando-Rodriguez, G.E. and S.B. Gibson, *Reactive Oxygen Species (ROS) Regulates Different Types of Cell Death by Acting as a Rheostat*. *Oxid Med Cell Longev*, 2021. **2021**: p. 9912436.
192. Brookes, P.S., et al., *Calcium, ATP, and ROS: a mitochondrial love-hate triangle*. *Am J Physiol Cell Physiol*, 2004. **287**(4): p. C817-33.
193. Gorlach, A., et al., *Calcium and ROS: A mutual interplay*. *Redox Biol*, 2015. **6**: p. 260-271.
194. Bauer, T.M. and E. Murphy, *Role of Mitochondrial Calcium and the Permeability Transition Pore in Regulating Cell Death*. *Circ Res*, 2020. **126**(2): p. 280-293.
195. Braun, J.S., et al., *Pneumolysin causes neuronal cell death through mitochondrial damage*. *Infect Immun*, 2007. **75**(9): p. 4245-54.
196. Galmiche, A. and J. Rassow, *Targeting of Helicobacter pylori VacA to mitochondria*. *Gut Microbes*, 2010. **1**(6): p. 392-5.
197. Muller, A., et al., *VDAC and the bacterial porin PorB of Neisseria gonorrhoeae share mitochondrial import pathways*. *EMBO J*, 2002. **21**(8): p. 1916-29.
198. Domanska, G., et al., *Helicobacter pylori VacA toxin/subunit p34: targeting of an anion channel to the inner mitochondrial membrane*. *PLoS Pathog*, 2010. **6**(4): p. e1000878.
199. Smaili, S.S., et al., *Bax translocation to mitochondria subsequent to a rapid loss of mitochondrial membrane potential*. *Cell Death Differ*, 2001. **8**(9): p. 909-20.
200. Karch, J., et al., *Bax and Bak function as the outer membrane component of the mitochondrial permeability pore in regulating necrotic cell death in mice*. *Elife*, 2013. **2**: p. e00772.
201. Whelan, R.S., et al., *Bax regulates primary necrosis through mitochondrial dynamics*. *Proc Natl Acad Sci U S A*, 2012. **109**(17): p. 6566-71.
202. Aits, S. and M. Jaattela, *Lysosomal cell death at a glance*. *J Cell Sci*, 2013. **126**(Pt 9): p. 1905-12.
203. Wang, F., R. Gomez-Sintes, and P. Boya, *Lysosomal membrane permeabilization and cell death*. *Traffic*, 2018. **19**(12): p. 918-931.

204. Guicciardi, M.E., M. Leist, and G.J. Gores, *Lysosomes in cell death*. *Oncogene*, 2004. **23**(16): p. 2881-90.
205. Mashimo, M., et al., *The 89-kDa PARP1 cleavage fragment serves as a cytoplasmic PAR carrier to induce AIF-mediated apoptosis*. *J Biol Chem*, 2021. **296**: p. 100046.
206. Chaitanya, G.V., A.J. Steven, and P.P. Babu, *PARP-1 cleavage fragments: signatures of cell-death proteases in neurodegeneration*. *Cell Commun Signal*, 2010. **8**: p. 31.
207. Cancino-Rodezno, A., et al., *Defense and death responses to pore forming toxins*. *Biotechnol Genet Eng Rev*, 2010. **26**: p. 65-82.
208. Hiyoshi, H., et al., *Contribution of Vibrio parahaemolyticus virulence factors to cytotoxicity, enterotoxicity, and lethality in mice*. *Infect Immun*, 2010. **78**(4): p. 1772-80.
209. Slee, E.A., C. Adrain, and S.J. Martin, *Executioner caspase-3, -6, and -7 perform distinct, non-redundant roles during the demolition phase of apoptosis*. *J Biol Chem*, 2001. **276**(10): p. 7320-6.
210. Nguyen, T.T.M., G. Gillet, and N. Popgeorgiev, *Caspases in the Developing Central Nervous System: Apoptosis and Beyond*. *Front Cell Dev Biol*, 2021. **9**: p. 702404.
211. Deveraux, Q.L., et al., *X-linked IAP is a direct inhibitor of cell-death proteases*. *Nature*, 1997. **388**(6639): p. 300-4.
212. Broker, L.E., F.A. Kruyt, and G. Giaccone, *Cell death independent of caspases: a review*. *Clin Cancer Res*, 2005. **11**(9): p. 3155-62.
213. Kroemer, G. and S.J. Martin, *Caspase-independent cell death*. *Nat Med*, 2005. **11**(7): p. 725-30.
214. Galluzzi, L., O. Kepp, and G. Kroemer, *Mitochondrial regulation of cell death: a phylogenetically conserved control*. *Microb Cell*, 2016. **3**(3): p. 101-108.
215. Ow, Y.P., et al., *Cytochrome c: functions beyond respiration*. *Nat Rev Mol Cell Biol*, 2008. **9**(7): p. 532-42.

216. Kim, H.E., et al., *Formation of apoptosome is initiated by cytochrome c-induced dATP hydrolysis and subsequent nucleotide exchange on Apaf-1*. Proc Natl Acad Sci U S A, 2005. **102**(49): p. 17545-50.
217. Patriarca, A., et al., *ATP acts as a regulatory effector in modulating structural transitions of cytochrome c: implications for apoptotic activity*. Biochemistry, 2009. **48**(15): p. 3279-87.
218. Von Ahsen, O., et al., *The 'harmless' release of cytochrome c*. Cell Death Differ, 2000. **7**(12): p. 1192-9.
219. Bratton, S.B., et al., *XIAP inhibition of caspase-3 preserves its association with the Apaf-1 apoptosome and prevents CD95- and Bax-induced apoptosis*. Cell Death Differ, 2002. **9**(9): p. 881-92.
220. Cregan, S.P., V.L. Dawson, and R.S. Slack, *Role of AIF in caspase-dependent and caspase-independent cell death*. Oncogene, 2004. **23**(16): p. 2785-96.
221. Orrenius, S., B. Zhivotovsky, and P. Nicotera, *Regulation of cell death: the calcium-apoptosis link*. Nat Rev Mol Cell Biol, 2003. **4**(7): p. 552-65.
222. Hajnoczky, G., et al., *Mitochondrial calcium signalling and cell death: approaches for assessing the role of mitochondrial Ca<sup>2+</sup> uptake in apoptosis*. Cell Calcium, 2006. **40**(5-6): p. 553-60.
223. Karch, J. and J.D. Molkenin, *Regulated necrotic cell death: the passive aggressive side of Bax and Bak*. Circ Res, 2015. **116**(11): p. 1800-9.
224. Westphal, D., R.M. Kluck, and G. Dewson, *Building blocks of the apoptotic pore: how Bax and Bak are activated and oligomerize during apoptosis*. Cell Death Differ, 2014. **21**(2): p. 196-205.
225. Kozjak-Pavlovic, V., et al., *Bacterial porin disrupts mitochondrial membrane potential and sensitizes host cells to apoptosis*. PLoS Pathog, 2009. **5**(10): p. e1000629.
226. Droga-Mazovec, G., et al., *Cysteine cathepsins trigger caspase-dependent cell death through cleavage of bid and antiapoptotic Bcl-2 homologues*. J Biol Chem, 2008. **283**(27): p. 19140-50.

227. Ray Chaudhuri, A. and A. Nussenzweig, *The multifaceted roles of PARP1 in DNA repair and chromatin remodelling*. Nat Rev Mol Cell Biol, 2017. **18**(10): p. 610-621.



# Synopsis



## Synopsis

**Title: Unraveling the molecular mechanisms underlying the cell death pathway induced by *Vibrio parahaemolyticus* Thermostable Direct Hemolysin, an atypical pore-forming toxin**

The plasma membrane, a vital structure in all living organisms, acts as a protective barrier that safeguards and preserves the cellular integrity, while also facilitating various biological processes [1]. Organisms have evolved mechanisms to disrupt the permeability barrier function of the plasma membrane by employing a distinct category of proteins known as ‘Pore-forming Proteins/Toxins’ (PFPs/PFTs) [2]. These unique proteins have the remarkable ability to punch holes on the plasma membrane, resulting in disturbed cellular homeostasis. PFPs are conserved across the diverse life forms, spanning from unicellular organisms like bacteria to the higher vertebrates like human [3].

Bacterial PFTs are the most extensively studied toxins and are considered invaluable machineries exploited by the bacteria for various purposes [4]. They play essential role in acquisition of the nutrients, elimination of competing bacteria, aiding the entry of other bacterial effectors, and facilitating pathogen’s dissemination and colonization [5-7]. Interaction of bacterial PFTs with the target host cells can induce numerous cellular responses, such as membrane-repair, cell survival, immunological or cell death responses [2]. Cell death is an inevitable consequence that can be triggered by either PFTs or by the host itself for their own benefit. PFTs may promote the pathogen spread or establishment of infection by killing the host cells. Conversely, the host may instigate a cell death response to contain the spread of infection by eliminating infected cells from the system. Multiple cell death pathways involving different molecular mechanisms have been documented in response to the different PFTs [8-13]. Understanding of distinct cell death responses and the underlying molecular mechanisms triggered by PFTs is crucial in comprehending their roles in bacterial pathogenesis and host-pathogen interaction processes.

Thermostable Direct Hemolysin (TDH) is a major protein toxin produced by *Vibrio parahaemolyticus*, a leading causative organism of acute gastroenteritis in humans [14]. Among several other virulence arsenals of the bacterium, TDH has been recognized

as the key virulence factor of the clinical strains of this bacterium [15]. It has been found to be associated with several outbreaks of seafood-borne gastrointestinal infections. TDH has been characterised as a membrane-damaging PFT [16]. TDH exhibits various biological activities such as hemolysis, enterotoxicity, cytotoxicity, and cardiotoxicity [17-19]. TDH has been established as a potent cytolytic PFT, and its cytotoxicity has been documented against a variety of nucleated mammalian cells [14]. Moreover, TDH has been shown to trigger programmed cell death with features resembling apoptosis in target nucleated cells [20]. However, the precise molecular details of the cell death pathway activated by TDH in nucleated mammalian cells remain relatively unexplored. Thus, the present study aims to unravel the intricate molecular mechanisms underlying the cell death pathway triggered by TDH.

The findings of the present thesis work revealed potent cytotoxicity of TDH against nucleated mammalian cells. Prominent morphological alterations such as cell shrinkage, increased cell granularity were recorded in response to TDH intoxication. Moreover, TDH instigated the flipping of phosphatidylserine on the outer leaflet of the membrane bilayer along with plasma membrane and nuclear disintegration in the target cells. Additionally, TDH was also found to trigger DNA fragmentation, displaying a characteristic DNA-laddering pattern. Collectively, these observations suggested that TDH induces features of programmed cell death that closely resembles apoptosis.

Furthermore, the involvement of caspases in the TDH-mediated programmed cell death was investigated, since caspases are considered as the hallmarks of apoptosis pathway of cell death. Intriguingly, the partial processing of caspase-3 indicating the unavailability of a functionally active form, and the lack of reduction in TDH-mediated cell death upon pan caspase-inhibitor pre-treatment, indicated that catalytic activity of caspases is not implicated in TDH-triggered cell death pathway. Therefore, TDH was found to induce a caspase-independent programmed cell death.

Considering the central role of mitochondria in various cell death pathways, the role of mitochondria was examined in TDH-mediated caspase-independent cell death. TDH was found to induce mitochondrial membrane permeability transition (MMPT), leading to notable mitochondrial damage, characterized by decreased ATP levels and release of mitochondrial factors like cytochrome c, apoptosis inducing factor (AIF) and endonuclease G (Endo G). Consequently, AIF and Endo G were found to translocate to

the nucleus of the target cells upon their mitochondrial release. Upon its nuclear translocation, Endo G generates DNA fragments of 100-200 base pairs, resulting in the characteristic DNA laddering pattern resembling apoptosis during TDH-mediated caspase-independent mode of programmed cell death.

Furthermore, the molecules/factors responsible for the mitochondrial pathway of programmed cell death were explored. Significant ROS production, including mitochondrial ROS, and ROS-mediated calcium influx were observed in the target cells in response to TDH. However, ROS and calcium did not appear to influence the TDH-mediated mitochondrial pathway of programmed cell death.

Interestingly, TDH exhibited prominent propensity to translocate to the mitochondria of the target cells. Nevertheless, its association with mitochondria was not enough to induce any mitochondrial damage. Thus, the possibility of a cytosolic factor or signal in inducing mitochondrial damage was explored. The increased *bax/bcl-2* levels and recruitment of active Bax to the mitochondria indicated the role of Bax as the cytosolic factor responsible for the mitochondrial damage upon TDH exposure.

In addition to investigating the role of mitochondria in the TDH-mediated caspase-independent programmed cell death, the study explored the involvement of other organelles, particularly, lysosomes. Interestingly, TDH intoxication was found to induce lysosomal damage, suggesting the possible engagement of lysosomes in TDH-mediated cell death. Furthermore, TDH was found to induce the cleavage of PARP-1 that can facilitate the translocation of AIF to the nucleus in certain pathways of cell death. While these findings suggest the potential role of lysosomes and PARP-1 in TDH-mediated cell death, further research will provide insights into their precise role in the pathway.

Overall, the present research work deciphers the intricate molecular mechanism of TDH-mediated cell death in the nucleated mammalian cells. Notably, TDH was found to induce caspase-independent programmed cell death, affecting mitochondria, AIF and Endo G-mediated chromatin condensation, and DNA fragmentation. The current study also highlighted the translocation of TDH to the target cell mitochondria, involvement of Bax in inducing mitochondrial damage, lysosomal damage and potential role of PARP-1 in the cell death pathway triggered by TDH. These findings contribute to the significant pathophysiological roles of TDH in the context of bacterial pathogenesis and host-

pathogen interaction processes. Moreover, considering TDH as a prototype bacterial PFT, this study extends our current understanding of cellular responses to such toxins.

### Publications

1. **Verma, P.\***, Chauhan, A.\*, Thakur, R., Lata, K., Sharma, A., Chattopadhyay, K., & Mukhopadhyaya, A. (2023). *Vibrio parahaemolyticus* thermostable direct haemolysin induces non-classical programmed cell death despite caspase activation. *Molecular microbiology*, 10.1111/mmi.15180. (\*equal contribution)
2. Bhutani, G., **Verma, P.**, Jayachandran, A., Paul, S., Chattopadhyay, K., & De, A. K. (2023). Unveiling the Role of Hidden Isomers in Large Stokes Shift in mKeima: Harnessing pH-Sensitive Dual-Emission in Bioimaging. *The journal of physical chemistry. B*, 127(14), 3197–3207.
3. Kaur, D.\*, **Verma, P.\***, Singh, M., Sharma, A., Lata, K., Mukhopadhyaya, A., & Chattopadhyay, K. (2022). Pore formation-independent cell death induced by a  $\beta$ -barrel pore-forming toxin. *FASEB journal : official publication of the Federation of American Societies for Experimental Biology*, 36(10), e22557. (\*equal contribution)
4. **Verma, P.**, & Chattopadhyay, K. (2021). Current Perspective on the Membrane-Damaging Action of Thermostable Direct Hemolysin, an Atypical Bacterial Pore-forming Toxin. *Frontiers in molecular biosciences*, 8, 717147.
5. **Verma, P.**, Gandhi, S., Lata, K., & Chattopadhyay, K. (2021). Pore-forming toxins in infection and immunity. *Biochemical Society transactions*, 49(1), 455–465.
6. Mondal, A. K., **Verma, P.**, Lata, K., Singh, M., Chatterjee, S., & Chattopadhyay, K. (2020). Sequence Diversity in the Pore-Forming Motifs of the Membrane-Damaging Protein Toxins. *The Journal of membrane biology*, 253(5), 469–478.
7. Kundu, N., **Verma, P.**, Kumar, A., Dhar, V., Dutta, S., & Chattopadhyay, K. (2020). N-Terminal Region of *Vibrio parahemolyticus* Thermostable Direct

Hemolysin Regulates the Membrane-Damaging Action of the Toxin. *Biochemistry*, 59(4), 605–614.

8. Mondal, A. K., Sreekumar, A., Kundu, N., Kathuria, R., Verma, P., Gandhi, S., & Chattopadhyay, K. (2018). Structural Basis and Functional Implications of the Membrane Pore-Formation Mechanisms of Bacterial Pore-Forming Toxins. *Advances in experimental medicine and biology*, 1112, 281–291.

### References

1. Blazek, A.D., B.J. Paleo, and N. Weisleder, *Plasma Membrane Repair: A Central Process for Maintaining Cellular Homeostasis*. Physiology (Bethesda), 2015. **30**(6): p. 438-48.
2. Verma, P., et al., *Pore-forming toxins in infection and immunity*. Biochem Soc Trans, 2021. **49**(1): p. 455-465.
3. Mondal, A.K., et al., *Structural Basis and Functional Implications of the Membrane Pore-Formation Mechanisms of Bacterial Pore-Forming Toxins*. Adv Exp Med Biol, 2018. **1112**: p. 281-291.
4. Dal Peraro, M. and F.G. van der Goot, *Pore-forming toxins: ancient, but never really out of fashion*. Nat Rev Microbiol, 2016. **14**(2): p. 77-92.
5. Lakey, J.H., F.G. van der Goot, and F. Pattus, *All in the family: the toxic activity of pore-forming colicins*. Toxicology, 1994. **87**(1-3): p. 85-108.
6. Jiang, J., et al., *Atomic structure of anthrax protective antigen pore elucidates toxin translocation*. Nature, 2015. **521**(7553): p. 545-9.
7. Seike, S., et al., *Delta-toxin from Clostridium perfringens perturbs intestinal epithelial barrier function in Caco-2 cell monolayers*. Biochim Biophys Acta Biomembr, 2018. **1860**(2): p. 428-433.
8. Braun, J.S., et al., *Pneumolysin causes neuronal cell death through mitochondrial damage*. Infect Immun, 2007. **75**(9): p. 4245-54.

9. Chassin, C., et al., *Pore-forming epsilon toxin causes membrane permeabilization and rapid ATP depletion-mediated cell death in renal collecting duct cells*. *Am J Physiol Renal Physiol*, 2007. **293**(3): p. F927-37.
10. Genestier, A.L., et al., *Staphylococcus aureus Panton-Valentine leukocidin directly targets mitochondria and induces Bax-independent apoptosis of human neutrophils*. *J Clin Invest*, 2005. **115**(11): p. 3117-27.
11. Goldmann, O., et al., *Streptococcus pyogenes induces oncosis in macrophages through the activation of an inflammatory programmed cell death pathway*. *Cell Microbiol*, 2009. **11**(1): p. 138-55.
12. Haslinger, B., et al., *Staphylococcus aureus alpha-toxin induces apoptosis in peripheral blood mononuclear cells: role of endogenous tumour necrosis factor-alpha and the mitochondrial death pathway*. *Cell Microbiol*, 2003. **5**(10): p. 729-41.
13. Kaur, D., et al., *Pore formation-independent cell death induced by a beta-barrel pore-forming toxin*. *FASEB J*, 2022. **36**(10): p. e22557.
14. Verma, P. and K. Chattopadhyay, *Current Perspective on the Membrane-Damaging Action of Thermostable Direct Hemolysin, an Atypical Bacterial Pore-forming Toxin*. *Front Mol Biosci*, 2021. **8**: p. 717147.
15. Letchumanan, V., K.G. Chan, and L.H. Lee, *Vibrio parahaemolyticus: a review on the pathogenesis, prevalence, and advance molecular identification techniques*. *Front Microbiol*, 2014. **5**: p. 705.
16. Honda, T., et al., *The thermostable direct hemolysin of Vibrio parahaemolyticus is a pore-forming toxin*. *Can J Microbiol*, 1992. **38**(11): p. 1175-80.
17. Kundu, N., et al., *Disulphide bond restrains the C-terminal region of thermostable direct hemolysin during folding to promote oligomerization*. *Biochem J*, 2017. **474**(2): p. 317-331.
18. Raimondi, F., et al., *Enterotoxicity and cytotoxicity of Vibrio parahaemolyticus thermostable direct hemolysin in in vitro systems*. *Infect Immun*, 2000. **68**(6): p. 3180-5.

19. Honda, T., et al., *Demonstration of the cardiotoxicity of the thermostable direct hemolysin (lethal toxin) produced by Vibrio parahaemolyticus*. *Infect Immun*, 1976. **13**(1): p. 163-71.
20. Naim, R., et al., *Vibrio parahaemolyticus thermostable direct hemolysin can induce an apoptotic cell death in Rat-1 cells from inside and outside of the cells*. *FEMS Microbiol Lett*, 2001. **195**(2): p. 237-44.